

**NON-PROPRIETARY VERSION**

**Attachment 2**

**Topical Report DOM-NAF-1**

**Qualification of the Studsvik Core Management System Reactor Physics Methods  
for Application to North Anna and Surry Power Stations**

**Virginia Electric and Power Company  
(Dominion)**

NON-PROPRIETARY VERSION

# Qualification of the Studsvik Core Management System Reactor Physics Methods for Application to North Anna and Surry Power Stations

NUCLEAR ANALYSIS AND FUEL DEPARTMENT  
DOMINION  
RICHMOND, VIRGINIA  
April, 2002

Prepared by:



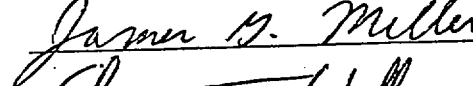
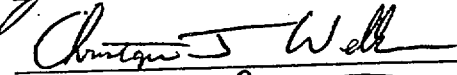
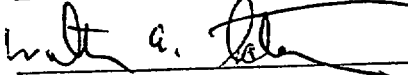
Robert A. Hall

Rebecca D. Kepler

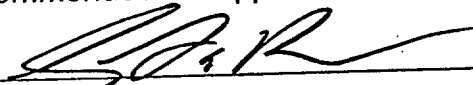
James G. Miller

Christopher J. Wells

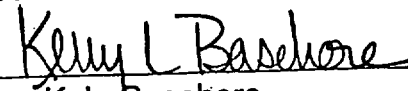
Walter A. Peterson

Recommended for Approval:

  
G. B. LaRoe  
Supervisor, Nuclear Core Design

Approved:

  
K. L. Basehore  
Director, Nuclear Analysis and Fuel

## ***NON-PROPRIETARY VERSION***

### **CLASSIFICATION/DISCLAIMER**

The data and analytical techniques described in this report have been prepared specifically for application by Dominion. Dominion makes no claim as to the accuracy of the data or techniques contained in this report if used by other organizations. Any use of this report or any part thereof must have the prior written approval of Dominion. Data withheld from publication in this non-proprietary version is denoted by [ ].

### **ABSTRACT**

As part of Dominion's continuing effort to improve its reload design methods, the Studsvik/CMS core modeling code package has been validated for use in the reload design process for the North Anna and Surry Power Stations. The primary codes in the CMS system are CASMO-4 and SIMULATE-3. The accuracy of the CMS system is demonstrated through comparisons with measurements from over 60 cycles of operation taken at the Surry and North Anna Nuclear Power Stations and through comparison with higher order Monte Carlo neutron transport calculations. The CMS system has been shown to meet or exceed the same standards for accuracy as models currently used by Dominion.

## Table of Contents

CLASSIFICATION/DISCLAIMER.....	2
ABSTRACT.....	2
TABLE OF CONTENTS .....	3
LIST OF TABLES .....	4
LIST OF FIGURES.....	5
SECTION 1 - INTRODUCTION .....	7
SURRY NUCLEAR POWER STATION OPERATING HISTORY .....	11
NORTH ANNA NUCLEAR POWER STATION OPERATING HISTORY .....	12
SECTION 2 – CODE AND MODEL DESCRIPTION .....	13
2.1 CASMO-4.....	13
2.2 CMS-LINK.....	14
2.3 SIMULATE-3 .....	15
2.4 AUXILIARY CODES .....	16
2.4.1 Monte Carlo Codes – Cross Section Library Benchmarking.....	16
2.4.2 ESCORE - Fuel Temperature Data.....	16
2.4.3 CECOR - Flux Map Reaction Rate Data.....	18
SECTION 3 – MODEL BENCHMARKING .....	19
3.1 CASMO BENCHMARKING .....	19
3.2 SIMULATE BENCHMARKING TO HIGHER ORDER CALCULATIONS .....	22
3.3 SIMULATE BENCHMARKING TO MEASURED CYCLE DATA.....	27
3.3.1 Critical Boron Concentration.....	27
3.3.2 Control Rod Worth .....	34
3.3.3 Isothermal Temperature Coefficient .....	42
3.3.4 Differential Boron Worth.....	45
3.3.5 Estimated Critical Position .....	51
3.3.6 Reaction Rate Comparisons.....	55
3.3.7 Normal Operation Power Transients.....	67
3.3.8 Xenon Oscillation Demonstration .....	90
SECTION 4 – UNCERTAINTY AND RELIABILITY FACTORS.....	92
4.1 DEFINITIONS.....	92
4.2 STATISTICAL METHODS .....	95
4.3 DETERMINATION OF NUCLEAR UNCERTAINTY FACTORS .....	99
4.3.1 Critical Boron Concentration.....	99
4.3.2 Integral Control Rod Worth.....	101
4.3.3 Peak Differential Control Rod Worth.....	105
4.3.4 Isothermal Temperature Coefficient .....	106
4.3.5 Differential Boron Worth.....	107
4.3.6 Estimated Critical Position .....	109
4.3.7 Reaction Rate Comparisons.....	112
4.3.8 Doppler Coefficients and Defects .....	114
4.3.9 Delayed Neutron and Prompt Neutron Lifetime .....	115
SECTION 5 - SUMMARY AND CONCLUSIONS .....	119
SECTION 6 - REFERENCES .....	121

## List of Tables

<b>Table</b>	<b>Title</b>	<b>Page</b>
1	Surry Nuclear Power Station Operating History	11
2	North Anna Nuclear Power Station Operating History	12
3	CASMO-4 Reactivity Benchmarking Versus MCNP-4B and KENO-V.a	20
4	CASMO-4 W-prime and Pin-to-Box Ratio Comparisons	26
5	SIMULATE Critical Boron Comparisons	32
6	SIMULATE Integral Control Rod Worth Comparisons	38
7	SIMULATE Peak Differential Control Rod Worth Comparisons	38
8	SIMULATE HZP BOC ITC Comparisons	44
9	SIMULATE HZP DBW Comparisons	49
10	SIMULATE ECP Error	53
11	Flux Map Database for Reaction Rate Comparison	59
12	Flux Map Reaction Rate Statistics	66
13	N1C11 Power Ascension Flux Map Reaction Rate Statistics	85
14	Approved NRF Values for Previous Design Models	94
15	SIMULATE Critical Boron NUF	100
16	SIMULATE Integral Rod Worth NUF	102
17	Rod Worth Measurement Uncertainty Estimate	104
18	SIMULATE Peak Differential Rod Worth NUF	105
19	SIMULATE Isothermal Temperature Coefficient NUF	106
20	SIMULATE Differential Boron Worth NUF	108
21	SIMULATE Estimated Critical Position NUF	111
22	Approximate Uncertainty Components for ECP Calculations	111
23	SIMULATE Reaction Rate NUF	113
24	SIMULATE FΔH and FQ NUF	113
25	Validation of CASMO-4 Prompt Neutron Lifetime Calculations	118

## List of Figures

<b>Figure</b>	<b>Title</b>	<b>Page</b>
1	Surry (15x15) Temperature Defects; CASMO-4 Versus MCNP-4B	21
2	North Anna (17x17) Temperature Defects; CASMO-4 Versus MCNP-4B	21
3	N2C5 Boron Letdown Curve	30
4	N2C12 Boron Letdown Curve	30
5	North Anna Critical Boron Difference; Simulate Minus Measured	31
6	Surry Critical Boron Difference; Simulate Minus Measured	31
7	Combined Critical Boron Difference; Simulate Minus Measured	33
8	North Anna Rod Worth Comparison	36
9	Surry Rod Worth Comparison	36
10	Combined Rod Worth Comparison	37
11	Combined Peak Differential Rod Worth Comparison	39
12	North Anna Unit 1, Cycle 4 Bank B Differential Rod Worth	40
13	North Anna Unit 2, Cycle 15 Bank B Differential Rod Worth	40
14	Surry Unit 2, Cycle 10 Bank B Differential Rod Worth	41
15	Surry Unit 1, Cycle 17 Bank B Differential Rod Worth	41
16	North Anna HZP BOC ITC Comparison	43
17	Surry HZP BOC ITC Comparison	43
18	Combined Reactivity Computer Bias Influence	49
19	Combined Differential Boron Worth Comparison	50
20	Combined DBW Error vs. Critical Boron Concentration	50
21	Combined ECP Results	54
22	Combined ECP Error Versus At-Power Critical Boron	54
23	In-core Moveable Detector Locations	58
24	Flux Map Thimble Reaction Rate Comparison; Integrated Trace Data	65
25	Flux Map Thimble Reaction Rate Comparison; 32 Axial Regions	65
26	S2C2 Load Follow Transient; Power and D-Bank Position Versus Time	69
27	S2C2 Load Follow Transient Delta-I Comparison	69
28	S2C2 Load Follow Transient Critical Boron Comparison	70

## List of Figures (continued)

<b>Figure</b>	<b>Title</b>	<b>Page</b>
29	S2C2 Load Follow Transient; Peak Core Average Axial Power Comparison	70
30	N1C3 Power Transient 1; Power and D-Bank Position Versus Time	72
31	N1C3 Power Transient 1 Delta-I Comparison	72
32	N1C3 Power Transient 1 Critical Boron Comparison	73
33	N1C3 Power Transient 2; Power and D-Bank Position Versus Time	73
34	N1C3 Power Transient 2 Axial Offset Comparison	74
35	N1C3 Power Transient 2 Critical Boron Comparison	74
36	N1C6 Power Transient; Power and D-Bank Position Versus Time	76
37	N1C6 Power Transient Delta-I Comparison	76
38	N1C6 Power Transient Critical Boron Comparison	77
39	N1C9 MTC Measurement Transient; Measured Inlet Temperature and Critical Boron Concentration	80
40	N1C9 MTC Measurement Transient; Delta-I Change from Beginning of Measurement	80
41	N1C9 MTC Measurement Transient; SIMULATE K-effective Drift	81
42	N1C11 Initial Power Ascension; Power and D-Bank Position Versus Time	83
43	N1C11 Initial Power Ascension Delta-I Comparison	83
44	N1C11 Initial Power Ascension Critical Boron Comparison	84
45	Core Average Axial Power Comparison; N1C11 Flux Map 1, 29.9% Power, D@124	84
46	Core Average Axial Power Comparison; N1C11 Flux Map 2, 74.0% Power, D@179	85
47	N2C14 Power Transient; Power and D-Bank Position Versus Time	88
48	N2C14 Power Transient Delta-I Comparison	88
49	N2C14 Power Transient Critical Boron Comparison	89
50	N2C14 Power Transient Delta-I Comparison; Sensitivity to Moderator Flow Rate	89
51	N1C15 Xenon Oscillation Demonstration	91
52	Control Rod Worth Comparison; SIMULATE Versus Measured	103

## SECTION 1 - INTRODUCTION

Virginia Electric and Power Company (Dominion) is updating its capability to perform nuclear utility reactor analyses in support of the Surry and North Anna nuclear power stations. The objectives of this report are to briefly describe the computational models to be validated, to describe the intended applications of the models in the reload design process, and to demonstrate the accuracy of the models by comparing calculated data to measurements from Surry and North Anna Units 1 and 2.

The updated models use the Studsvik Core Management System (CMS) core modeling code package, consisting primarily of the CASMO-4 (CASMO, references 1-4) and SIMULATE-3 (SIMULATE, references 5-6) codes. The CMS package was developed by Studsvik AB and Studsvik of America (currently Studsvik Scandpower, Inc.). The CMS package is used and accepted in the nuclear industry both in the United States and worldwide in its current and previous versions. A brief description of the theory and function of the computer codes used for core modeling and for verification of model accuracy is presented in Section 2.

The primary focus of this report is to demonstrate the validity and accuracy of the CMS package as implemented at Dominion for core reload design, core follow, and calculation of key core parameters for reload safety analysis. An integral part of the implementation is a rigorous modeling approach that begins with higher order computer codes to identify and eliminate significant model bias prior to performing core calculations. The types of calculations that can be performed by the CMS model include:

- Three-dimensional assembly power and flux distributions, relative radial peaking factors ( $F_{xy}(Z)$ ), enthalpy rise hot channel factors ( $F_{\Delta H}(X,Y)$ ), assembly average axial power distribution, core average axial power distribution ( $F(Z)$ ), and heat flux hot channel factor ( $F_Q(X,Y,Z)$ )
- Soluble boron concentration and boron worth
- Fuel and burnable poison nuclide concentrations as a function of fuel burnup
- Integral and differential control rod bank worths
- Abnormally positioned control rod worths



- Moderator and Doppler temperature coefficients and defects
- Power coefficients and defects
- Operational transient simulation
- Delayed neutron parameters and prompt neutron lifetime
- Detector reaction rates, coupling coefficients, and peaking factors for flux map analysis
- Fuel burnup
- Scoping studies for the evaluation of alternative fuel management strategies, fuel design changes, burnable poison product changes, and alternate control rod designs

These calculations are currently performed with other core models (References 7-10) as described in those and other Topical Reports (References 11-13, 18, 39). The benchmarking data presented in this report demonstrate that the CMS models, including appropriate uncertainty factors derived herein, are fully capable of and acceptable for performing these types of calculations. Use of the CMS models does not change the essential methodology of those reports, but may alter details of the methodology. For example, because SIMULATE models the entire core in three dimensions, it is no longer necessary to perform 1-D/3-D peaking factor synthesis. Due to the efficient run-time of the SIMULATE models, 1-D calculations formerly required due to computer time limitations are no longer necessary. These cases may now be run directly in full-core 3-D geometry, eliminating approximations inherent in quarter-core modeling and the synthesis process.

The Surry Nuclear Power Station and the North Anna Nuclear Power Station, each consisting of two operating units, have been selected for verification of the CMS model. Measurements from Surry cycles S1C1-S1C17 and S2C1-S2C17 and from North Anna cycles N1C1-N1C15 and N2C1-N2C15 will be used for model benchmarking and determination of model reliability factors.

These cycles represent evolutionary changes in core design over more than 60 cycles of operation including transitions in fuel enrichment, fuel density, fuel loading pattern strategy, spacer grid design and material, fuel vendor, core operating conditions (full

power average moderator temperature and rated thermal power) and burnable poison material and design. Loading pattern strategy variations include out-in and low-low-leakage designs, axially zoned fixed poison rods for reactor pressure vessel fluence reduction, transition to axially and radially zoned burnable poisons, and a range of operating cycle lengths from 202 to 582 effective full power days (EFPD) with and without temperature and power coastdown. Types of core measurements used for model benchmarking include:

- Critical boron concentration
  - Hot full power (HFP)
  - Hot zero power (HZP) beginning of cycle (BOC)
  - HZP for restarts following reactor trips or mid-cycle outages
- Startup Physics Tests (HZP, BOC)
  - Integral control rod worth (via boron dilution and rod swap methods)
  - Differential control rod worth (boron dilution method)
  - Isothermal temperature coefficient (ITC)
  - Differential boron worth (DBW)
- Estimated Critical Position (ECP)
  - Return to HZP critical conditions following an outage
  - Verification of reactivity effect of control rods, power defect, soluble boron, xenon and other isotopic changes
- Flux maps
  - Instrument thimble reaction rates
- Operational transients
  - Similar to load follow maneuvers
  - Verification of reactivity effects (critical boron vs. time)
  - Verification of correct axial power distribution effects (axial offset or delta-I versus time)
  - Verification of undamped xenon oscillation axial power distribution behavior (correct balance between Doppler feedback and axial xenon oscillations)

The Surry Units 1 and 2 are identical Westinghouse designed three coolant loop pressurized water reactors with thermal ratings of 2546 MWt (Initially rated 2441 MWt). Initial criticality was achieved for Surry Unit 1 on July 1, 1972 and for Surry Unit 2 on March 7, 1973. Cycle operating summaries for the Surry units are listed in Table 1.

The North Anna Units 1 and 2 are identical Westinghouse designed three coolant loop pressurized water reactors with thermal ratings of 2893 MWt (initially rated 2775 MWt). Initial criticality was achieved for North Anna Unit 1 on April 5, 1978 and for North Anna

Unit 2 on June 6, 1980. Cycle operating summaries for the North Anna units are listed in Table 2.

**Table 1**  
**Surry Nuclear Power Station Operating History**

<b>Cycle</b>	<b>On Line Date</b>	<b>Off Line Date</b>	<b>Length (Months)</b>	<b>Rating (MWt)</b>	<b>Loading (MTM)</b>	<b>EFPD</b>	<b>MWD/MTU</b>	<b>Load Factor</b>
S1C1	09/12/72	10/24/74	25.4	2441	70.45	391	13548	51
S1C2	02/03/75	09/26/75	7.7	2441	71.27	202	6919	86
S1C3	12/08/75	10/17/76	10.3	2441	70.83	260	8960	83
S1C4	01/24/77	04/22/78	14.9	2441	71.65	385	13116	85
S1C5	07/09/78	09/14/80	26.2	2441	71.7	423	14401	53
S1C6	07/06/81	02/07/83	19.1	2441	71.75	485	16500	83
S1C7	05/30/83	09/26/84	15.9	2441	71.81	353	11999	73
S1C8	12/26/84	05/10/86	16.4	2441	71.91	414	14053	83
S1C9	07/12/86	04/09/88	20.9	2441	72.18	475	16064	75
S1C10	07/14/88	09/14/88	2	2441	72.33	53	1789	85
S1C10A	07/05/89	10/06/90	15	2441	72.33	417	14073	91
S1C11	12/17/90	02/29/92	14.4	2441	72.41	414	13956	94
S1C12	05/01/92	01/22/94	20.7	2441	72.47	582	19603	92
S1C13	03/24/94	09/08/95	17.5	2441	72.38	483	16289	91
S1C14	10/19/95	03/07/97	16.6	2546	72.31	485	17077	96
S1C15	04/28/97	10/19/98	17.7	2546	72.38	495	17412	92
S1C16	11/19/98	04/16/00	16.9	2546	72.43	499	17540	97
S1C17	05/08/00	10/14/01	17.2	2546	72.45	512	17992	98
S2C1	03/19/73	04/26/75	25.2	2441	70.46	429	14862	56
S2C2	06/19/75	04/22/76	10.1	2441	71.03	263	9038	85
S2C3	06/10/76	09/10/77	15	2441	71.21	275	9427	60
S2C4	10/12/77	02/04/79	15.8	2441	71.86	403	13689	84
S2C5	08/19/80	11/07/81	14.6	2441	71.88	411	13957	92
S2C6	12/31/81	06/30/83	17.9	2441	71.87	471	15997	86
S2C7	09/25/83	03/20/85	17.8	2441	71.89	437	14838	81
S2C8	06/27/85	10/04/86	15.2	2441	71.95	394	13367	85
S2C9	11/30/86	09/10/88	21.4	2441	72.12	464	15705	71
S2C10	09/16/89	03/30/91	18.4	2441	72.21	442	14941	79
S2C11	06/05/91	03/06/93	21	2441	72.28	551	18608	86
S2C12	05/04/93	02/03/95	21	2441	72.38	550	18549	86
S2C13	03/19/95	05/03/96	13.5	2546	72.37	377	13055	92
S2C14	06/05/96	10/06/97	16	2546	72.42	464	16312	95
S2C15	10/30/97	04/18/99	17.6	2546	72.43	518	18208	97
S2C16	05/25/99	10/01/00	16.3	2546	72.41	474	16666	96
S2C17	10/30/00	Operating	Operating	2546	72.48	Operating	Operating	Operating

Note: Data from Reference 14. MWD/MTU and loading is approximate.

**Table 2**  
**North Anna Nuclear Power Station Operating History**

<b>Cycle</b>	<b>On Line Date</b>	<b>Off Line Date</b>	<b>Length (Months)</b>	<b>Rating (MWt)</b>	<b>Loading (MTM)</b>	<b>EFPD</b>	<b>MWD/MTU</b>	<b>Load Factor</b>
N1C1	04/23/78	09/25/79	17.1	2775	72.15	413	15885	79
N1C2	01/24/80	12/28/80	11.1	2775	72.18	279	10726	82
N1C3	04/10/81	05/17/82	13.2	2775	72.27	347	13324	86
N1C4	11/18/82	05/12/84	17.8	2775	72.12	350	13467	65
N1C5	09/25/84	11/04/85	13.3	2775	72.29	349	13397	86
N1C6	12/23/85	04/19/87	15.8	2893	72.41	401	15694	83
N1C7	06/29/87	02/25/89	19.9	2893	72.62	423	16851	70
N1C8	07/15/89	01/12/91	17.9	2893	72.74	485	19289	89
N1C9	03/07/91	01/04/93	22.0	2893	72.78	503	19994	75
N1C10	04/09/93	09/09/94	17.0	2893	72.74	494	19647	95
N1C11	10/08/94	02/11/96	16.1	2893	72.81	474	18834	97
N1C12	03/10/96	05/11/97	14.0	2893	72.78	419	16655	98
N1C13	06/10/97	09/13/98	15.1	2893	72.78	452	17967	98
N1C14	10/07/98	03/12/00	17.1	2893	72.87	509	20208	98
N1C15	04/07/00	09/09/01	17.1	2893	72.91	498	19760	96
N2C1	08/23/80	03/07/82	18.4	2775	72.06	376	14480	67
N2C2	06/02/82	04/02/83	10.0	2775	72.2	220	8456	72
N2C3	05/29/83	08/02/84	14.2	2775	72.26	383	14708	89
N2C4	11/02/84	02/20/86	15.6	2775	72.5	416	15923	88
N2C5	04/01/86	08/24/87	16.8	2893	72.61	443	17455	87
N2C6	11/03/87	02/20/89	15.6	2893	72.74	449	17858	95
N2C7	05/07/89	08/21/90	15.5	2893	72.83	454	18034	96
N2C8	11/01/90	02/26/92	15.8	2893	72.75	459	18253	95
N2C9	04/22/92	09/07/93	16.5	2893	72.74	469	18653	93
N2C10	10/26/93	03/25/95	16.9	2893	72.8	485	19273	94
N2C11	05/31/95	09/08/96	15.3	2893	72.74	458	18215	98
N2C12	10/12/96	04/05/98	17.7	2893	72.73	487	19372	90
N2C13	05/03/98	09/12/99	16.3	2893	72.79	491	19515	99
N2C14	10/09/99	03/11/01	17.0	2893	72.81	499	19827	96
N2C15	04/09/01	Operating	Operating	2893	72.89	Operating	Operating	Operating

Note: Data from Reference 14. MWD/MTU and loading is approximate.

## SECTION 2 – CODE AND MODEL DESCRIPTION

### 2.1 CASMO-4

CASMO-4 (CASMO) is a multigroup two-dimensional transport theory code for burnup calculations on BWR and PWR assemblies or simple pin cells. The code handles a geometry consisting of cylindrical fuel rods of varying composition in a square pitch array. Fuel rods may be loaded with integral poisons such as gadolinium or boron. The fuel assembly model may contain burnable absorber rods, cluster control rods, in-core instrument channels, water gaps, boron steel curtains, and cruciform control rods in the regions separating fuel assemblies. Typical fuel storage rack geometries can also be handled. Some characteristics of CASMO are listed below:

- Nuclear data are collected in a library containing microscopic cross sections in 70 energy groups. Neutron energies cover the range 0 to 10 MeV.
- CASMO can accommodate non-symmetric fuel bundles containing up to 25 by 25 rods. Full, half, quadrant or octant symmetry (mirror symmetry) can be utilized in the calculations.
- Absorber rods or water holes covering 1x1, 2x2 pin cell positions or larger areas are allowed in the assembly.
- Effective resonance cross sections are calculated individually for each fuel pin.
- A fundamental mode calculation is performed to account for leakage effects.
- The microscopic depletion is calculated in each fuel and burnable absorber pin. Isotopic depletion as a function of irradiation is calculated for each fuel pin and for each region containing a burnable absorber.
- Discontinuity factors are calculated at the boundary between bundles and for reflector regions.

In order to generate a neutronic data library for SIMULATE-3 a series of CASMO depletions and branch cases is required. This series of calculations is defined within CMS as the "SIMULATE-3 Case Matrix." This case matrix consists of a series of depletions and instantaneous branch cases vs. exposure as a function of varied boron concentration,

moderator temperature, fuel temperature, and shutdown cooling time, as well as cases with control rods and without removable burnable poison in guide tube locations.

## **2.2 CMS-LINK**

CMS-LINK (Ref. 33) is a linking code that processes CASMO card image files into a binary formatted nuclear data library for use by SIMULATE-3. The code collects the following data from CASMO card image files:

- Two-group macroscopic cross sections
- Two-group discontinuity factors
- Fission product data
- Detector data
- Pin power reconstruction data
- Kinetics data
- Isotopics data
- Spontaneous fission data

CMS-LINK is capable of processing data for the following segment types:

- Standard hot and cold PWR segments (fuel regions) with and without burnable poison
- Pulled and reinserted burnable poison for PWR segments
- Standard cold and hot PWR reflector segments

Functional dependencies for key core condition variables are predefined in the code. A diverse set of CASMO cases provide data covering a range of reactor conditions between hot or cold shutdown and full power operation. Branch cases include changes in soluble boron, moderator temperature, fuel temperature, insertion and removal of burnable poison rods, insertion of control rods, and isotopic decay after shutdown. The cumulative effect of long term changes in individual variables such as soluble boron, moderator temperature or fuel temperature are treated as “history” effects by CMS-LINK and subsequently in SIMULATE.

### **2.3 SIMULATE-3**

SIMULATE-3 (SIMULATE) is an advanced two-group nodal code for the analysis of both PWRs and BWRs. The code is based on the QPANDA neutronics model (Ref. 6) which employs fourth-order polynomial representations of the intranodal flux distributions in both the fast and thermal groups. Key features of SIMULATE are:

- Pin power reconstruction
- No normalization required against higher order calculations
- Explicit representation of the reflector region
- Coupled neutronics/thermal-hydraulics
- Internal calculation of the effect of spacer grids on axial power distributions
- Calculation of intra-nodal axial power distribution effect on FQ

SIMULATE cross-section input is provided from CASMO with linkage through CMS-LINK.



## **2.4 AUXILIARY CODES**

### **2.4.1 Monte Carlo Codes – Cross Section Library Benchmarking**

Monte Carlo method codes such as KENO-V.a (Ref. 15) and MCNP-4C (Ref. 16) are used to benchmark CASMO and SIMULATE calculations. Monte Carlo fuel assembly models are used to identify any biases in the CASMO model key parameters (such as control rod worth, burnable poison worth, fuel temperature (Doppler) defect, and soluble boron worth). [

]

Monte Carlo models are also used to verify the accuracy of peak-to-average pin power calculations in CASMO and SIMULATE. In conjunction with comparisons of measured and predicted flux thimble reaction rates, the Monte Carlo models support the derivation of overall uncertainty and reliability factors for peaking factor predictions using the CMS system.

### **2.4.2 ESCORE - Fuel Temperature Data**

In SIMULATE, the average temperature of the fuel pellets in a node is calculated by:

$$TFU = TMO + A (x ,y ) \times P + B \times P^2$$

where  $TMO$  is the moderator temperature,  $P$  is the nodal power density relative to core-averaged power density at 100% of rated power,  $A$  is the linear coefficient of the fuel temperature with respect to nodal power density (this can be a table that is a function of up to two state variables,  $x$  and  $y$ ), and  $B$  is a quadratic coefficient of fuel temperature with respect to nodal power density. For the North Anna and Surry models, fuel temperature data based on the EPRI ESCORE code (Ref. 17) are represented via  $A(x,y)$  in the above equation. The coefficient  $A$  is a function of local burnup and power level. Model benchmarking which supports the use of ESCORE fuel data coupled with CASMO cross sections [ ] includes:

- 1) Comparison of HZP and HFP critical boron (measured versus predicted).  
Doppler feedback is a major contributor to the power defect near BOC.  
Consistency between the HZP and HFP boron agreement supports a conclusion of accurate power defect predictions.
- 2) Comparison of measured and predicted axial offset during undamped xenon oscillations following operational transients and return to full power. Axial xenon variations tend to cause unstable axial offset oscillations. Doppler feedback is the primary damping force. Comparison of the measured and predicted axial offset behavior demonstrates whether the model has the proper xenon / Doppler balance.
- 3) Comparison of measured and predicted critical conditions for mid-cycle reactor restarts (also known as Estimated Critical Position or ECP calculations). ECP calculations are a reactivity balance (typically between HFP and HZP) which incorporate changes in control bank position, soluble boron, xenon, power defect, and other less significant changing isotopic concentrations to predict conditions for the return to criticality following a reactor trip or shutdown. The power defect is a significant component in all ECPs, and the Doppler feedback is a large portion of the power defect.

### **2.4.3 CECOR - Flux Map Reaction Rate Data**

CECOR (Ref. 10, 18) is used for movable in-core detector flux map analysis. The primary use in the benchmarking of the North Anna and Surry SIMULATE models is to provide instrument thimble detector reaction rate data for comparison to predicted reaction rates. A Dominion post-processor code reads SIMULATE and CECOR reaction rates and provides normalized comparisons. Reaction rate comparisons are a key component used to determine peaking factor uncertainty factors.

## SECTION 3 – MODEL BENCHMARKING

### 3.1 CASMO BENCHMARKING

CASMO-4 has been extensively benchmarked against critical experiments and Monte Carlo calculations. These benchmarks encompass criticality, pin power predictions, fuel isotopic concentrations, new LEU fuel, burned LEU fuel, and MOX fuel. A sampling of relevant papers are listed in References 19 through 22. As part of the development of the North Anna and Surry models, Dominion has performed a comparison of CASMO and Monte Carlo code calculations of reactivity worth for soluble boron, burnable poison rods (BP), AIC (silver-indium-cadmium) control rods, Hafnium flux suppression rods, temperature defect, and Doppler defect. [

]

Table 3 and Figures 1 and 2 show the results of the CASMO reactivity benchmarking. Statistical uncertainty associated with each Monte Carlo calculation was limited to a range of 0.0001 to 0.00037  $\Delta K$  (one standard deviation). For all but the Doppler defects, the data represents a range of fuel enrichments from 2.6 to 5.0 w/o U-235, soluble boron concentration from 0 to 2000 ppm, and temperature from 100 to 547 °F. Doppler comparisons are for enrichments of 3.0 and 4.0 w/o U-235 (burned and new fuel) over a fuel temperature range of 300 to 900 K. [

]

**Table 3****CASMO-4 Reactivity Benchmarking Versus MCNP-4B and KENO-V.a**

<b>Component</b>	<b>Fuel Type</b>	<b>Mean (% difference)</b>	<b>Std. Deviation (% difference)</b>	<b>Number of Observations</b>
<b>AIC Control Rods</b>	North Anna (17x17)	[ ]	[ ]	12
	Surry (15x15)	[ ]	[ ]	12
<b>Hf Rods</b>	Surry (15x15)	[ ]	[ ]	12
<b>Soluble Boron</b>	North Anna (17x17)	[ ]	[ ]	36
	Surry (15x15)	[ ]	[ ]	24
<b>8 BP Rods @ 0.95 w/o B4C</b>	North Anna (17x17)	[ ]	[ ]	12
<b>20 BP Rods @ 0.95 w/o B4C</b>	North Anna (17x17)	[ ]	[ ]	12
<b>8 BP Rods @ 3.0 w/o B4C</b>	North Anna (17x17)	[ ]	[ ]	12
	Surry (15x15)	[ ]	[ ]	12
<b>20 BP Rods @ 3.0 w/o B4C</b>	North Anna (17x17)	[ ]	[ ]	12
	Surry (15x15)	[ ]	[ ]	12
<b>Doppler Defect</b>	North Anna (17x17)	[ ]	[ ]	3
	Surry (15x15)	[ ]	[ ]	3

Note: % Difference is  $100 \times (\text{CASMO WORTH} - \text{MONTE CARLO WORTH}) / (\text{MONTE CARLO WORTH})$

**Figure 1**



**Figure 2**



### **3.2 SIMULATE BENCHMARKING TO HIGHER ORDER CALCULATIONS**

Comparison of CASMO/SIMULATE and Monte Carlo code calculations of pin-to-box ratios and flux thimble instrument reaction rate ratios are used in combination with normalized flux map reaction rate comparisons to determine appropriate peaking factor ( $F_{\Delta H}$  and  $F_Q$ ) uncertainty factors. Comparison of pin-to-box ratios and flux thimble reaction rate ratios ( $W$ -primes) exercises the entire CMS system (CASMO, CMS-LINK, and SIMULATE). Pin-to-box ratios are defined here to be the ratio of pin power to assembly average power.  $W$ -prime is defined as the normalized ratio of assembly power to flux thimble instrument reaction rate.

When assessing the ability of core design codes to predict pin powers, predicted pin powers would ideally be compared directly to measured values. Unfortunately, in most power reactors there is no method available to directly measure individual pin powers. Power reactor measured pin powers are reconstructed using measured instrument thimble reaction rates, predicted  $W$ -prime values, and predicted pin-to-box ratios. The key components associated with measured and predicted peaking factors are described as follows:

Predicted peak pin power = Predicted assembly power x predicted pin-to-box ratio

Measured peak pin power = Measured thimble reaction rate x predicted  $W$ -prime  
x predicted pin-to-box ratio

Uncertainty associated with predicted peak pin power is therefore different than the uncertainty associated with measured peak pin power. The uncertainty factor for predicted peaking factors will be derived by combining the uncertainty factor from measured and predicted thimble reaction rate comparisons with the pin-to-box uncertainty factor derived from comparisons of SIMULATE and MCNP.

Thimble reaction rate comparisons will be used to determine a conservative approximation of the predicted assembly power uncertainty. It is conservative because it

inherently includes not only predicted power uncertainty, but measurement uncertainty and uncertainty associated with reconstructing the predicted thimble reaction rate (W-prime uncertainty). Appropriate uncertainty for measured peaking factors is composed of a combination of the W-prime uncertainty (from comparisons of SIMULATE and MCNP), the pin-to-box uncertainty, and any other desired factors (such as the effect of manufacturing tolerances on FQ).

In order to estimate the W-prime and pin-to-box uncertainty for the Surry and North Anna models, two-by-two assembly models have been constructed using both SIMULATE and MCNP. These models are comprised of identical fresh fuel assemblies with two diagonally opposite assemblies containing control rods. Periodic boundary conditions were used. The fuel assembly designs and operating conditions include North Anna and Surry fuel assembly designs, a range of fuel enrichments, and a range of soluble boron concentrations. The SIMULATE model setup, to the extent possible, paralleled that of the North Anna and Surry CMS core models to ensure that the results of these calculations are applicable to the production models.

The set of cases modeled (six 2x2 cases for 15x15 fuel and six 2x2 cases for 17x17 fuel) is not exhaustive in scope. However, extreme inter-assembly and intra-assembly flux and power gradients are caused by the presence of the control rods. Strong gradients increase pin-to-box factors and result in challenging and conservative conditions for both W-prime and pin-to-box uncertainty determinations.

Additional conservatism results from different treatment of the gamma contribution to the pin power distribution in SIMULATE and MCNP. CASMO/SIMULATE uses a gamma smoothing technique to account for redistribution of fission energy released as gamma radiation. This method redistributes approximately 7% of the assembly power, effectively flattening the intra-assembly pin power distribution. Various references (Ref. 27, 28) support long range (~ 100 cm) gamma energy contributions from prompt fission gammas, capture gammas, and fission product decay gammas of 7% - 12% of total recoverable energy. Gamma smoothing was not incorporated into the MCNP model. MCNP will therefore conservatively model the variation in intra-assembly pin powers, resulting in a



conservatively larger pin-to-box uncertainty for CMS as determined by comparison to MCNP. Statistics will also be provided for SIMULATE predictions without gamma smoothing, which effectively provides a comparison of fission rates.

Results of the SIMULATE / MCNP 2x2 model comparisons are presented in Table 4. All W-prime data was determined to be normal and all pin-to-box ratio data was determined to be non-normal using the Shapiro-Wilk W-test. Because the W-prime data is normal and simple tests of the mean and variance (simplified versions of the T-test and F-test, Ref. 25) indicated that there is no reason to believe that the Surry and North Anna samples are from different populations, the data were pooled. Due to the non-normality of the pin-to-box data, no pooling was performed. One-sided tolerance intervals (95% probability, 95% confidence) were calculated based on the sample size, mean and standard deviation (Ref. 25) for W-prime and based on the sample size (Ref. 26) for pin-to-box. Additional discussion on statistical tests and tolerance intervals is provided in Section 4.2.

The pin-to-box cases of primary significance in Table 4 are the statistics for the unrodded assemblies, because in none of the cases does the rodded assembly have an RPD (relative power density) above unity. In fact despite the larger pin-to-box ratios in the rodded assemblies, typically only one or two pins in the rodded assembly exceeded an RPD of one, whereas typically all of the pins in the unrodded assembly exceeded an RPD of one. The pin-to-box errors of the rodded assemblies would not play a role in determining the maximum core-wide peaking factors. The range of standard deviations in Table 4 for pin-to-box ratio [ ] is consistent with pin power RMS (root mean square) differences for CASMO-4 comparisons to three sets of critical experiment measurements (Ref. 20). The reported RMS differences range from [ ] and represent typical pin fission rate measured-versus-predicted differences for the small cores. Note that RMS and standard deviation are directly comparable if the population mean associated with the RMS value is zero.

MCNP statistical uncertainty for W-prime is approximately 0.8% (one standard deviation). The MCNP uncertainty contribution to the tolerance limit is relatively small for the pin-to-

box ratio, but is significant for the W-prime, resulting in a very conservative estimate of [ ] for the W-prime tolerance interval. Excluding the MCNP uncertainty reduces the W-prime uncertainty to [ ].

MCNP statistical uncertainty for pin-to-box ratios is approximately 0.4% (one standard deviation), therefore its contribution to the pin-to-box ratio tolerance interval is modest. Because the magnitude of the SIMULATE gamma smearing (7%) appears to be reasonable compared to values previously referenced, the statistics from Table 4 without the influence of gamma smearing are taken to be the most appropriate for determining the pin-to-box tolerance interval. The tolerance interval for assemblies with pin powers above unity is [ ] for both fuel types. The cases modeled here represent extreme inter-assembly flux gradients due to the rodded assemblies. However, it is possible that less significant insert components (such as discrete burnable poison rods) which have not been modeled here could result in assemblies with above average power and pin-to-box uncertainty larger than for the unrodded assemblies. In consideration of this possibility, the tolerance interval is chosen to be [ ]. The RSS (root sum square) combination of W-prime and pin-to-box uncertainty for use in determining measured peaking factors is [ ] using the conservative W-prime tolerance and [ ] using the W-prime tolerance with the MCNP uncertainty removed.

**Table 4**

**CASMO-4 W-prime and Pin-to-box Ratio Comparisons**

<b>Fuel Type / Parameter</b>	<b>Assembly</b>	<b>Mean (%)</b>	<b>Std. Dev. (%)</b>	<b>Normal</b>	<b>Tolerance Limit</b>
<b>Surry 15x15 W-prime</b>	Rodded	[ ]	[ ]	Yes	[ ]
	Unrodded	[ ]	[ ]	Yes	[ ]
	Combined	[ ]	[ ]	Yes	[ ]
<b>North Anna 17x17 W-prime</b>	Rodded	[ ]	[ ]	Yes	[ ]
	Unrodded	[ ]	[ ]	Yes	[ ]
	Combined	[ ]	[ ]	Yes	[ ]
<b>Combined data W-prime</b>	Combined	[ ]	[ ]	Yes	[ *]
<b>Pin-to-box Ratio Statistics (Including Gamma Smearing)</b>					
<b>Surry 15x15 Pin-to-box ratio</b>	Rodded	[ ]	[ ]	No	[ ]
	Unrodded	[ ]	[ ]	No	[ ]
	Combined	[ ]	[ ]	No	[ ]
<b>North Anna 17x17 Pin-to-box ratio</b>	Rodded	[ ]	[ ]	No	[ ]
	Unrodded	[ ]	[ ]	No	[ ]
	Combined	[ ]	[ ]	No	[ ]
<b>Pin-to-box Ratio Statistics (Excluding Gamma Smearing)</b>					
<b>Surry 15x15 Pin-to-box ratio</b>	Rodded	[ ]	[ ]	No	[ ]
	Unrodded	[ ]	[ ]	No	[ ]
	Combined	[ ]	[ ]	No	[ ]
<b>North Anna 17x17 Pin-to-box ratio</b>	Rodded	[ ]	[ ]	No	[ ]
	Unrodded	[ ]	[ ]	No	[ ]
	Combined	[ ]	[ ]	No	[ ]

\* Eliminating the MCNP W-prime uncertainty component (conservatively set at [ ] ) by root sum square results in a W-prime tolerance interval of [ ].

### **3.3 SIMULATE BENCHMARKING TO MEASURED CYCLE DATA**

The following sections present the results of comparisons of SIMULATE-3 predictions with measurements from the North Anna and Surry power stations. Most calculations were performed using full core, 32 axial node, 2x2 X-Y mesh per assembly geometry. Depending on the type of calculation, this geometry can sometimes be relaxed to a lower level of detail without significantly changing the results.

All comparisons of SIMULATE predictions with measured data will by nature represent a combination of SIMULATE bias, SIMULATE uncertainty, measurement bias, and measurement uncertainty. These comparisons will be used to derive appropriate uncertainty factors for SIMULATE predictions. In cases where the comparison data lead to unrealistically high estimates for SIMULATE uncertainty, attempts to quantify and account for measurement bias and uncertainty will be made. Statistical methods are discussed in Section 4.2. Specific uncertainty factors based on the results given in this section are developed in Section 4.3. In the statistics presented, the sign convention used is such that a positive value indicates over-prediction of the magnitude of a parameter by SIMULATE, and a negative value indicates under-prediction by SIMULATE.

#### **3.3.1 Critical Boron Concentration**

Critical boron concentrations were obtained from three sources. Startup physics tests provided measured critical boron at HZP, ARO conditions. HFP critical boron concentrations were obtained from routine daily boron measurements. Measured HZP boron concentrations for plant restarts (ECPs) were also used for cases near BOC and EOC.

Sources of boron concentration uncertainty unrelated to SIMULATE include titration (used to measure the boron concentration) and  $B^{10}$  depletion.  $B^{10}$  depletion is a reduction in the natural  $B^{10}/B$  atom ratio caused by loss of  $B^{10}$  by neutron capture as boron in the coolant passes through the operating core. If there is little boron inventory turnover in the primary

system then the  $B^{10}/B$  ratio can decrease continuously. Because only the  $B^{10}$  in boron contributes to the boron worth and the boron concentration measured by titration includes both  $B^{10}$  and  $B^{11}$ , the measured and predicted boron concentrations may not reflect the same  $B^{10}/B$  ratio assumptions and should not be compared without consideration of the  $B^{10}$  depletion effect.

Only equilibrium HFP data near BOC (up to 700 MWD/MTU) and EOC (between 50 and 5 ppm critical boron concentration) was used for the comparisons due to the complication of accounting for  $B^{10}$  depletion. The  $B^{10}/B$  atom ratio is typically equal to the ratio for fresh boron (0.198 – 0.2) at BOC due to the addition of fresh boric acid during refueling. Near EOC,  $B^{10}$  depletion is not significant due to the low boron concentration. All SIMULATE calculations assume 0.198  $B^{10}/B$  ratio.

Soluble boron measurement uncertainty is approximately  $\pm 10$  ppm for titration. In addition, near BOC there is potential  $B^{10}/B$  variation of approximately  $\pm 1\%$  (equivalent to approximately  $\pm 10$  to  $\pm 20$  ppm) due to natural boron isotopic ratio variation. Near EOC, the  $B^{10}/B$  isotopic ratio variation is estimated to contribute about  $+5/-0$  ppm measurement uncertainty (0 to 10%  $B^{10}$  depletion). The BOC  $B^{10}$  isotopic content can range high depending on the source of fresh boron used and can range low due to a limited amount of  $B^{10}$  depletion that can occur for the near-BOC data (up to 700 MWD/MTU).  $B^{10}$  depletion can reduce the  $B^{10}/B$  ratio to 0.18 or less at EOC (approximately 10% reduction in boron worth). To minimize the effect of  $B^{10}$  depletion, EOC data is limited to measured boron concentrations of 50 ppm or less.

Figures 3 and 4 demonstrate the effect of  $B^{10}$  depletion on boron letdown curve agreement. Figure 3 is representative of a cycle with relatively little  $B^{10}$  depletion effect. The  $B^{10}/B$  ratio tends to be re-established to the natural boron ratio by relatively high primary system leakage (continuous) or outages (periodic). Figure 4 is representative of a cycle with significant  $B^{10}$  depletion effect (due to low primary system leakage and few outages). The effect of an outage (partial restoration of the  $B^{10}/B$  ratio by mixing with fresh boron) is visible in Figure 4 at about 15 GWD/MTU burnup.

Figures 5 and 6 present the difference between SIMULATE and measured boron concentrations in histogram format. Each histogram bin represents  $\pm 5$  ppm about the indicated bin midpoint value. Table 5 presents boron difference statistics. Data is based on SIMULATE core models for 29 North Anna cycles and 33 Surry cycles. Figure 7 presents a histogram of all Surry and North Anna data combined.

Figure 3

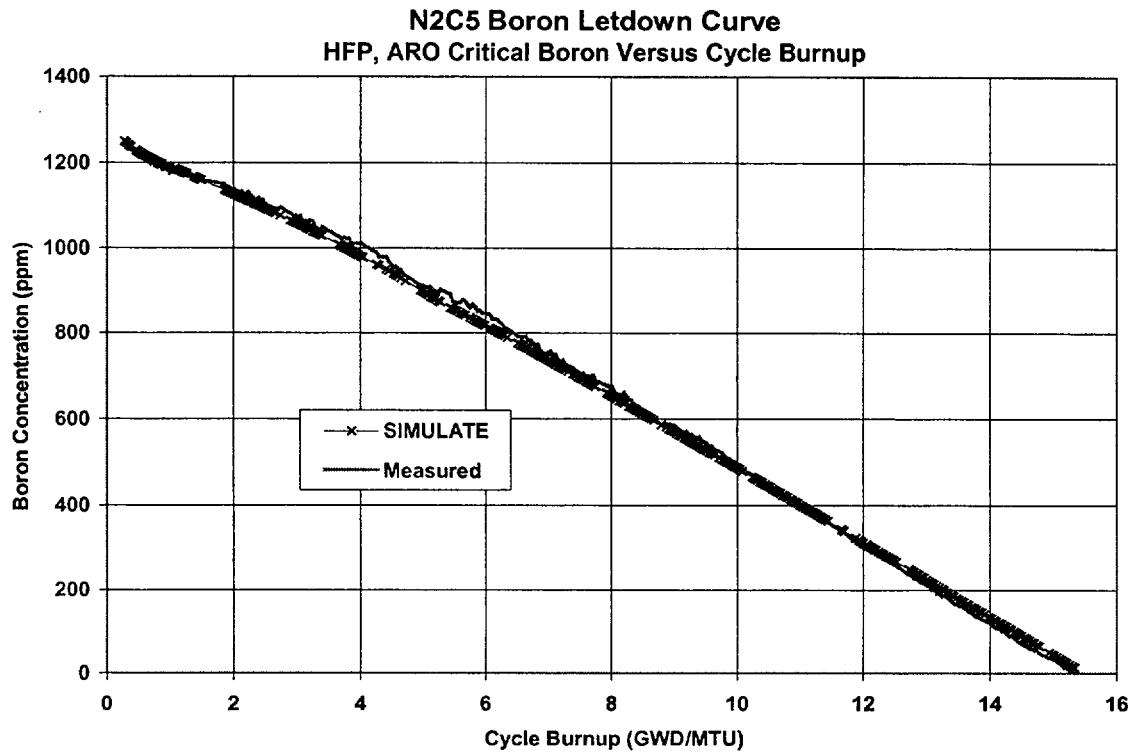
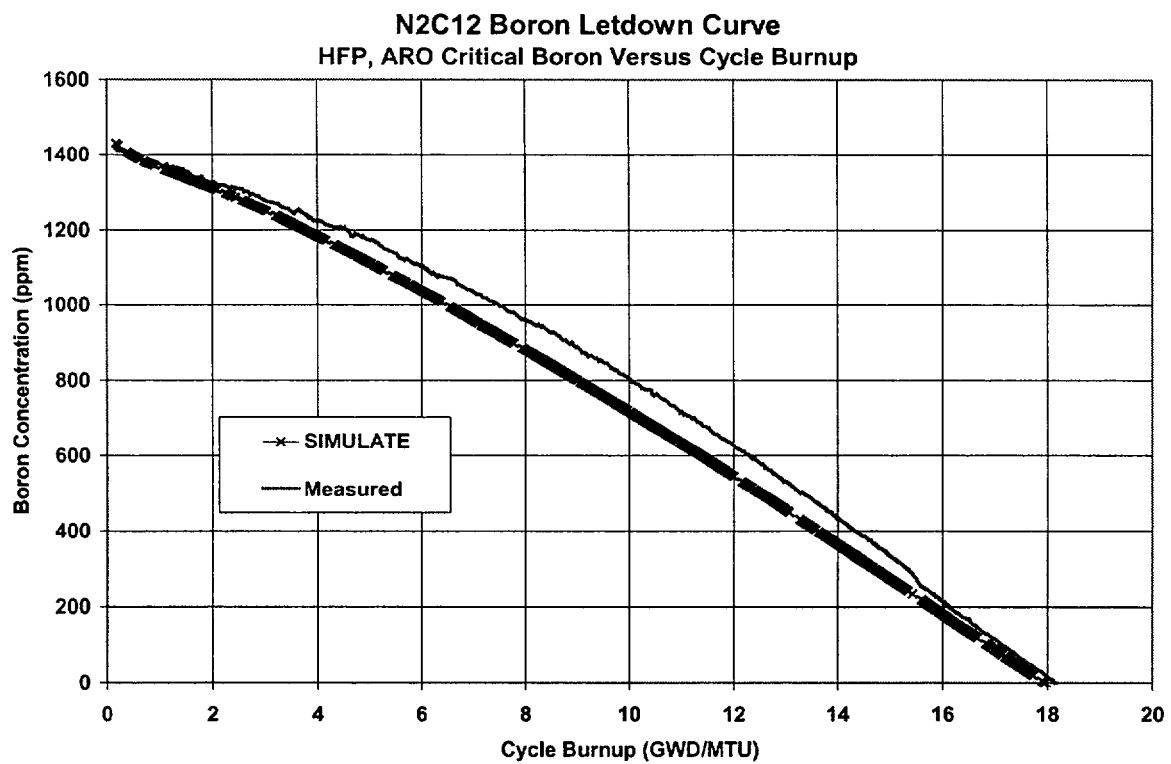
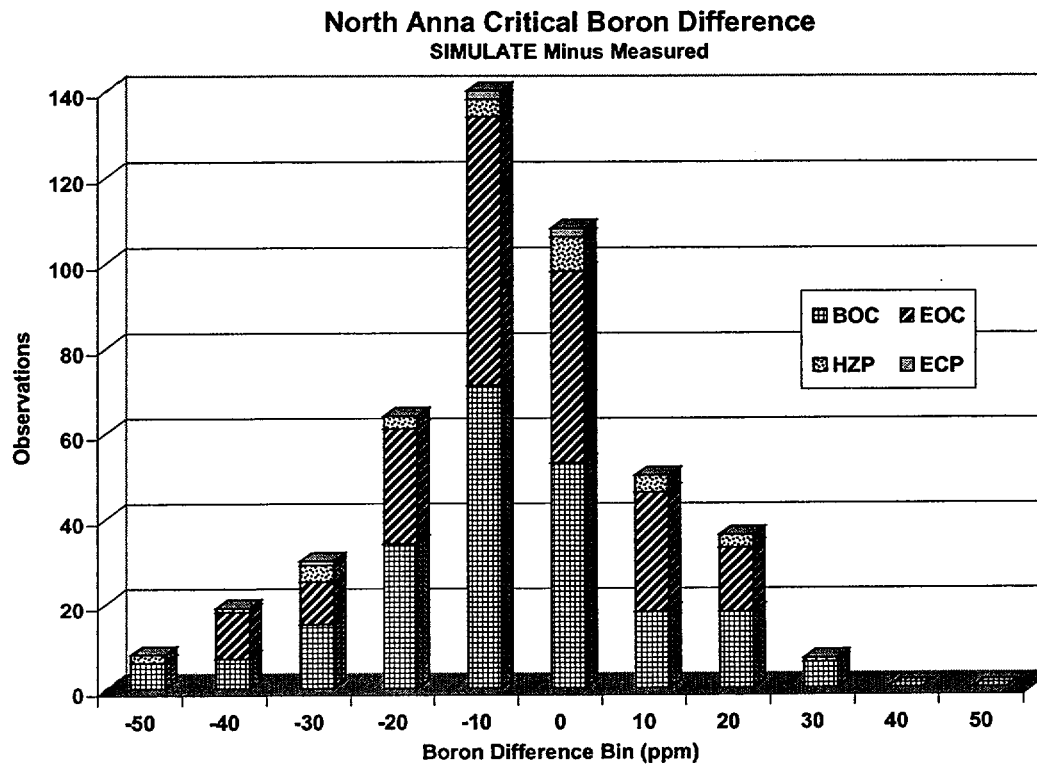


Figure 4



# Figure 5



# Figure 6

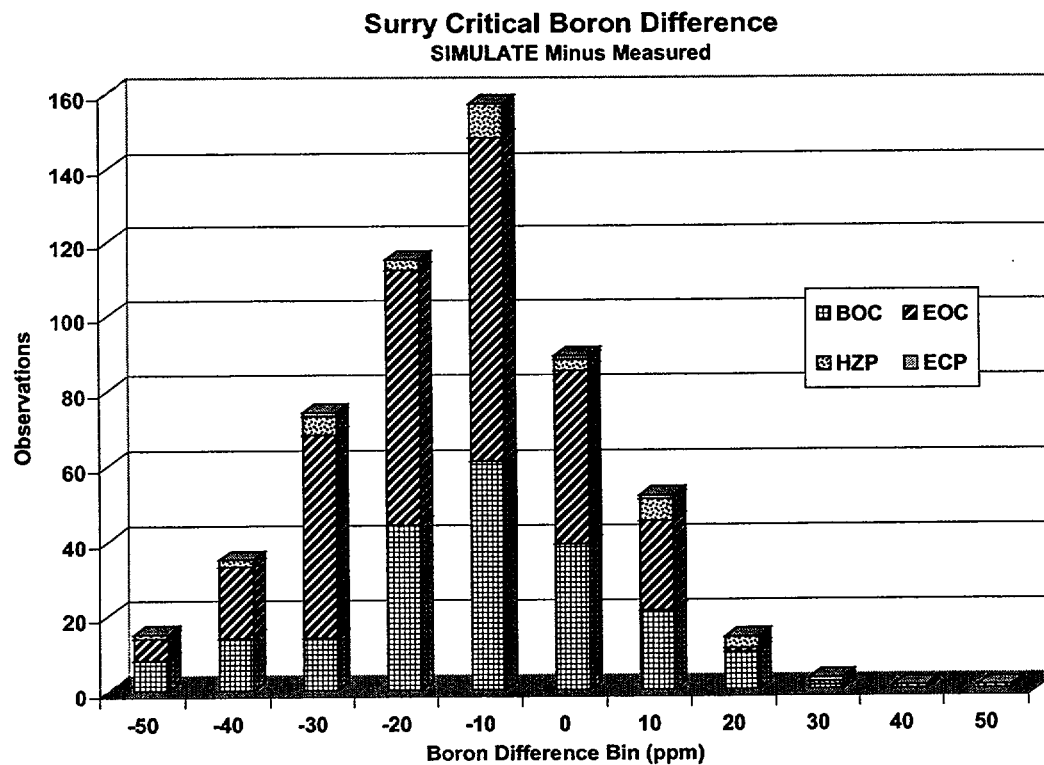




Table 5

## SIMULATE Critical Boron Comparisons

Plant	Condition	Mean (ppm)	Std. Dev. (ppm)	Number Of Obs.	Max.	Min.	Normal
North Anna	BOC HZP	-8.1	20.3	30	30	-53	Yes
	BOC HFP	-7.2	16.4	228	30	-51	Yes*
	EOC HFP	-5.9	14.6	199	24	-39	Yes^
	ECP	-10.1	13.2	5	4	-31	N/A
	ALL	-6.7	15.9	462	30	-53	Yes'
Surry	BOC HZP	-5.0	23.4	35	48	-49	Yes
	BOC HFP	-11.2	16.5	212	35	-54	Yes*
	EOC HFP	-14.8	14.6	305	16	-48	Yes*
	ECP	2.8	24.4	4	30	-31	N/A
	ALL	-12.7	16.3	556	48	-54	Yes
Combined	BOC HZP	-6.4	21.9	65	48	-53	Yes
	BOC HFP	-9.1	16.5	440	35	-54	Yes'
	EOC HFP	-11.2	15.2	521	24	-48	Yes*
	ECP	-4.3	18.9	9	30	-31	N/A
	ALL	-10.0	16.4	1018	48	-54	Yes^

Note: Critical boron difference is SIMULATE – Measured (ppm)

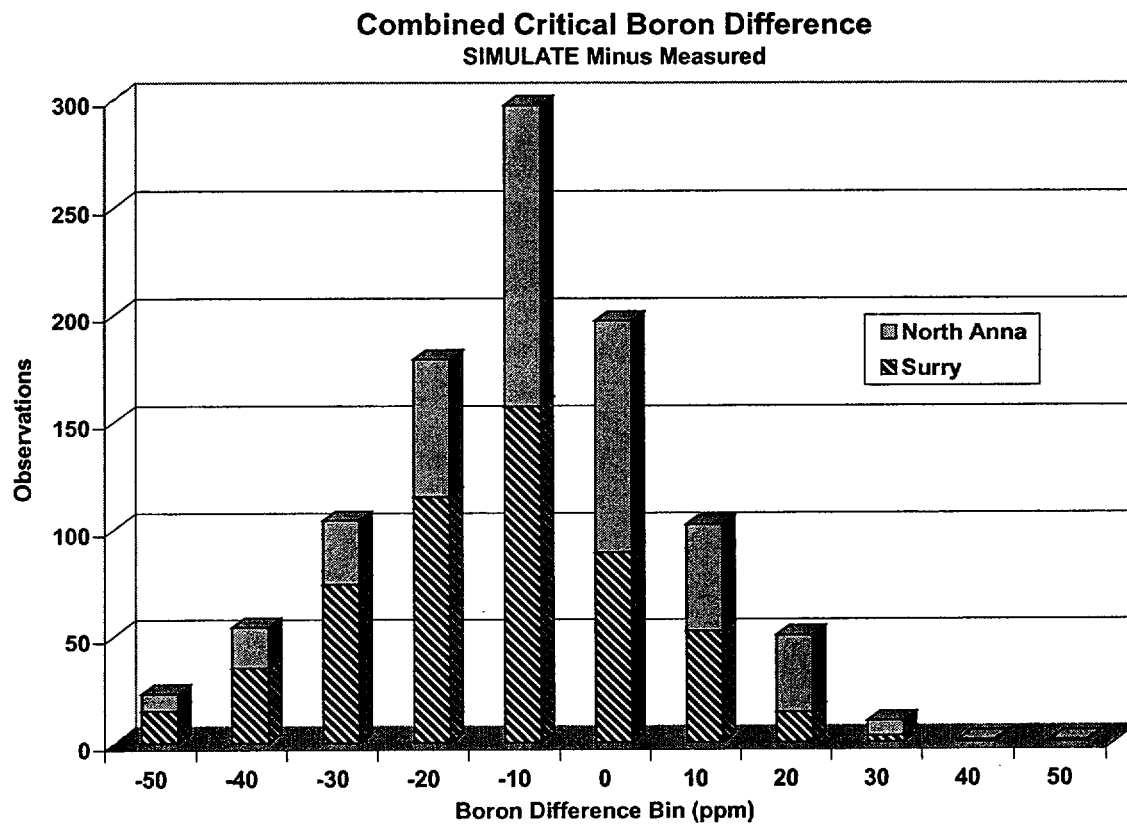
Yes - Passed all test (D', K-S, and Kuiper tests)

Yes\* - Failed the D' test but passed the K-S and Kuiper tests

Yes' - Failed the D' and K-S tests but passed the Kuiper test

Yes^ - Failed the K-S test but passed the D' and Kuiper tests

Figure 7



### 3.3.2 Control Rod Worth

The methods used for measuring control rod bank worth for Startup Physics Testing are described in Reference 13, and include the boron dilution method and the rod swap method. Measured rod swap bank worth accuracy is dependent on the accuracy of the reference (highest worth) bank worth measurement determined via the boron dilution method.

Sources of measurement uncertainty using the boron dilution method include boron measurement (titration) uncertainty, reactivity computer bias, and reactivity computer uncertainty. Reactivity computer bias and uncertainty is presumed to result primarily from the calculated delayed neutron data used in the kinetics equations. Delayed neutron data uncertainty is generally considered to be about  $\pm 5\%$  (Ref. 23 and Section 4.3.9) and has been estimated by indirect means to add significantly to the variance between predicted and measured rod worth (Section 3.3.4). Additional sources of measurement uncertainty include reactivity computer drift due to uncompensated background current and the manual measurement of each partial segment of the reference bank worth (roughly 20 segments per bank measurement which are also used to determine the differential rod worth).

Figures 8, 9, and 10 present the difference between SIMULATE and measured integral control rod worth for North Anna, Surry, and data for both units combined. Each histogram bin represents  $\pm 1\%$  about the indicated bin midpoint value. Table 6 presents the same data in statistical format.

For control rod banks measured using the boron dilution method, the differential rod worth (DRW) is also measured. Statistics for the difference (%) between the SIMULATE and measured peak differential rod worth for 65 measurements are shown in Table 7. There is a significant tendency for SIMULATE to over-predict the peak DRW. No distinction is made concerning the rod position at which the peak DRW occurs because the most important use of the DRW is for the rod withdrawal from subcritical accident. That accident is terminated after a few seconds and the

maximum DRW is usually conservatively assumed to occur for the entire withdrawal sequence. Previous assessments of DRW uncertainty (Ref. 12) developed an uncertainty factor based on the DRW difference in units of pcm/step. However, it is more appropriate and conservative to determine the uncertainty in terms of % difference, because it results in a much larger DRW conservatism for accident conditions at which the predicted DRW is much higher than any of the cases in the measured database.

A histogram for the Table 7 data is shown in Figure 11 with each bin representing the indicated midpoint  $\pm 0.25$  pcm/step. A sampling of four differential rod worth curve comparisons (DRW vs. rod position) is presented in Figures 12 through 15.

Figure 8

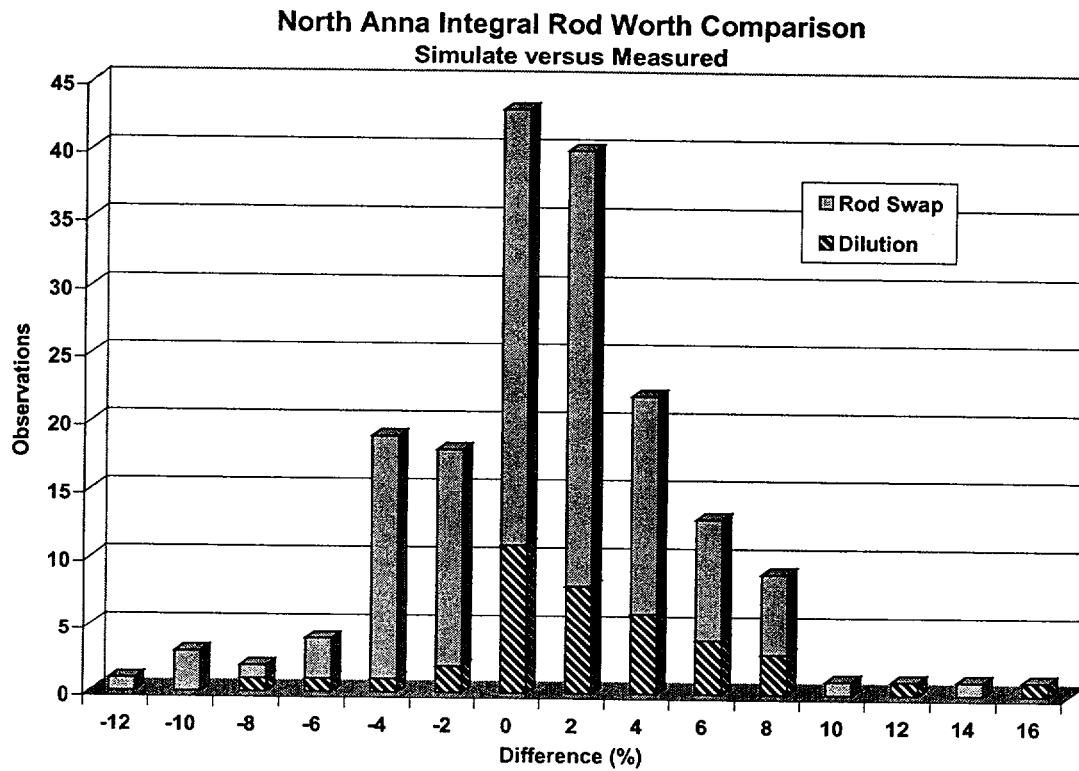


Figure 9

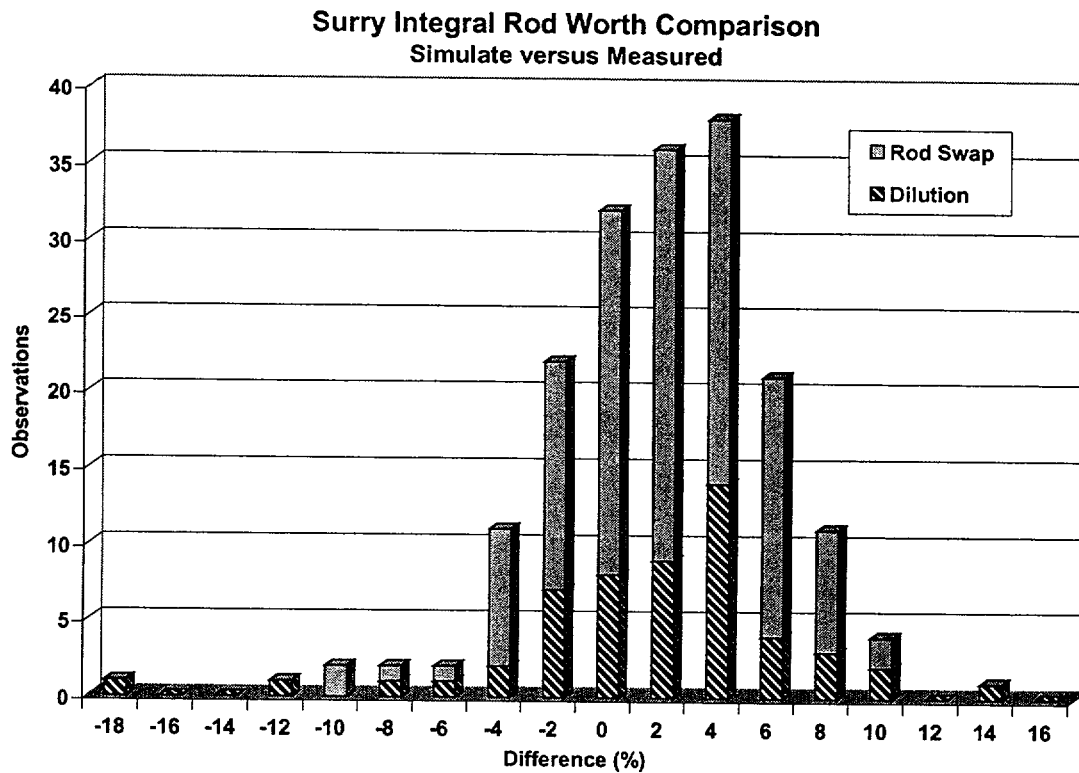
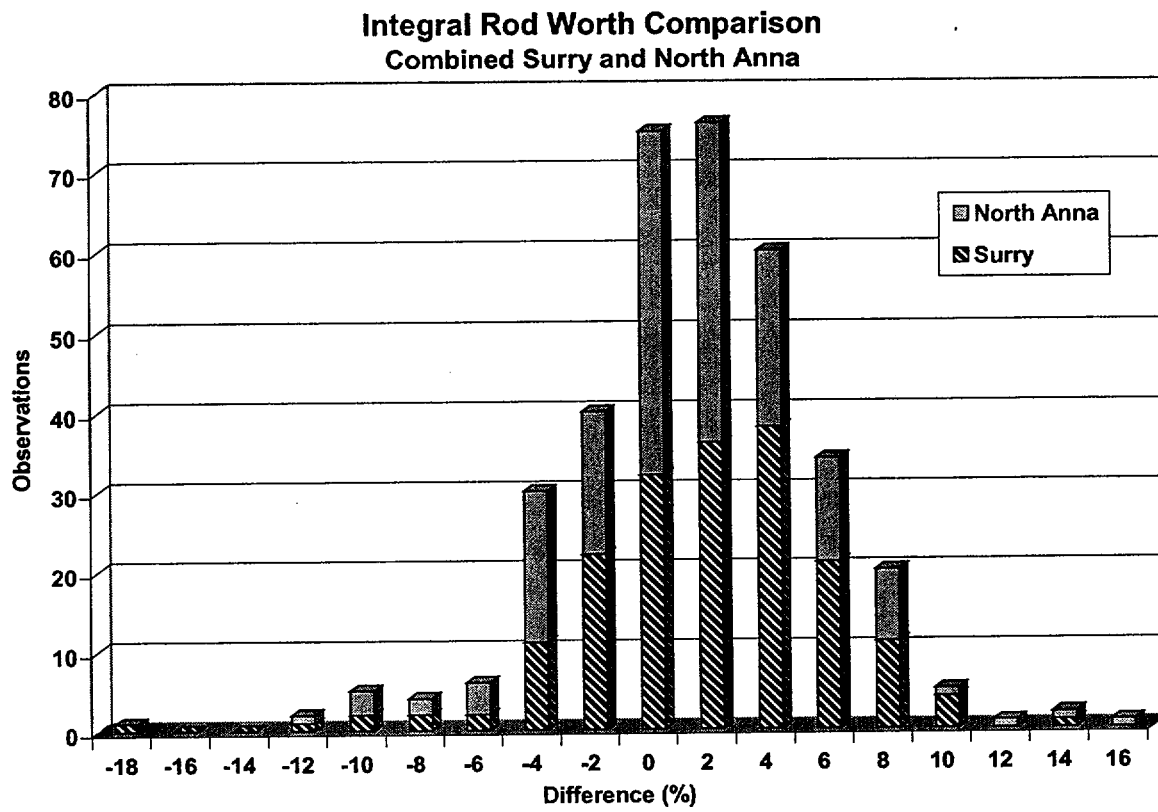


Figure 10



**Table 6**

**SIMULATE Integral Control Rod Worth Comparisons**

Plant	Type	Mean (%)	Std. Dev. (%)	Number Of Obs.	Max.	Min.	Normal
North Anna	Dilution	2.4	4.3	39	16.1	-7.3	Yes
	Rod Swap	0.6	4.1	139	13.4	-12.4	Yes*
	<b>ALL</b>	<b>0.9</b>	<b>4.2</b>	<b>178</b>	<b>16.1</b>	<b>-12.4</b>	<b>Yes*</b>
Surry	Dilution	1.7	5.2	54	13.6	-17.4	Yes*
	Rod Swap	1.8	3.7	130	10.4	-9.7	Yes
	<b>ALL</b>	<b>1.8</b>	<b>4.2</b>	<b>184</b>	<b>13.6</b>	<b>-17.4</b>	<b>Yes*</b>
Combined	Dilution	2.0	4.8	93	16.1	-17.4	Yes*
	Rod Swap	1.2	3.9	269	13.4	-12.4	Yes*
	<b>ALL</b>	<b>1.4</b>	<b>4.2</b>	<b>362</b>	<b>16.1</b>	<b>-17.4</b>	<b>Yes*</b>

**Note:** Rod worth difference is (SIMULATE – Measured) / SIMULATE)

Yes\* - Failed the D' test but passed the K-S test and the Kuiper test

**Table 7**

**SIMULATE Peak Differential Control Rod Worth Comparisons**

Plant	Mean (%)	Std. Dev. (pcm/step)	Number Of Obs.	Max.	Min.	Normal
North Anna	5.0	8.0	39	30.6	-12.2	Yes
Surry	6.0	8.3	54	20.1	-17.0	Yes
Combined	5.6	8.1	93	30.6	-17.0	Yes

Note: Differential rod worth difference is (SIMULATE – Measured)/SIMULATE (%)

# Figure 11

## Combined Peak Differential Rod Worth Comparison

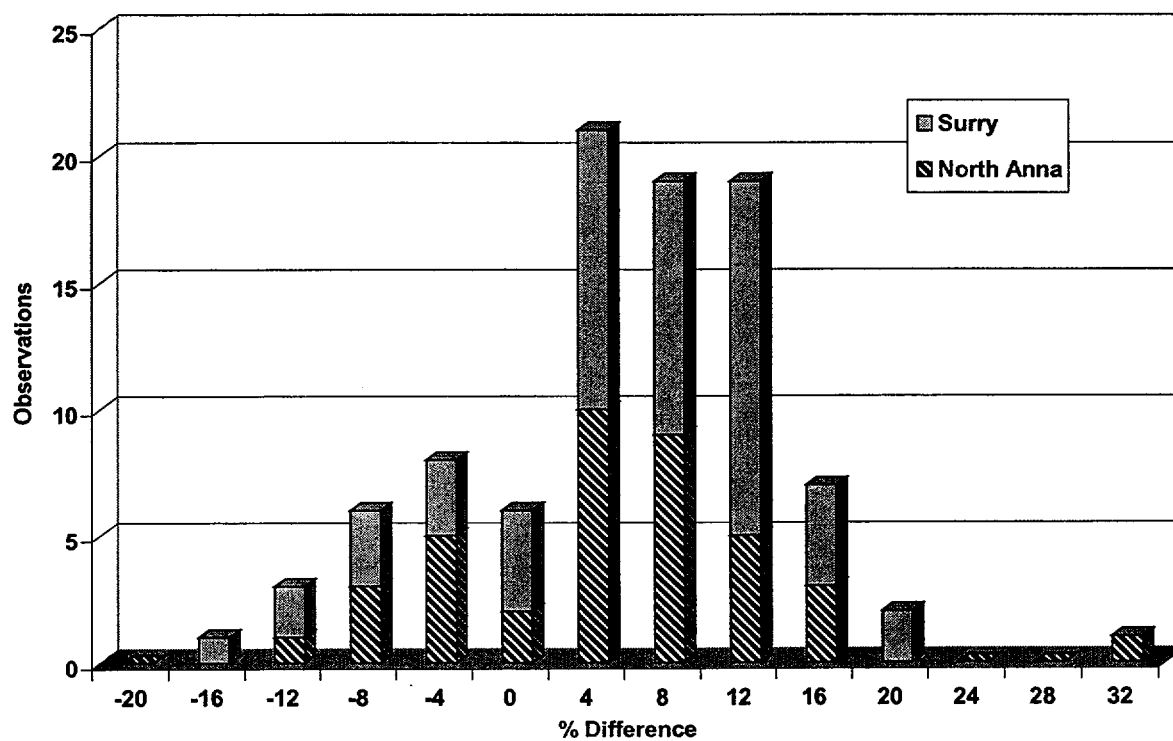




# Figure 12

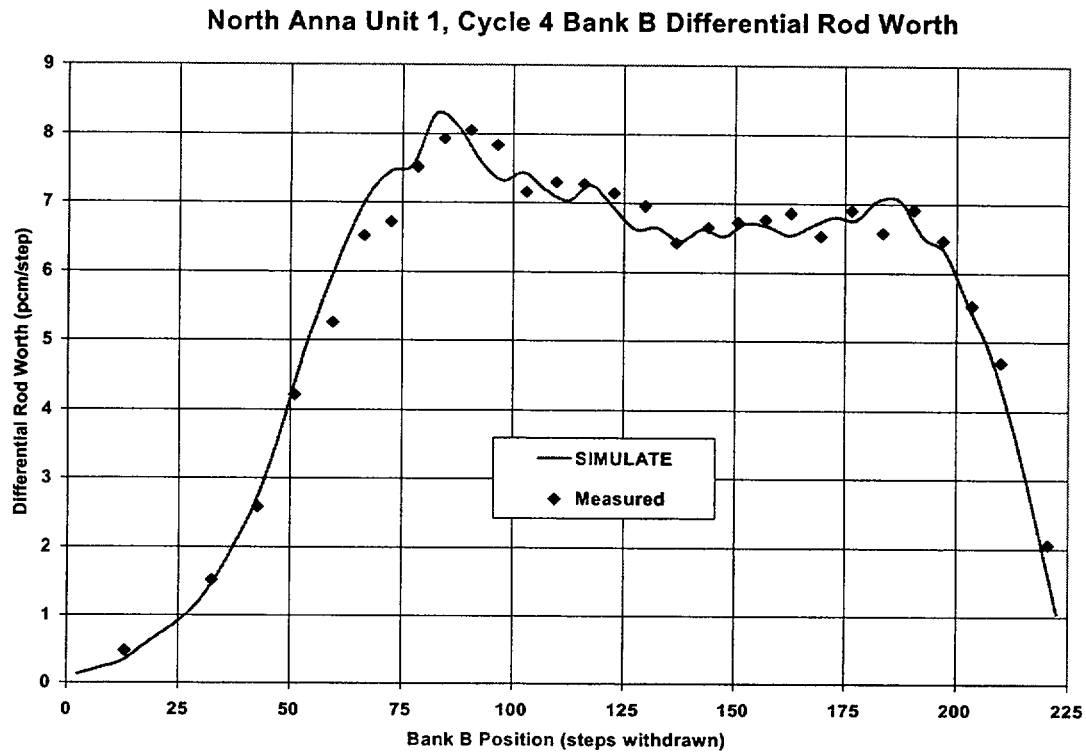


# Figure 13

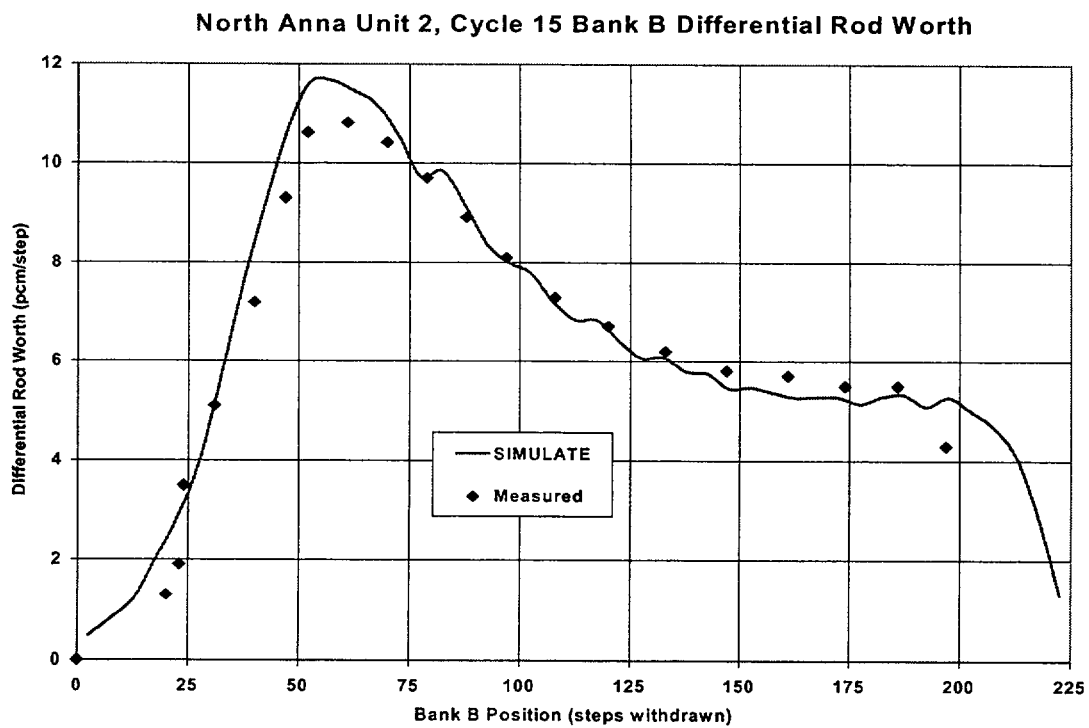


# Figure 14

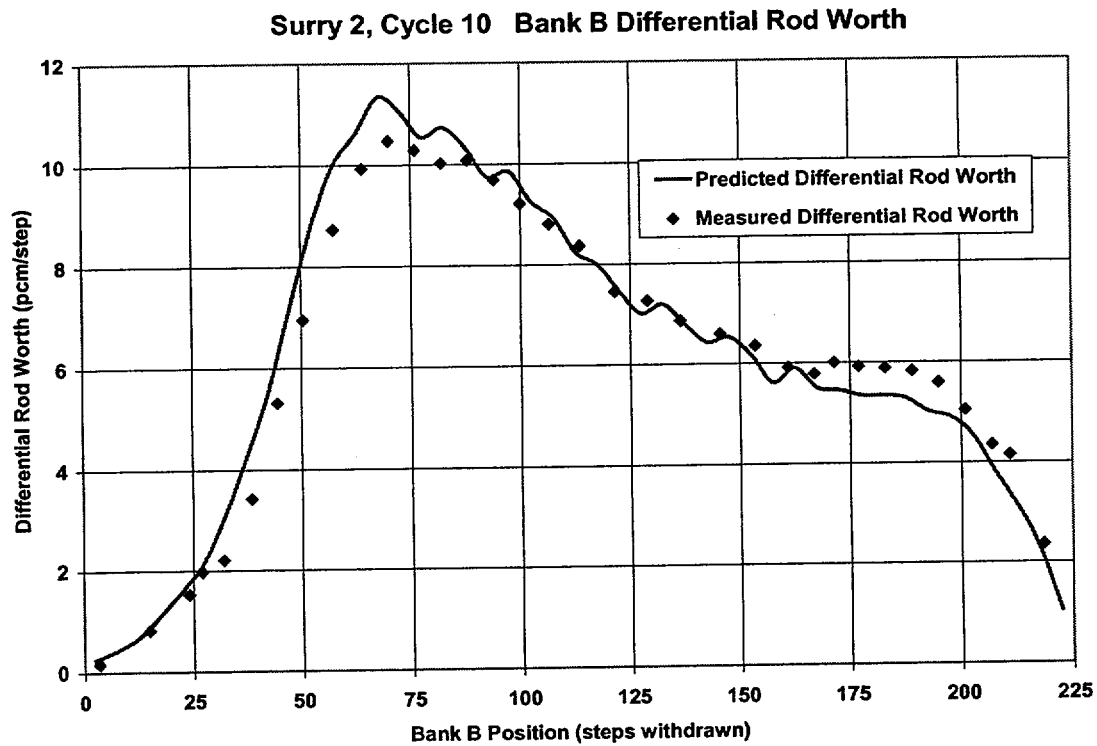
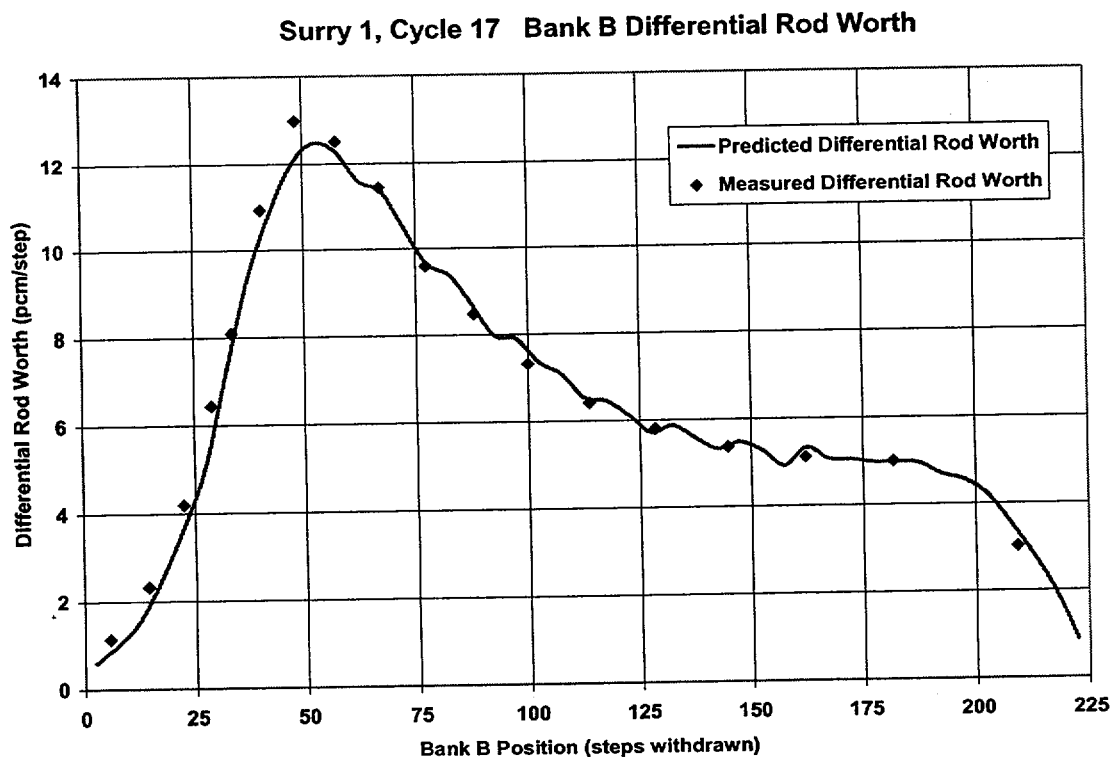


# Figure 15



### 3.3.3 Isothermal Temperature Coefficient

The isothermal temperature coefficient is measured at BOC, HZP as part of startup physics testing. Earlier core measurements included unrodded as well as several rodded configurations for the ITC measurement. Later cycles typically include only the ARO condition. The temperature change for the ITC is usually 3-5 °F.

Sources of measurement uncertainty for the ITC include reactivity computer bias, reactivity computer uncertainty, and uncertainty in the measurement of the temperature change. Reactivity computer accuracy is determined during startup physics testing by verifying that measured and predicted doubling and halving times for a given reactivity insertion match within  $\pm 4\%$ . Using assumed uncertainty values of 4% for the reactivity computer and 0.1 °F for the temperature change (about 2.5%) leads to a root sum square (RSS) estimate of ITC measurement uncertainty of about 5%. The measured ITC is usually determined using the average of a heatup measurement and a cooldown measurement. Ideally, the two measurements should be the same. In practice, they can vary and are considered acceptable measurements if they agree within 1 pcm / °F. An estimate of measurement uncertainty based on acceptable differences between heatup and cooldown measurements is therefore  $\pm 0.5$  pcm / °F.

Figures 16 and 17 present the SIMULATE versus measured ITCs for North Anna and Surry, respectively. Uncertainty bands of  $\pm 3$  pcm/°F about the 45° line (measured = predicted) are shown for reference. A least squares fit through the pairs of points (SIMULATE, measured) shows excellent correlation of the slope, but with a slight SIMULATE bias of less than +1 pcm/°F. Table 8 presents the same data in statistical format, including the data for Surry and North Anna combined. Although only the ITC is measured, the same comparison statistics are used for the MTC. The Doppler coefficient portion of the MTC is small (between 1 and 2 pcm/°F) and nearly constant at all reactor operating conditions, whereas the MTC component is highly dependent on fuel enrichment, soluble boron concentration, and moderator density.

# Figure 16

North Anna HZP BOC ITC Comparison

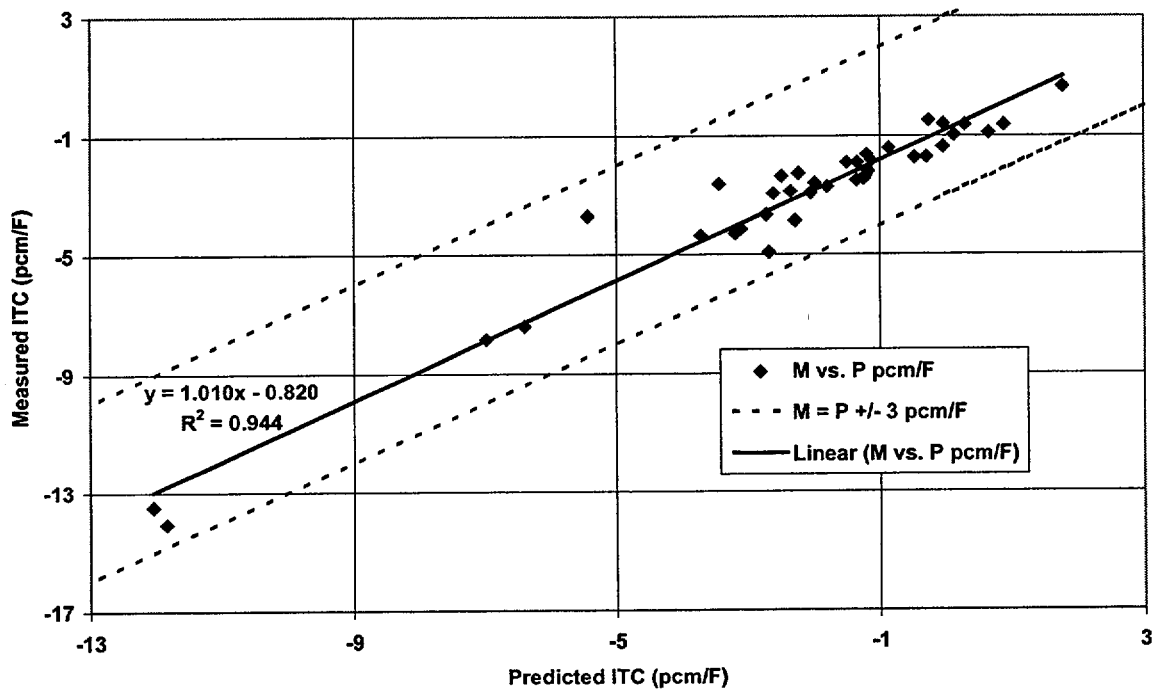


# Figure 17

Surry HZP BOC ITC Comparison

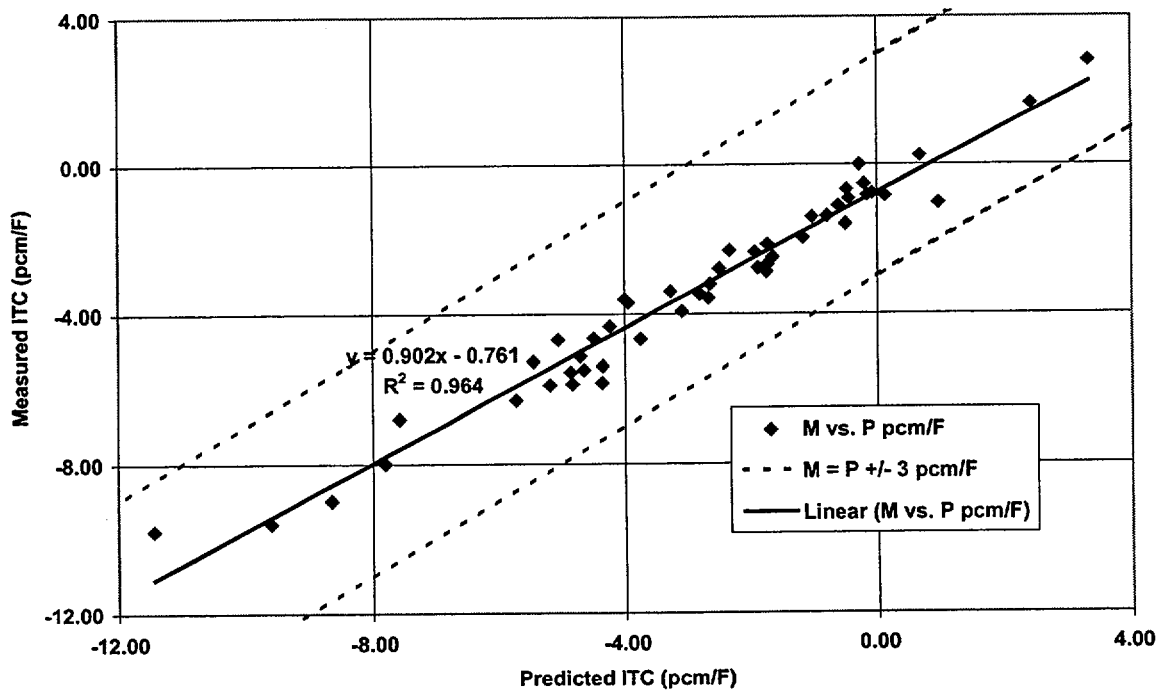


**Table 8**

**SIMULATE HZP BOC ITC Comparisons**

<b>Plant</b>	<b>Mean (pcm/°F)</b>	<b>Std. Dev. (pcm/°F)</b>	<b>Number Of Obs.</b>	<b>Max.</b>	<b>Min.</b>	<b>Normal</b>
<b>North Anna</b>	0.84	0.73	38	2.24	-1.72	Yes'
<b>Surry</b>	0.44	0.55	49	1.49	-1.64	Yes'
<b>COMBINED</b>	0.62	0.66	87	2.24	-1.72	Yes*

**Note:** ITC difference is (SIMULATE – Measured)

Yes' – Failed the W test but passed the K-S test and the Kuiper test

Yes\* - Failed the D' test but passed the K-S test and the Kuiper test

### 3.3.4 Differential Boron Worth

The differential boron worth (DBW) is measured at BOC, HZP as part of startup physics testing. Measured differential boron worth is determined by dividing the measured control rod worth (boron dilution method) by the change in critical boron from the same bank worth measurement. Prior to the use of the rod swap technique, several bank worth measurements were made in sequence (i.e. D-bank, D+C-bank, D+C+B-bank, etc.) using the dilution method. These measurements can be collapsed into a single total rod worth and total boron change, or can be treated as multiple measurements of essentially the same quantity (the differential boron worth is only a weak function of boron concentration). Later cycles typically include only the reference bank worth measurement.

#### **Assessment of DBW Measurement Uncertainty**

Sources of measurement uncertainty for the DBW include reactivity computer bias and uncertainty (contained in the measured rod worth), uncertainty in the manual measurement of each partial segment of the measured bank worth, and measurement of the two critical boron concentration endpoints. Uncertainty in the boron measurement has varied over time with procedural changes (number of multiple measurements and measurement consistency requirements) as well as equipment changes (manual versus automatic titration).

An estimate of critical boron measurement uncertainty can be made based on ANSI/ANS Standard 19.6.1-1997 (Ref. 24), which recommends continuing boron sampling until three consecutive samples are obtained which (1) show no trend and (2) are within 10 ppm of the three sample average. This implies a maximum acceptable boron measurement uncertainty of approximately  $\pm 10$  ppm. The boron change for single bank measurements has averaged roughly 175 ppm at North Anna and Surry. For two endpoint measurements (three-sample average), the RSS uncertainty for two boron endpoint measurements is 14 ppm, which represents a maximum measurement uncertainty in the boron worth measurement *due to boron measurement uncertainty alone* of about 8%. For early cycles with multiple dilution-

type rod worth measurements, the use of the total rod worth and boron change for multiple banks will reduce this uncertainty by approximately a factor of 3. However, only a few cycles used the dilution method for multiple rod banks. It is therefore likely that an uncertainty factor for the predicted boron worth derived from comparison to measurements will be unrealistically high by several percent.

**Effect of Reactivity Computer Bias on DBW Measurement Uncertainty**

A technique for estimating the magnitude of the reactivity computer bias can be developed using the following observations. [

Figure 19 is a histogram of the raw DBW data. Each bin represents  $\pm 1\%$  about the indicated midpoint % difference value.



### **Indirect Evidence of DBW Uncertainty**

Indirect indication of the SIMULATE DBW uncertainty comes from the critical boron data discussed in Section 3.2.1. The raw DBW data in Table 9 indicates a  $2\sigma$  SIMULATE DBW uncertainty of about 7% and a maximum observed difference of 9.6%. These data were measured for soluble boron concentrations ranging from approximately 1000 ppm to over 2000 ppm. Figure 20 confirms that there is no significant trend of DBW error with critical boron concentration, therefore the SIMULATE *integral* boron worth can be expected to exhibit bias and uncertainty similar to the SIMULATE *differential* boron worth. Based on this observation, critical boron differences *due to boron worth error alone* in the range of 70 ppm ( $7\% \times 1000$  ppm) to 192 ppm ( $9.6\% \times 2000$  ppm) are expected to be observed in the critical boron data. However, the largest observed boron difference for all BOC measurements *due to all sources of bias and uncertainty combined* is 54 ppm (absolute value from Table 5). This suggests that the true DBW uncertainty is significantly lower than the DBW statistics indicate.

**Figure 18**

**Table 9**

**SIMULATE HZP DBW Comparisons**

<b>Plant</b>	<b>Data Adjustment</b>	<b>Mean (% diff.)</b>	<b>Std. Dev. (% diff.)</b>	<b>Number Of Obs.</b>	<b>Max.</b>	<b>Min.</b>	<b>Normal</b>
<b>North Anna</b>	None	0.0	3.2	30	7.6	-6.1	Yes
<b>Surry</b>	None	0.3	4.2	35	9.6	-7.8	Yes
<b>Combined</b>	None	0.2	3.7	65	9.6	-7.8	Yes
<b>Combined</b>	[ ]	[ ]	[ ]	[ ]	[ ]	[ ]	Yes

Note: DBW % difference is  $100 \times (\text{SIMULATE} - \text{Measured}) / \text{SIMULATE}$

Figure 19

Combined Differential Boron Worth Comparison

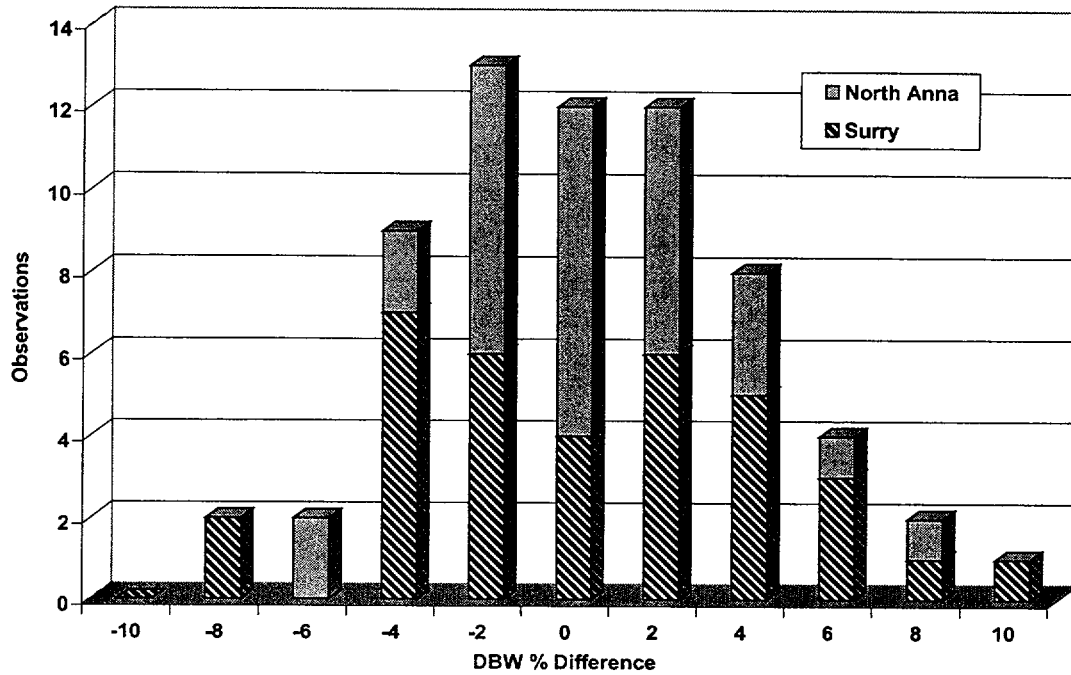
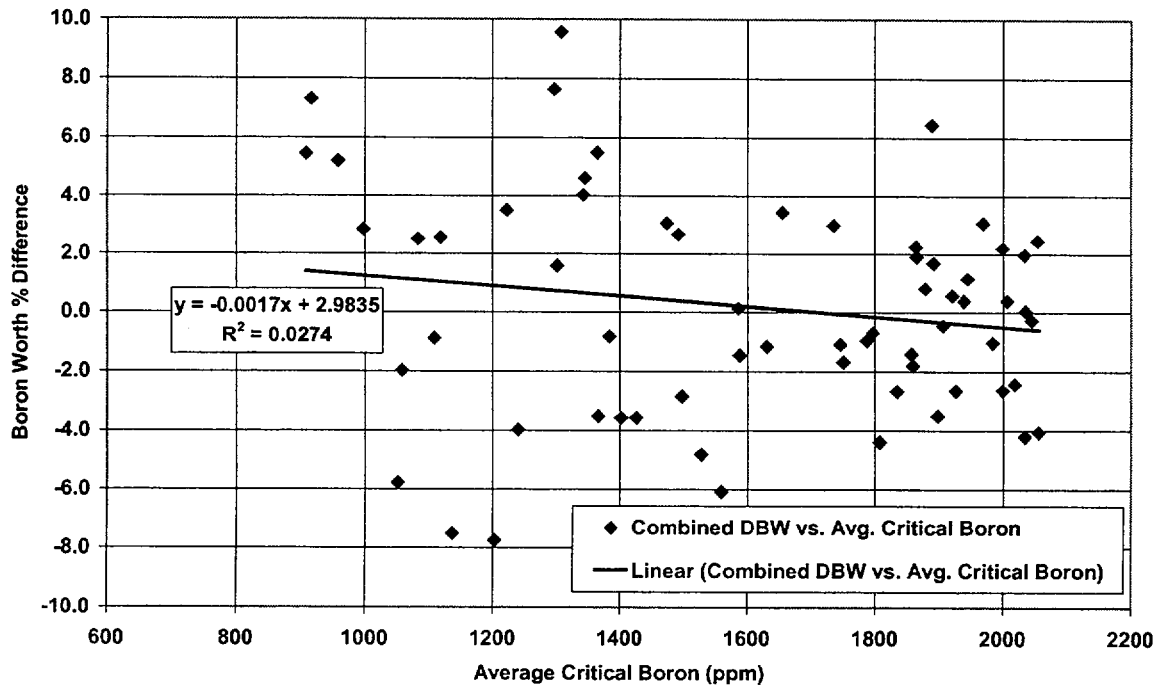


Figure 20

Combined DBW Error vs. Critical Broron Concentration



### 3.3.5 Estimated Critical Position

An estimated critical rod position (ECP) calculation is required prior to restarting a reactor after a period of time at zero power (such as after a trip or maintenance outage). All reactivity elements of the CMS model are tested in this calculation because soluble boron worth, power defect, partially inserted control rod worth, axial flux redistribution effects, transient fuel isotope and fission product worth (such as  $\text{Xe}^{135}$ ,  $\text{Sm}^{149}$ ,  $\text{Np}^{239}$  decay to  $\text{Pu}^{239}$ , and others) are all involved. The xenon concentration and boron concentration may be higher or lower than the HFP equilibrium value depending on the power history, down time, and desired control rod position.

There are two primary sources of measurement uncertainty for an ECP calculation. The largest is the measurement uncertainty of the critical boron concentrations for a critical condition prior to the outage and for the critical re-start condition. A second source of uncertainty is the exact timing and power history for the ramp down or trip prior to the outage. For long outages, xenon completely decays away and the timing uncertainty is negligible. For short outages, xenon can change at the rate of about 150 pcm / hour. Although there is no reliability factor associated with the ECP calculation, an administrative limit of  $\pm 500$  pcm is typically used to screen for unexpected reactivity anomalies. The ECP calculation is a useful indicator of overall model accuracy for reactivity calculations.

A total of 71 ECP calculations were run for seven Surry Unit 1 cycles, ten Surry Unit 2 cycles, ten North Anna Unit 1 cycles, and eight North Anna Unit 2 cycles. For the Surry cycles, core burnup ranged from 78 to 16653 MWD/MTU, D-bank position at restart ranged from 82 to 212 steps withdrawn (ARO position is 225 steps), and down time ranged from 7.8 to 1798 hours. For the North Anna cycles, core burnup ranged from 225 to 14632 MWD/MTU, D-bank position at restart ranged from 16 to 215 steps withdrawn (ARO position is 225 steps), and down time ranged from 6.3 to 2150 hours. Two SIMULATE cases were run for each ECP. The first represents a critical condition (typically HFP, equilibrium Xe) measured just prior to the outage.

The second represents the measured critical restart condition. The ECP error is calculated as follows:

$$\text{ECP Error (pcm)} = (K_{\text{startup}} - K_{\text{previous}})/(K_{\text{startup}} * K_{\text{previous}}) * 100000$$

where  $K_{\text{previous}}$  is the SIMULATE K-effective for the critical at power condition prior to the outage and  $K_{\text{startup}}$  is the SIMULATE K-effective for the restart critical conditions. Note that because the error is calculated relative to a known previous critical condition, the ECP error is free of overall reactivity bias. The startup K-effective can also be used directly to estimate critical boron difference (see Table 5).

Table 10 presents the ECP error statistics. Figure 21 is a histogram of the same ECP error data. There is a slight positive bias (SIMULATE restart K-effective higher than measured). Figure 22 demonstrates that the source of the bias is primarily in the middle of the boron range (the critical boron of the critical condition prior to the outage). This is most likely due to reduced  $B^{10}$  depletion effects for the restart condition caused by boration and dilution during the outage.  $B^{10}$  depletion effects are not significant at high boron concentration (near BOC) or at low boron concentration (insignificant boron reactivity). The data used for ECP error statistics has not been adjusted to eliminate the effect of  $B^{10}$  depletion. Inclusion of the effects of  $B^{10}$  depletion will tend to increase the bias and standard deviation of the ECP error. A more complete discussion of  $B^{10}$  depletion effects is provided in Section 3.3.1.

The results presented in Table 10 and in Figures 21 and 22 indicate excellent SIMULATE agreement with measured data and preclude any large bias or uncertainty related to power defect, xenon worth, control rod worth, or boron worth.

**Table 10**  
**SIMULATE ECP Error**

Plant	Mean (pcm)	Std. Dev. (pcm)	Number Of Obs.	Max.	Min.	Normal
North Anna	22	107	38	297	-231	Yes
Surry	42	142	33	322	-213	Yes
COMBINED	31	124	71	322	-231	Yes

**Note:** ECP Error (pcm) is  $(K_{\text{startup}} - K_{\text{previous}})/(K_{\text{startup}} * K_{\text{previous}}) * 100000$  where  $K_{\text{previous}}$  is the SIMULATE K-effective for the critical at power condition prior to the outage and  $K_{\text{startup}}$  is the SIMULATE K-effective for the restart critical conditions.

# Figure 21

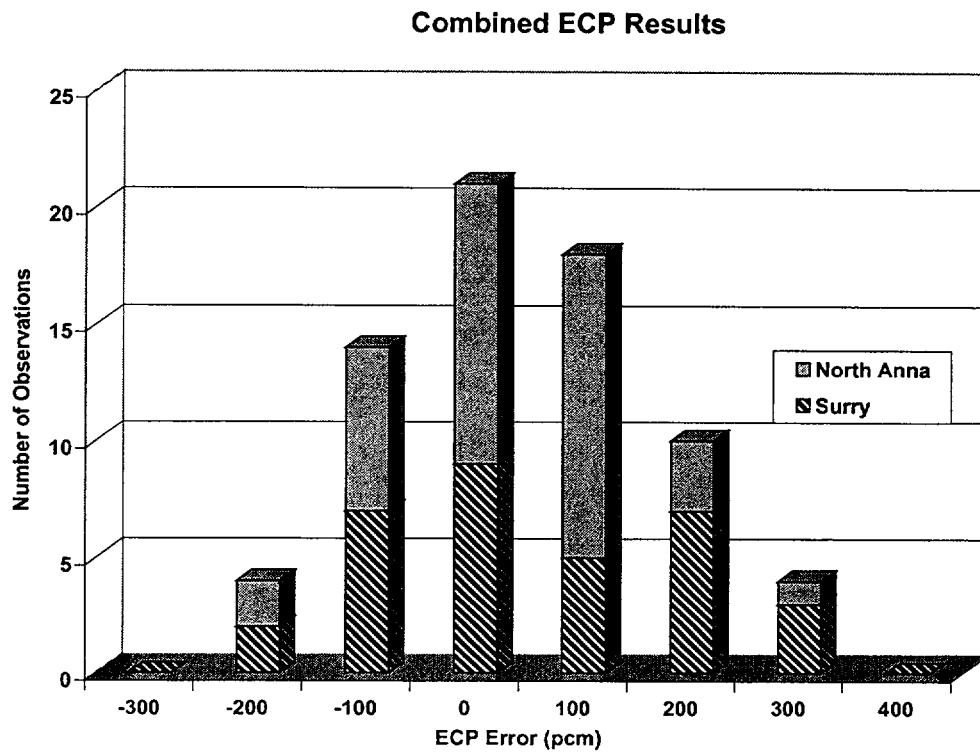
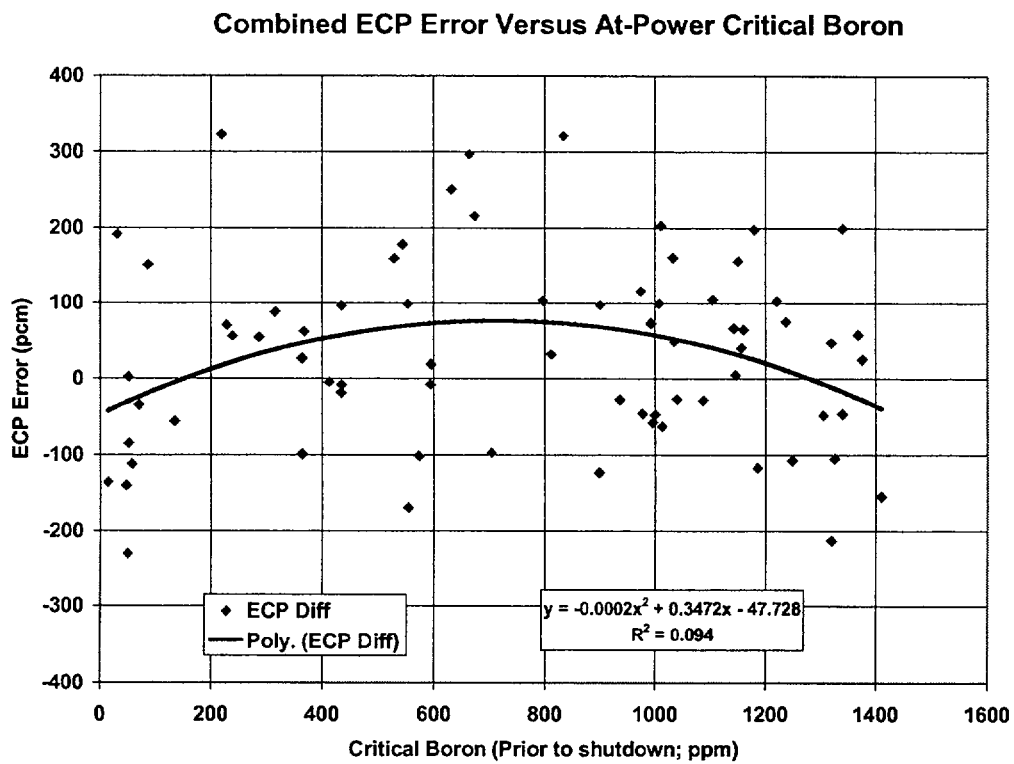


# Figure 22



### 3.3.6 Reaction Rate Comparisons

Flux mapping is routinely performed using movable in-core fission chamber detectors for each cycle on a monthly basis and at approximately 30% and 70% power during initial power ascension following a refueling. Figure 23 shows the in-core detector flux thimble locations (identical for North Anna and Surry). For routine flux mapping, the CECOR code (Ref. 18) is used to align, calibrate, and normalize the reaction rate data obtained using five independent detectors so that the core power distribution and peaking factors can be synthesized.

Each axial flux trace (a pass) is obtained by withdrawing the detector and drive cable through the flux thimble from the top of the fuel assembly to the bottom at a fixed rate. A total of 61 or 610 "snapshots" are collected at equally spaced time intervals during each pass. CECOR performs a synthesis of measured reaction rate data, predicted reaction rate data, and predicted assembly power and peaking factor data to obtain the core power distribution, including RPD,  $F(z)$ ,  $F\Delta H$ , and  $FQ(z)$ . RPD (relative power density) is the average of the axially integrated power of all fuel pins in a fuel assembly divided by the core average axially integrated fuel pin power.  $F(z)$  is the core average axial power distribution.  $F\Delta H$  is the enthalpy rise hot channel factor (also referred to as the "peak pin") and represents the highest axially integrated fuel pin power divided by the core average axially integrated fuel pin power.  $FQ(z)$  is the ratio of the highest local pin power at each elevation divided by the core average axially integrated fuel pin power.

In the flux mapping process described above, only the reaction rates are directly measured. Therefore, in order to determine an appropriate reliability factor for  $F\Delta H$ ,  $FQ(z)$ , and peak  $FQ$ , the uncertainty of the following components of the process must be assessed and combined:

- 1) Thimble reaction rate uncertainty (integral for RPD and  $F\Delta H$ , 32 node for  $FQ(z)$ ). This uncertainty will be derived using SIMULATE predictions and measured thimble reaction rates from the flux maps for each cycle.



- 2) Uncertainty in the reconstruction of measured assembly RPD (and local RPD(z)) from the thimble reaction rates. This component is discussed in Section 3.1.
- 3) Uncertainty in the reconstruction of  $F\Delta H$  and  $FQ(z)$  from the RPD. This component is also discussed in Section 3.1.

Two separate sets of reaction rate comparison statistics are needed. Axially integrated reaction rates are needed to develop uncertainty factors for 2-D quantities RPD and  $F\Delta H$ . Reaction rates at multiple axial locations are needed to develop uncertainty factors for  $FQ$ .

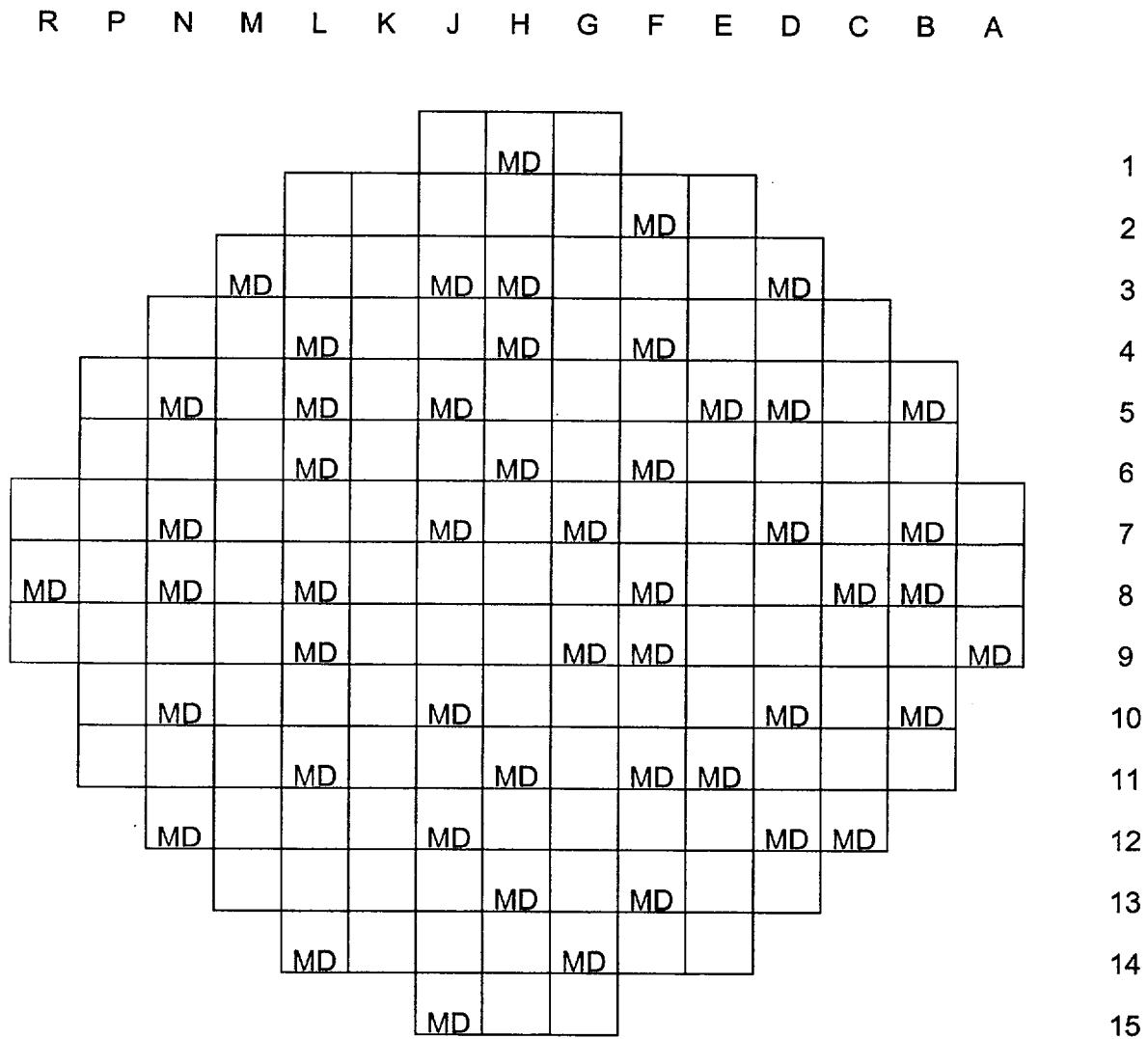
For each flux map, measured reaction rates are normalized to the average of all measured reaction rates in instrumented assemblies. For the same set of fuel assemblies, predicted reaction rates are normalized to the average of all predicted reaction rates. The normalized measured and predicted integral reaction rates are then accumulated for all maps for the calculation of integral difference statistics. Normalized integral reaction rates of 1.0 or less are discarded because they represent fuel assemblies with less than core average relative power. Low power assemblies not only have higher measurement uncertainty, but they are also not of interest for the determination of peaking factor uncertainty factors, because high peaking factors are found in high power assemblies.

Reaction rates at multiple axial locations are needed to develop uncertainty factors for  $FQ$ . Normalized measured and predicted reaction rates at 32 axial locations are accumulated for all maps for the calculation of difference statistics. These reaction rates correspond to the “mini” integrals over 32 equally spaced axial core regions (with a 1:1 correspondence with each SIMULATE axial node). The measured axial reaction rates are collapsed from 61 measured points to 32 integrals by trapezoidal integration of the measured data. As with RPD and  $F\Delta H$ , reaction rates of 1.0 or less are discarded.

A listing of flux maps used to develop the reaction rate comparison statistics is provided in Table 11. Flux mapping is typically only performed when the core is axially stable (no more than 1% per hour axial offset change). SIMULATE predictions are also normally based on equilibrium xenon conditions. However, transient modeling of the N1C11 startup in Section 3.3.7 demonstrates that maps (particularly during initial power ascension) are sometimes taken at relatively stable but non-equilibrium xenon conditions, and that the axial offset can vary significantly from the equilibrium value. Therefore, to get a valid comparison of measured and predicted reaction rates, both the core and the model need to be close to equilibrium conditions (as with most full power flux maps), or the reactor history needs to be modeled in detail (as with the N1C11 startup). Because detailed operating history modeling is impractical for the large number of flux maps needed to develop the uncertainty factors, a tolerance of  $\pm 4\%$  axial offset difference was used as a filter for probable mismatches between measured conditions and the assumed equilibrium SIMULATE conditions.

Figure 24 is a histogram of the thimble integral differences. The difference is defined as the  $(\text{Predicted} - \text{Measured}) / \text{Predicted} (\%)$  for all normalized reaction rates  $> 1.0$ . Figure 25 is a corresponding histogram of the 32 node differences. In both Figures, each bin represents  $\pm 0.5\%$  about the value indicated. Table 12 contains the difference data statistics for Surry maps, North Anna maps, and for all maps combined.

**Figure 23**  
**In-core Moveable Detector Locations**



MD – Moveable Detector

**Table 11**

**Flux Map Database for Reaction Rate Comparison**

<b>CYCLE</b>	<b>Map #</b>	<b>Burnup (MWD/MTU)</b>	<b>D-bank (steps w/d)</b>	<b>Core Power (%)</b>	<b>CECOR A/O (%)</b>	<b>SIMULATE A/O (%)</b>	<b>A/O Difference (C – S)</b>
N1C1	9	50	210	49	-2.6	-4.1	1.5
	25	300	216	96	-8.3	-8.6	0.3
N1C2	12	110	192	45	6.7	5.8	0.9
	21	1129	220	99	0.5	-0.1	0.6
	30	4490	215	100	-1.7	-3.5	1.8
	47	8811	228	100	-0.4	-2.2	1.8
N1C3	87	12433	214	99	-1.9	-2	0.1
N1C4	5	41	188	52	4.2	1.2	3.0
	7	305	221	100	0.2	-0.5	0.7
	18	6834	214	100	-4.6	-3.6	-1.0
	29	12241	222	100	-2.7	-2.4	-0.3
N1C5	23	6831	224	100	-2.3	-2.8	0.5
	34	12983.2	228	100	-0.9	-1.2	0.3
N1C6	3	55	170	49	-3.2	-3.2	0.0
	6	69	181	75	-4.8	-4.8	0.0
	9	378	219	100	-1.6	-2.2	0.6
	19	8170	228	96	-2.0	-1.9	-0.1
	29	14340	228	100	-1.2	-1.6	0.4
N1C7	2	37	179	49	2.8	1	1.8
	19	7404	228	100	-2.6	-2.9	0.3
	29	15400	228	100	-1.6	-1.7	0.1
N1C8	1	14	163	29	-1.7	-0.3	-1.4
	2	47	192	74	0.5	-0.5	1.0
	6	1243	228	100	0.2	-1	1.2
	13	9462	228	100	-2.5	-2.6	0.1
	21	16201	228	100	-0.6	-1.8	1.2
N1C9	1	14	133	24	-13.7	-11.8	-1.9
	6	305	228	99	-2.4	-5.7	3.3
	19	9842	228	100	-2.7	-2.7	0.0
	29	16830	228	95	0.5	-1	1.5
N1C10	1	6	137	30	-7.3	-8.9	1.6
	4	1452	225	100	-2.0	-4.2	2.2
	12	9513	225	100	-2.4	-2.5	0.1
	18	16233	225	100	-0.9	-1.2	0.3
N1C11	1	4	124	30	-12.7	-13.7	1.0
	2	37	179	74	-6.3	-6	-0.3
	4	1908	225	100	-1.7	-3.9	2.2
	11	9852	225	100	-2.1	-2.7	0.6
	17	16963	225	100	0.0	-1	1.0

**Table 11 (continued)**

<b>CYCLE</b>	<b>Map #</b>	<b>Burnup (MWD/MTU)</b>	<b>D-bank (steps w/d)</b>	<b>Core Power (%)</b>	<b>CECOR A/O (%)</b>	<b>SIMULATE A/O (%)</b>	<b>A/O Difference (C – S)</b>
N1C12	1	5	152	30	-3.4	-3.5	0.1
	2	25	213	74	3.3	2.2	1.1
	4	1792	225	100	-1.1	-2	0.9
	10	8698	225	100	-2.4	-2.7	0.3
	16	15591	225	100	-1.0	-1.7	0.7
N1C13	2	36	189	74	-2.3	-4.4	2.1
	4	1758	225	100	0.6	-1.9	2.5
	10	8590	225	100	-1.0	-2	1.0
	19	16618	225	100	-0.7	-1.3	0.6
N1C14	1	8	156	29	-2.5	-3.6	1.1
	2	31	183	71	-1.6	-3.3	1.7
	4	1553	227	100	0.3	-1.2	1.5
	11	9782	227	100	-1.5	-2.5	1.0
	18	17911	227	100	-1.4	-1.3	-0.1
N1C15	2	30.3	194	70	-0.5	-3.2	2.7
	4	1303	225	100	-1.2	-4.2	3.0
	10	8678	225	100	-1.6	-2.5	0.9
	17	17073	225	100	-0.9	-0.9	0.0
N2C1	19	280	186	76	-14.1	-10.9	-3.2
	40	8011	203	100	-3.7	-3.3	-0.4
N2C2	17	1700	223	100	2.6	0.3	2.3
	21	4110	228	100	-0.8	-1.7	0.9
	30	7844	218	100	-2.4	-3.4	1.0
N2C3	2	0	177	31	1.0	1.9	-0.9
	13	671	228	100	-3.6	-4.1	0.5
	25	7647	217	100	-2.3	-3.8	1.5
	38	13299	221	100	-0.5	-1.7	1.2
N2C4	2	65	162	50	-3.9	-5.8	1.9
	7	230	216	100	-1.3	-3.3	2.0
	23	7906	222	100	-2.3	-2.7	0.4
	34	14612	228	100	-1.2	-1.4	0.2
N2C5	2	5	145	27	-8.1	-8.3	0.2
	8	250	228	100	-0.4	-1.9	1.5
	22	8370	228	100	-2.6	-3.0	0.4
	35	15295	228	100	-1.4	-1.6	0.2
N2C6	4	222	228	100	-1.3	-3.5	2.2
	16	8586	228	100	-2.9	-3.0	0.1
	24	15516	228	100	-1.1	-1.6	0.5

**Table 11 (continued)**

<b>CYCLE</b>	<b>Map #</b>	<b>Burnup (MWD/MTU)</b>	<b>D-bank (steps w/d)</b>	<b>Core Power (%)</b>	<b>CECOR A/O (%)</b>	<b>SIMULATE A/O (%)</b>	<b>A/O Difference (C – S)</b>
N2C7	1	19	123	30	-11.0	-9.7	-1.3
	8	800	228	100	-0.2	-2.4	2.2
	15	8339	228	100	-1.6	-1.8	0.2
	24	15823	228	100	-1.3	-1.7	0.4
N2C8	1	18	150	28	-2.6	-5.1	2.5
	7	1505	228	100	-0.5	-2.2	1.7
	14	9129	228	100	-2.5	-2.9	0.4
	25	16640	228	100	-0.9	-1.7	0.8
N2C9	3	159	225	100	2.3	0.3	2.0
	11	8571	225	100	-2.1	-2.9	0.8
	21	16086	225	100	-1.3	-1.9	0.6
N2C10	3	46	173	73	-4.1	-6.5	2.4
	6	1782	225	100	-2.7	-3.4	0.7
	14	10811	225	100	-2.6	-2.7	0.1
	20	17126	225	100	0.8	-1.2	2.0
N2C11	1	8	130	29	-6.5	-8.6	2.1
	2	46	192	74	-2.3	-1.9	-0.4
	4	1517	225	100	0.0	-2.2	2.2
	11	9713	225	100	-1.9	-2.6	0.7
	17	16107	225	100	-1.1	-1.6	0.5
N2C12	1	4	125	30	-10.0	-11	1.0
	2	27	186	72	-1.5	-1.3	-0.2
	4	1109	225	100	0.8	-0.5	1.3
	12	10449	225	100	-1.9	-2.5	0.6
	19	16589	225	100	-1.2	-1.7	0.5
N2C13	2	20	191	70	-2.2	-2.7	0.5
	4	1445	225	100	-0.5	-3	2.5
	12	9985	225	100	-1.5	-2	0.5
	18	17042	225	100	-0.8	-1.3	0.5
N2C14	3	56	190	75	-0.6	-2.2	1.6
	4	289	225	100	0.8	-0.8	1.6
	12	9429	225	100	-1.9	-2.4	0.5
	19	17746	225	100	-0.8	-1.4	0.6

**Table 11 (continued)**

<b>CYCLE</b>	<b>Map #</b>	<b>Burnup (MWD/MTU)</b>	<b>D-bank (steps w/d)</b>	<b>Core Power (%)</b>	<b>CECOR A/O (%)</b>	<b>SIMULATE A/O (%)</b>	<b>A/O Difference (C – S)</b>
S1C04	19	6968	207	100	-4.7	-4.8	0.1
S1C05	10	150	221	100	-0.3	-3.4	3.1
S1C06	56	7518	228	100	-0.9	-2.0	1.1
	74	14752	226	100	-0.1	-1.5	1.4
S1C07	3	6	180	51	0.7	-3.1	3.8
	11	1612	227	100	1.0	-1.9	2.9
	24	9593	225	100	-1.9	-2.5	0.6
S1C08	36	6873	227	100	-1.8	-2.5	0.7
	50	13212	212	99	-0.6	-3.6	3.0
S1C09	2	14	168	50	-0.1	-3.6	3.5
	6	240	220	100	1.0	0.8	0.2
	29	8640	228	100	-0.9	-2.1	1.2
S1C10A	19	3373	217	100	-1.0	-2.8	1.8
	29	7419	224	100	-0.1	-2.4	2.3
	48	13908	224	94	2.9	0.6	2.3
S1C11	7	626	219	100	-0.1	-3.5	3.4
	15	6670	224	100	-1.1	-2.4	1.3
	21	12640	224	100	-1.0	-1.5	0.5
S1C12	3	28.4	163	69	-5.1	-7.1	2.0
	5	178	220	100	4.1	0.6	3.5
	14	9266	224	100	-1.0	-1.8	0.8
	23	16789	223	100	-0.5	-1.8	1.3
S1C13	2	19	196	70	-3.1	-6.5	3.4
	13	7836	224	96	0.9	0.1	0.8
	24	14678	224	100	1.8	1.0	0.8
S1C14	2	28	181	54	-5.1	-7.0	1.9
	4	1500	224	100	-2.8	-5.2	2.4
	14	8600	226	100	-0.2	-1.0	0.8
	22	15978	225	100	1.1	1.3	-0.2
S1C15	4	88	192	68	0.0	-2.1	2.1
	5	238	225	100	-0.5	-1.8	1.3
	13	8723	225	100	-0.4	-0.9	0.5
	20	15870	226	100	0.6	0.0	0.6
S1C16	3	35	193	69	0.2	-3.0	3.2
	5	1332	227	100	-0.2	-2.3	2.1
	13	8705	228	100	-0.7	-1.2	0.5
	19	14098	228	100	0.7	0.0	0.7

**Table 11 (continued)**

<b>CYCLE</b>	<b>Map #</b>	<b>Burnup (MWD/MTU)</b>	<b>D-bank (steps w/d)</b>	<b>Core Power (%)</b>	<b>CECOR A/O (%)</b>	<b>SIMULATE A/O (%)</b>	<b>A/O Difference (C – S)</b>
S1C17	2	22.5	200	68	-1.0	-2.5	1.5
	6	2243	225	100	-1.3	-3.0	1.7
	12	8551	225	100	-0.7	-1.1	0.4
	20	16856	225	100	1.0	0.5	0.5
S2C04	17	4524	218	100	-1.0	-3.1	2.1
	36	13200	222	100	0.5	-1.6	2.1
S2C05	13	450	215	100	2.3	0.5	1.8
	24	6653	227	100	0.5	-1.7	2.2
S2C06	4	17	180	59	-5.3	-5.3	0.0
	7	1116	228	100	-0.9	-2.8	1.9
	18	7390	228	100	-1.5	-2.3	0.8
	31	15326	228	100	-0.5	-1.1	0.6
S2C07	2	10	178	47	0.9	-3.0	3.9
	5	198	228	100	-0.1	-2.1	2.0
	45	14150	223	100	-0.6	-1.4	0.8
S2C08	3	31	157	46	-7.5	-9.9	2.4
S2C09	17	6887	223	100	0.3	-2.0	2.3
S2C10	22	8016	222	100	-1.3	-2.6	1.3
	50	13935	222	90	0.3	0.0	0.3
S2C11	3	43	182	68	-1.0	-3.1	2.1
	13	2986	221	100	0.0	-1.2	1.2
	22	9650	223	100	-1.2	-2.2	1.0
	32	17246	223	100	-0.6	-1.6	1.0
S2C12	2	28	165	57	-2.8	-5.4	2.6
	4	646	224	100	1.5	-0.9	2.4
	16	9368	217	94	-0.5	-0.8	0.3
	28	17575	224	100	0.0	-0.9	0.9
S2C13	2	20	177	69	-3.4	-5.1	1.7
	4	890	225	100	-0.2	-1.6	1.4
	10	4876	224	100	-1.6	-1.8	0.2
	11	5416	224	100	-1.7	-1.9	0.2
	18	12044	226	100	-1.5	-1.6	0.1
S2C14	2	19	184	71	0.7	-1.9	2.6
	4	1126	226	100	1.8	0.7	1.1
	11	8204	225	100	-1.6	-1.5	-0.1
	19	15356	223	100	-1.3	-1.5	0.2
S2C15	4	178	228	100	0.2	-3.3	3.5
	13	8514	227	100	-0.7	-1.2	0.5
	20	15909	228	100	-0.1	-0.6	0.5



**Table 11 (continued)**

<b>CYCLE</b>	<b>Map #</b>	<b>Burnup (MWD/MTU)</b>	<b>D-bank (steps w/d)</b>	<b>Core Power (%)</b>	<b>CECOR A/O (%)</b>	<b>SIMULATE A/O (%)</b>	<b>A/O Difference (C – S)</b>
S2C16	4	1412	225	100	0.2	-1.8	2.0
	11	8762	225	100	-1.8	-2.0	0.2
	19	15314	225	100	-0.4	-0.9	0.5
S2C17	2	34.8	185	66	2.0	-1.2	3.2

Figure 24

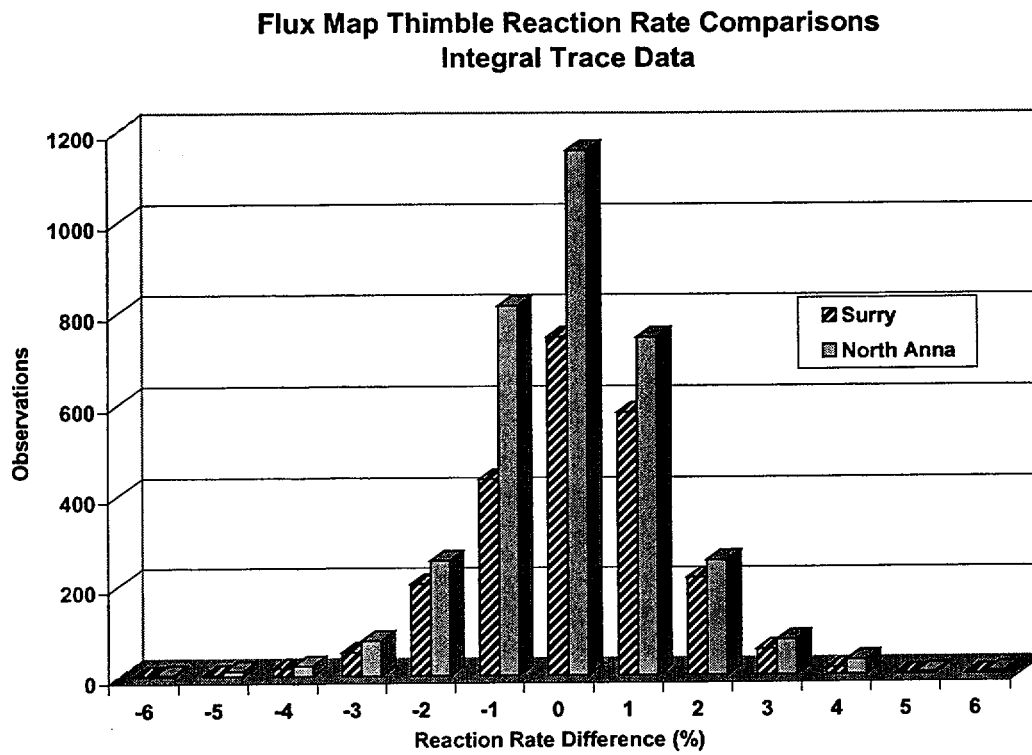
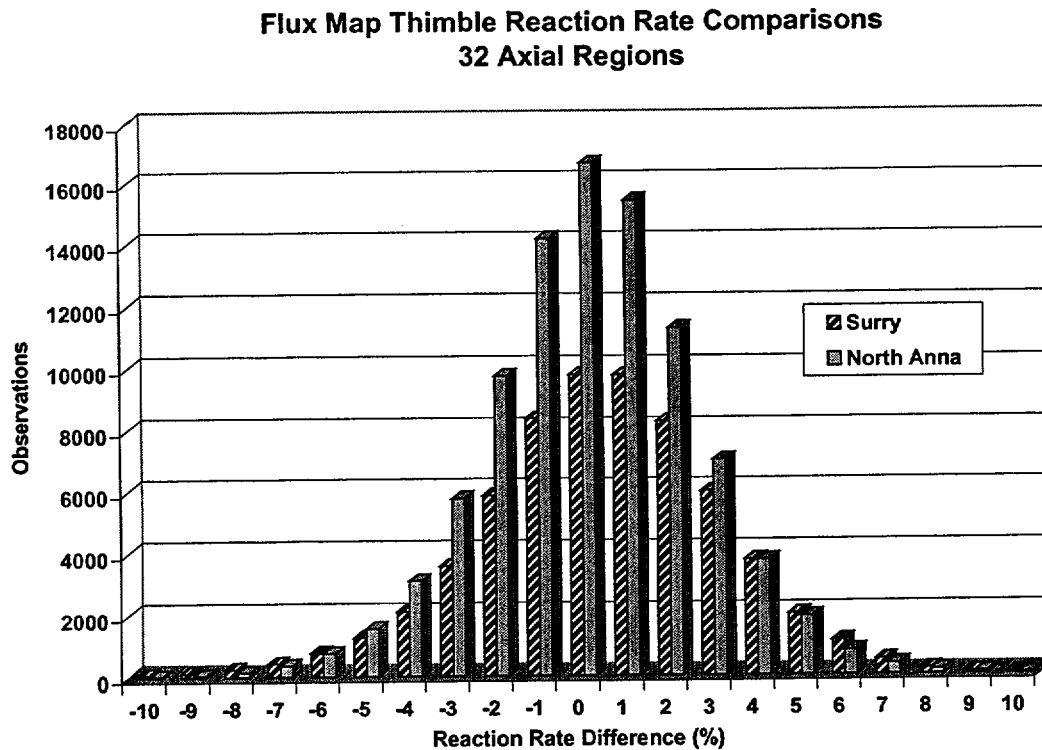


Figure 25



**Table 12****Flux Map Reaction Rate Statistics**

<b>Plant</b>	<b>Data Type</b>	<b>Mean (% Diff.)</b>	<b>Std. Dev. (% Diff.)</b>	<b>Number Of Obs.</b>	<b>Max. (% Diff.)</b>	<b>Min. (% Diff.)</b>	<b>Normal</b>
<b>North Anna</b>	Integral	-0.02	1.34	3453	5.8	-6.2	No
<b>Surry</b>	Integral	0.07	1.34	2322	5.1	-6.1	No
<b>Combined</b>	Integral	0.01	1.34	5775	5.8	-6.2	No
<b>North Anna</b>	32 Node	0.14	2.41	93070	16.4	-12.8	No
<b>Surry</b>	32 Node	0.38	2.79	64354	13.8	-15.1	No
<b>Combined</b>	32 Node	0.24	2.58	157424	16.4	-15.1	No

**Note:** Reaction rate difference is  $((\text{SIMULATE} - \text{Measured}) / \text{SIMULATE}) \times 100\%$  for all normalized reaction rates  $> 1.0$ .

### 3.3.7 Normal Operation Power Transients

Normal operation plant transient modeling provides an opportunity to test the performance of the SIMULATE model in a dynamic manner. Operational transients involve all reactivity components of the model, including thermal-hydraulic feedback, power and temperature defects, boron worth, control rod worth, and transient xenon worth. Reactivity performance can be assessed using measured critical boron concentrations. These reactivity components also have an impact on the core axial power distribution, which can be monitored via the ex-core instrumentation (measured delta-I or axial offset). In some cases, a limited amount of in-core flux map information is also available.

Measured plant transients were modeled for the following:

- S2C2 - 24 hour 100-50-100 load follow test on 8/1-8/2/75.
- N1C3 - two EOC return to power scenarios on 4/16-4/20/82 and 4/30-5/2/82.
- N1C6 - power transient initiated on 12/26/86.
- N1C9 - 95% power EOC MTC measurement on 6/15/92.
- N1C11 - BOC power ascension to 100% 10/8/94-10/17/94.
- N2C14 - power transient initiated 10/14/00.

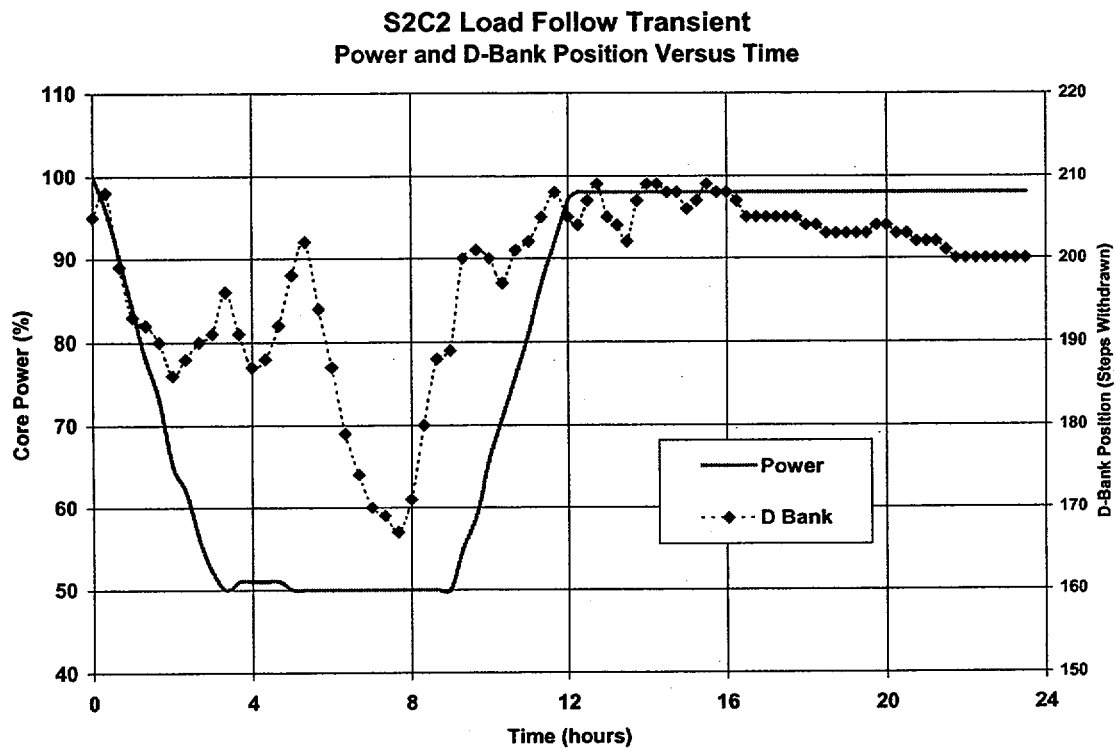
Comparison to measured data includes critical boron concentration, axial offset, delta-I, and peak  $F(z)$ . Axial offset (AO) is a measure of axial core power imbalance. AO is defined as the power in the top half of the core minus the power in the bottom half of the core divided by the total core power. Delta-I is equal to AO times the core relative power (fraction of full power). Peak  $F(z)$  is the maximum point in the core average relative axial power distribution  $F(z)$ .

### **S2C2 Load Follow Demonstration**

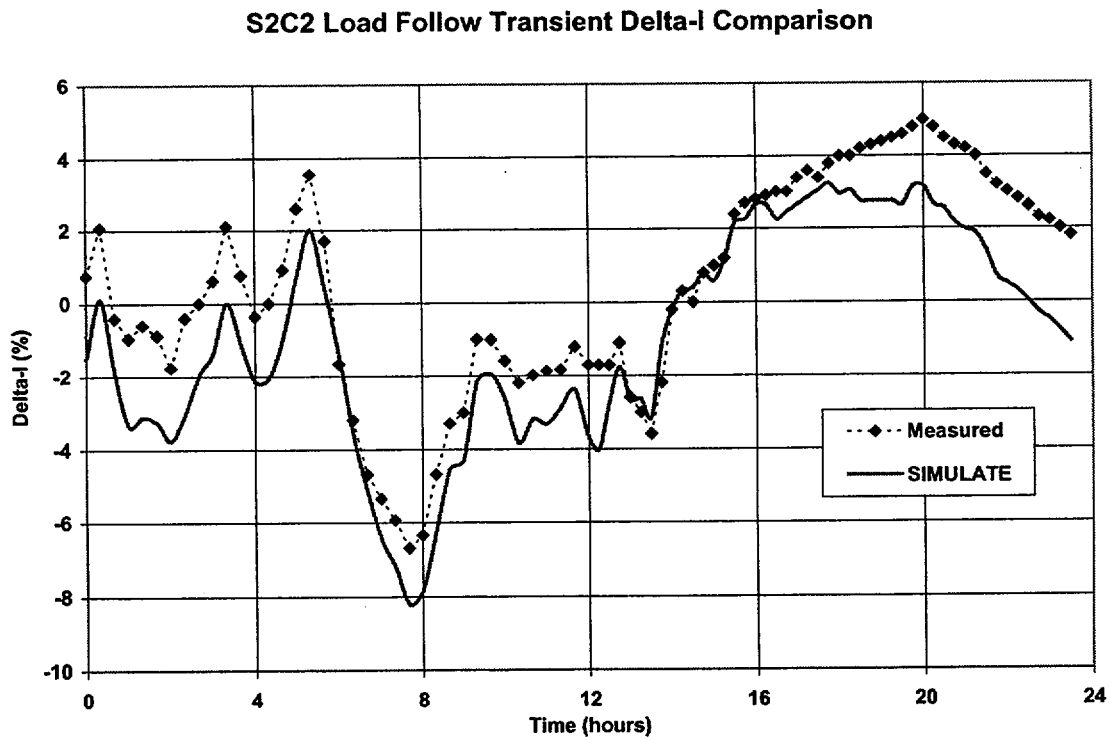
A twenty-four hour 100-50-100 load follow test was conducted for S2C2. Measured data was gathered every twenty minutes for delta-I, peak core average axial power  $F(z)$ , and critical boron concentration.

Figure 26 provides the core power and D-bank position as a function of time. Figures 27, 28, and 29 show the comparison of SIMULATE and measured delta-I, critical boron concentration, and peak  $F(z)$ , respectively. SIMULATE calculated delta-I versus time follows the measured values to within about +3% / -1% after accounting for an initial bias of roughly -2%. SIMULATE critical boron values follow the measured values within about +14 ppm / -20 ppm after accounting for an initial bias of -34 ppm. SIMULATE calculated peak  $F(z)$  values are low by 0.01-0.04, but follow the trend well. Comparison of Figures 27 and 29 demonstrates that delta-I agreement based on calibrated ex-core detectors is a relatively good indicator of axial power shape agreement (represented by peak  $F(z)$  from in-core measurements).

# Figure 26



# Figure 27



# Figure 28

## S2C2 Load Follow Transient Critical Boron Comparison

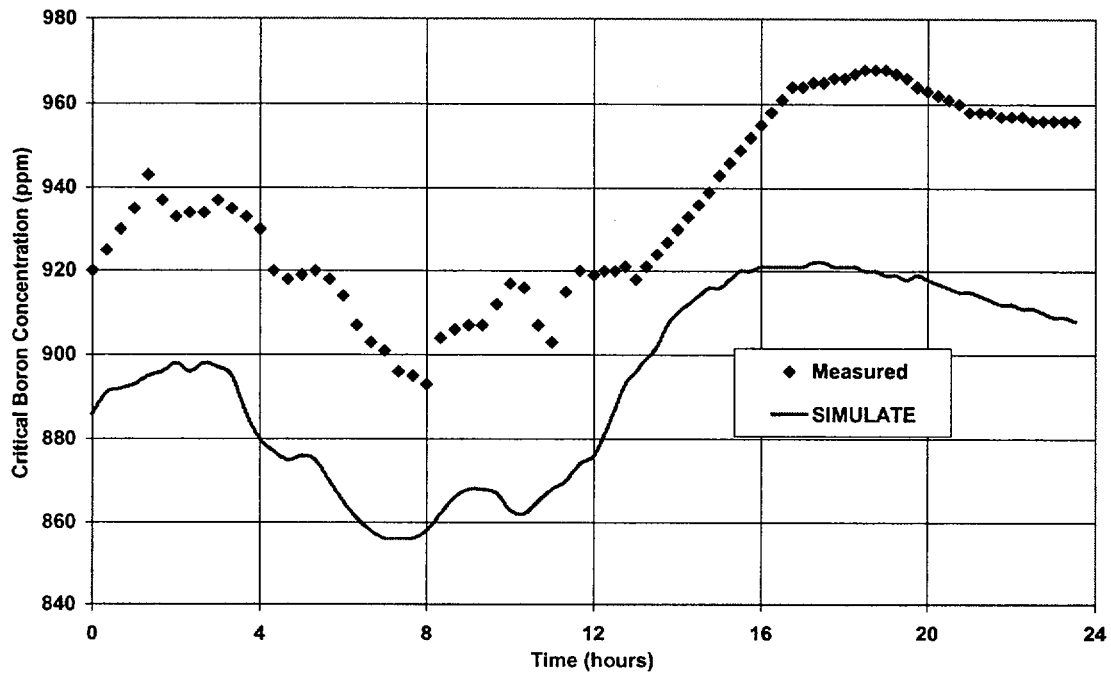
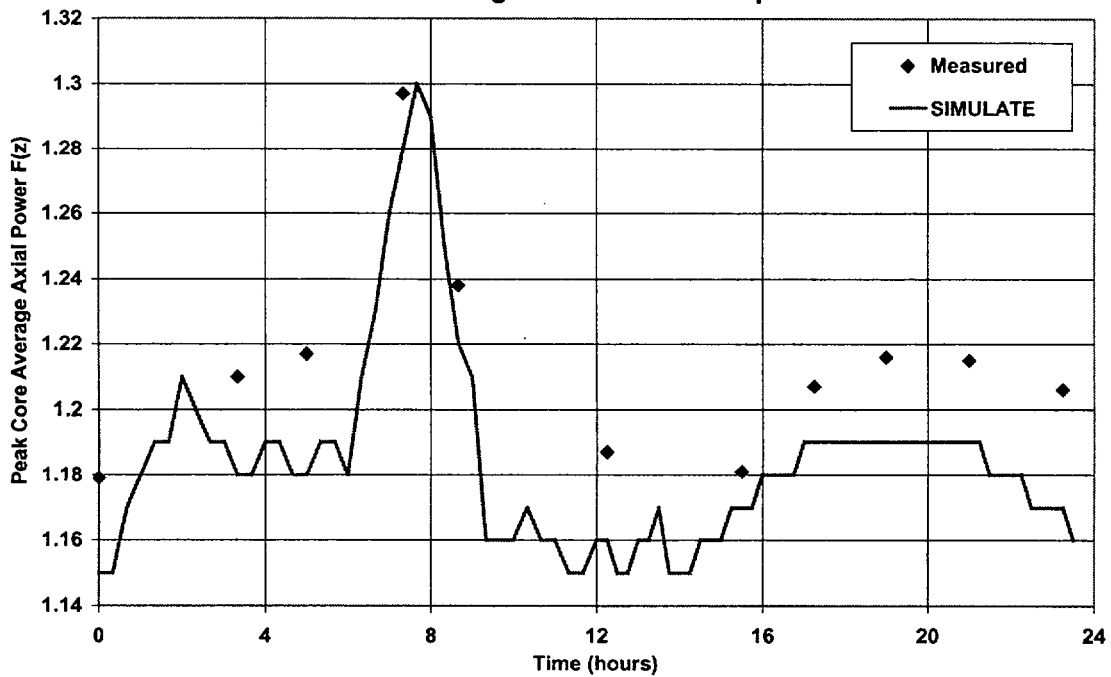


# Figure 29

## S2C2 Load Follow Transient Peak Core Average Axial Power Comparison



### **N1C3 Trip and Return to Power**

Two sets of measured data were recorded near the end of North Anna unit 1, Cycle 3 during power escalations following reactor trips. The first incident (transient 1) occurred on April 16-20, 1982, and the second (transient 2) on April 30 - May 2, 1982. Hourly readings of delta-I and eight critical boron measurements were taken during transient 1. During transient 2, both ex-core delta-I readings and in-core axial offset measurements were performed, because delta-I cannot be measured accurately at very low power levels. Note that in-core measurements were performed on only four or five assemblies each time and may therefore not be completely representative of core average behavior. The delta-I readings have been converted to axial offsets in order to compare SIMULATE results to both types of data.

Figure 30 provides the core power and D-bank position as a function of time for case 1. Figures 31, and 32 show the case 1 comparison of SIMULATE and measured delta-I and critical boron concentration respectively. Figure 33 provides the core power and D-bank position as a function of time for case 1. Figures 34, and 35 show the case 2 comparison of SIMULATE and measured delta-I and critical boron concentration respectively. The two N1C3 transients are very wide ranging in both reactivity (critical boron) and delta-I. For both transients the SIMULATE delta-I (or axial offset) and critical boron predictions are in excellent agreement with the measured data. In the transient 1 delta-I plot, a small difference that oscillates from positive to negative and back with a period of about 30 hours is apparent. This could be due to a pre-existing xenon oscillation.



Figure 30

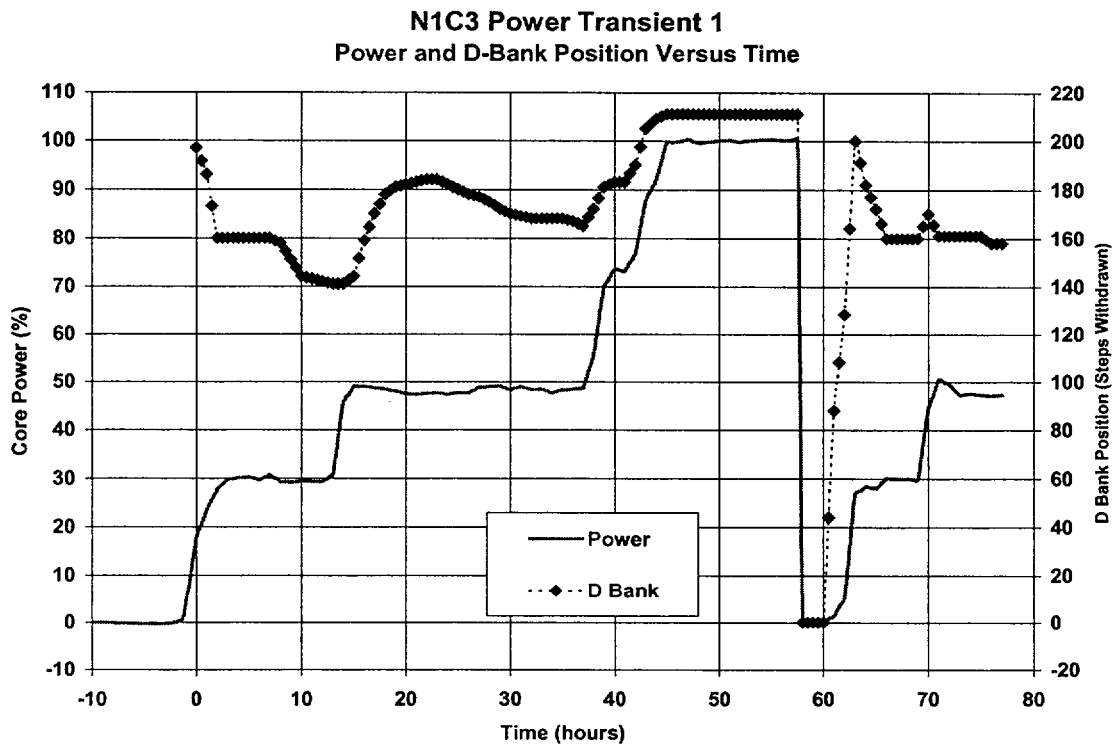
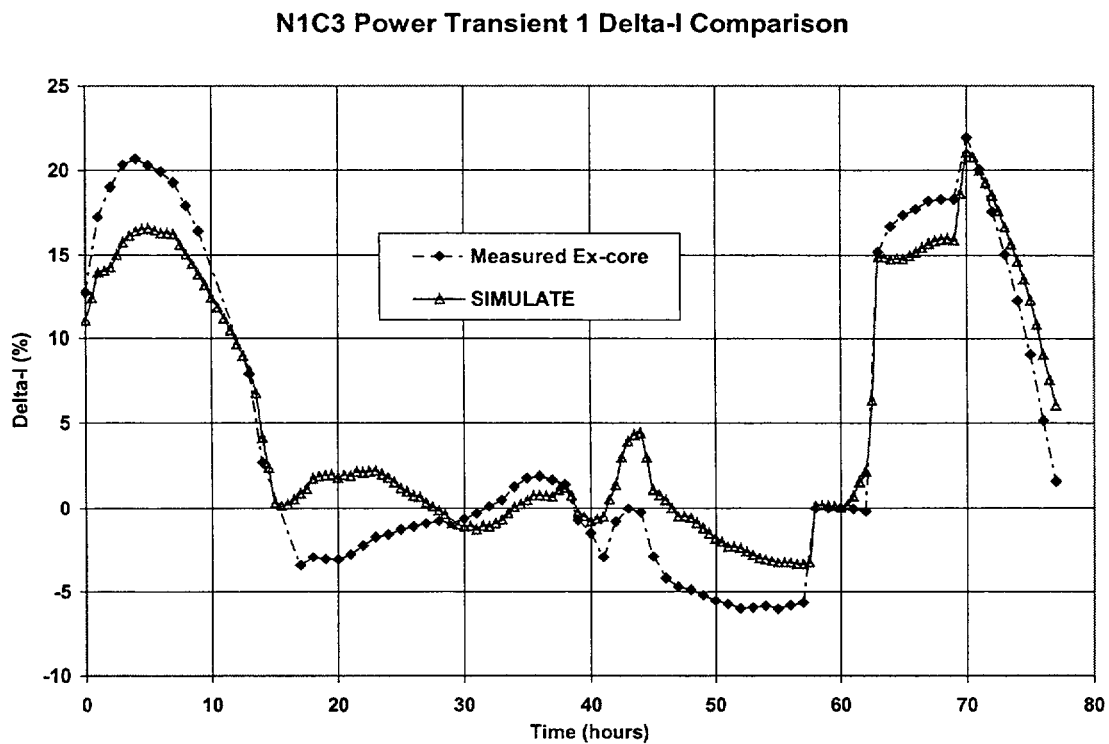
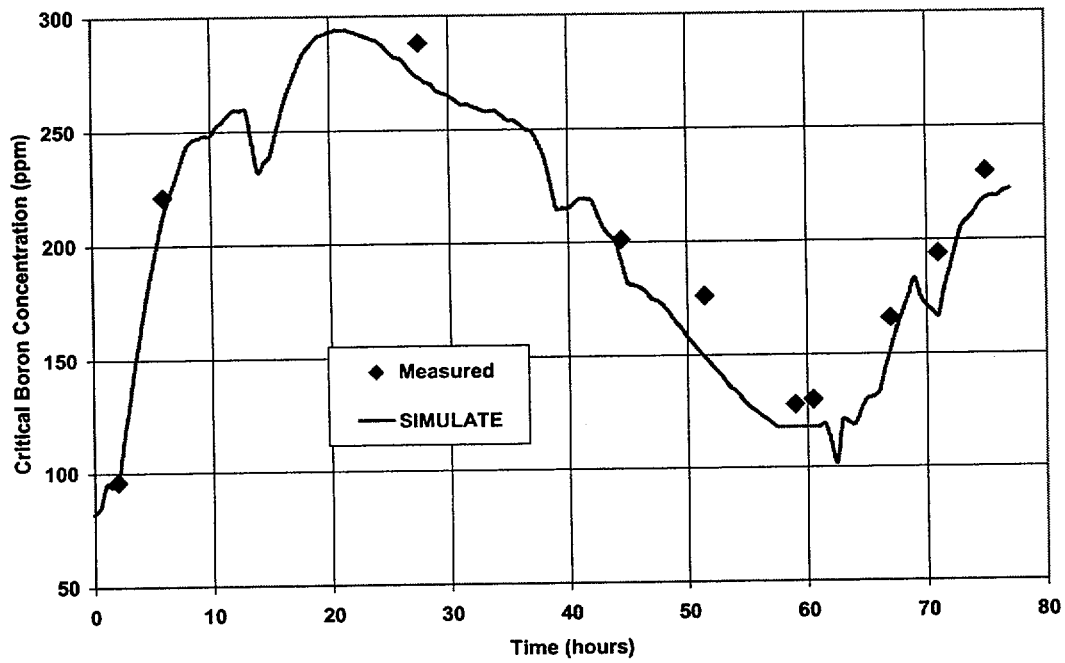


Figure 31



# Figure 32

## N1C3 Power Transient 1 Critical Boron Comparison



# Figure 33

## N1C3 Power Transient 2 Power and D-Bank Position Versus Time

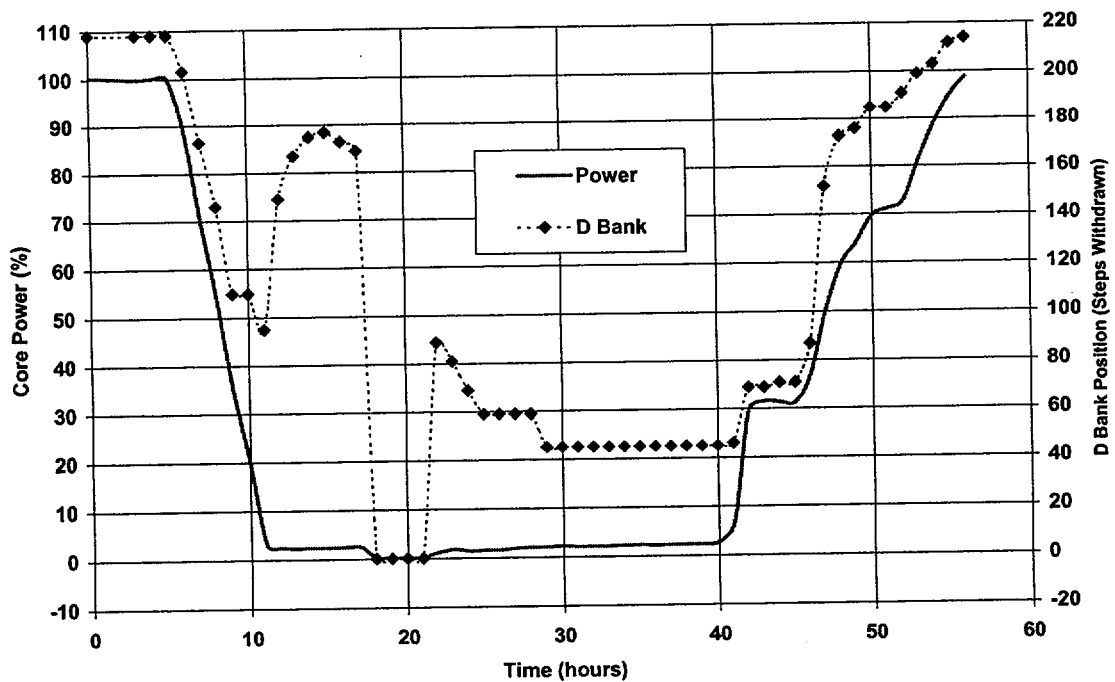


Figure 34

N1C3 Power Transient 2 Axial Offset Comparison

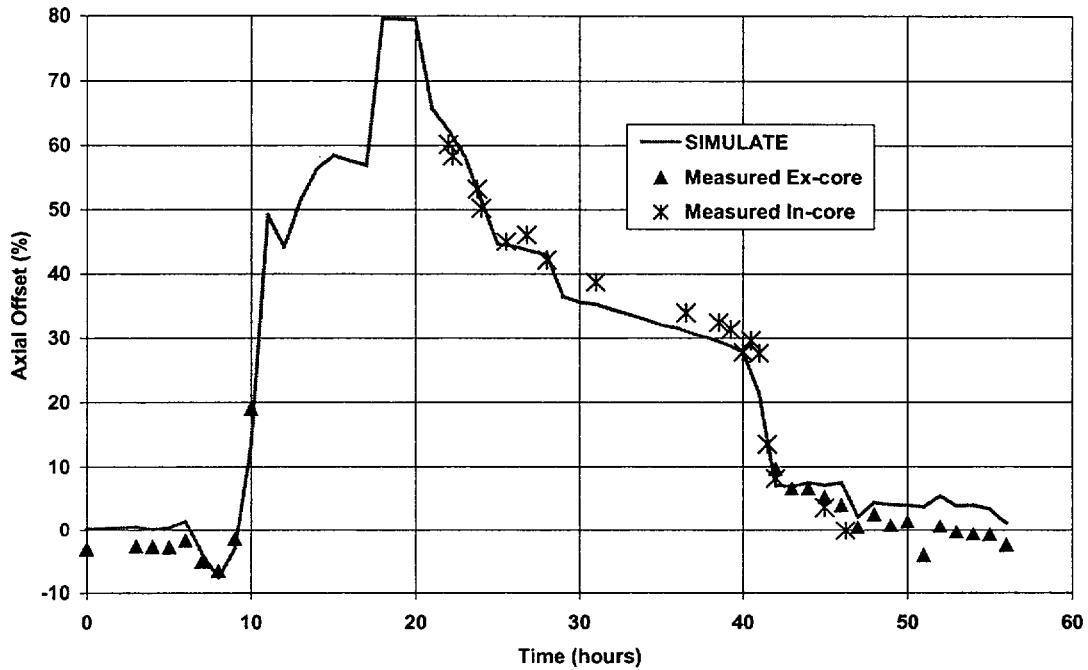
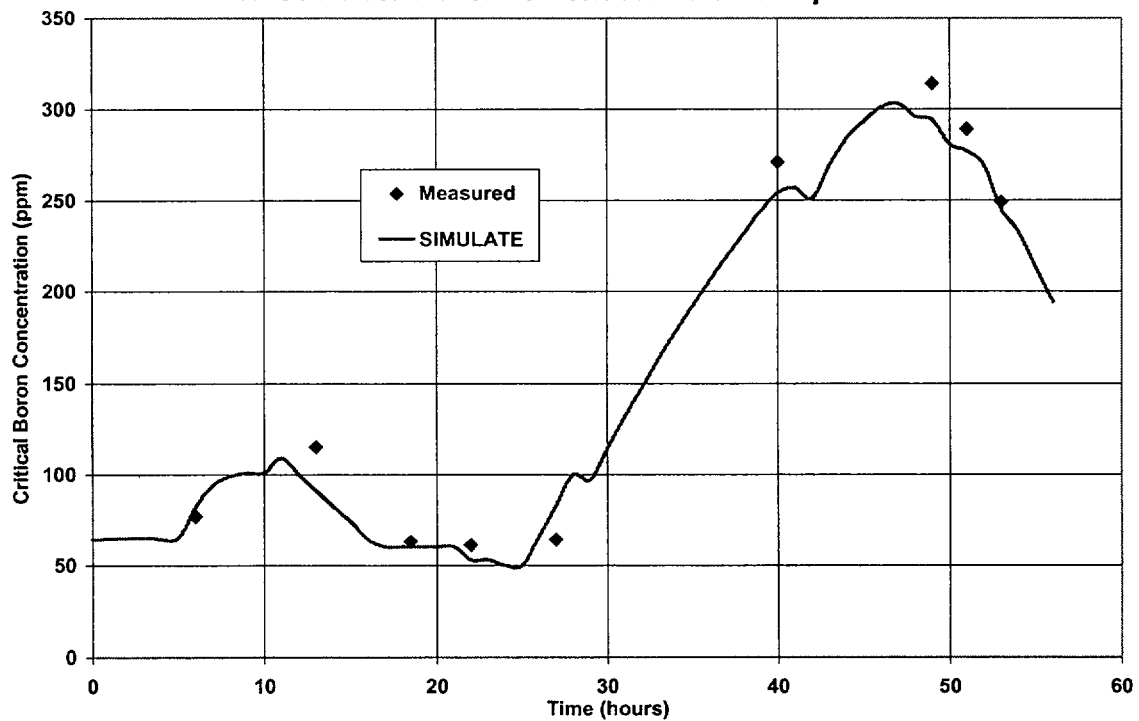


Figure 35

N1C3 Power Transient 2 Critical Boron Comparison



### **N1C6 Pipe Inspection**

During N1C6 operation, power was reduced from 100% to 20% during a secondary side pipe inspection on December 25 through December 29, 1986. The reactor was at HFP, ARO equilibrium conditions prior to the inspection. Power was reduced at a rate of about 15% per hour down to approximately 17% but was soon stabilized at 20% power. This power level proved to be low enough that the water flow through the pipe to be inspected could be stopped for the testing procedure. However, at 20% power with control rods deeply inserted, power was forced to the top of the core.

During this event, the axial power distribution changed dramatically due to changing thermal hydraulic feedback (core power changes), control rod insertion for both reactivity and axial power control, and an induced axial iodine and xenon transient. Figure 36 provides the core power and D-bank position as a function of time. Figures 37, and 38 show the comparison of SIMULATE and measured delta-I and critical boron concentration, respectively. SIMULATE calculated delta-I versus time follows the measured values to within about +2% / -3% after accounting for an initial bias of roughly +2%. SIMULATE critical boron values follow the measured values within about +18 ppm / -15 ppm after accounting for an initial bias of -24 ppm.

An interesting feature of this transient is the full-power xenon oscillation beginning at about 50 hours (see Figure 37). The measured delta-I indicates stable or slightly naturally damped behavior. The good agreement of the measured and predicted magnitude and timing of the axial oscillation over more than one full period indicates that the tradeoff of xenon and Doppler reactivity is in proper balance. If the Doppler feedback were too small the xenon oscillation would be divergent. If the Doppler feedback were too large, the xenon oscillation would damp out too rapidly.

# Figure 36

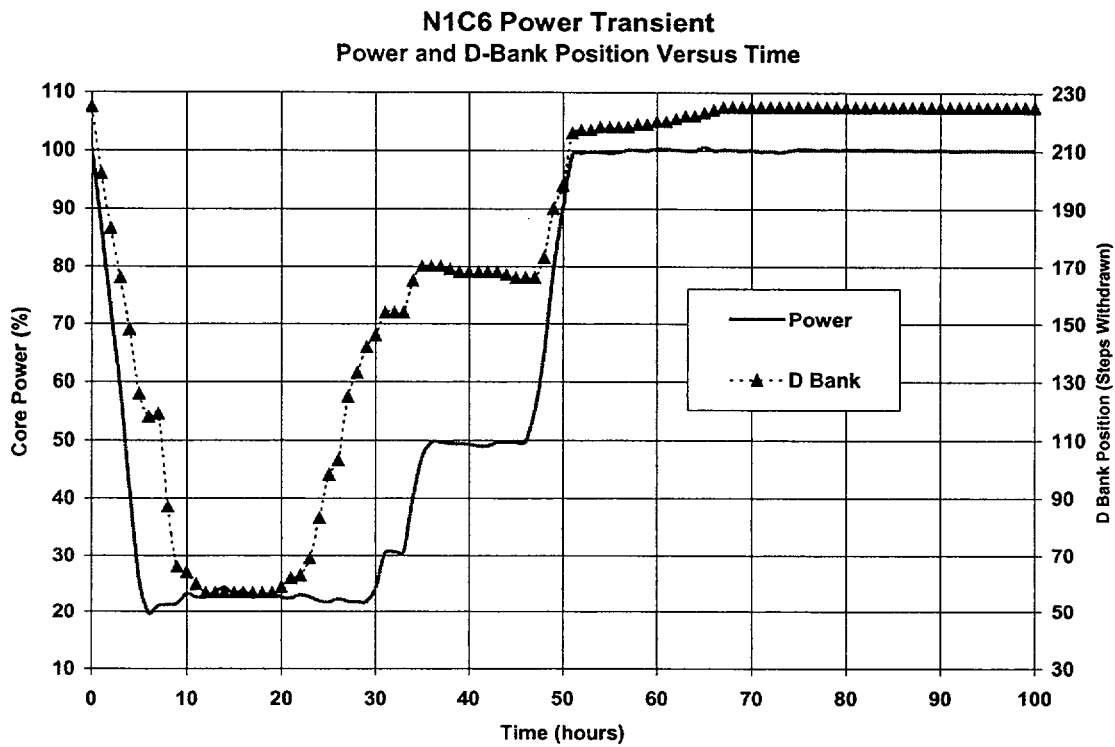


# Figure 37

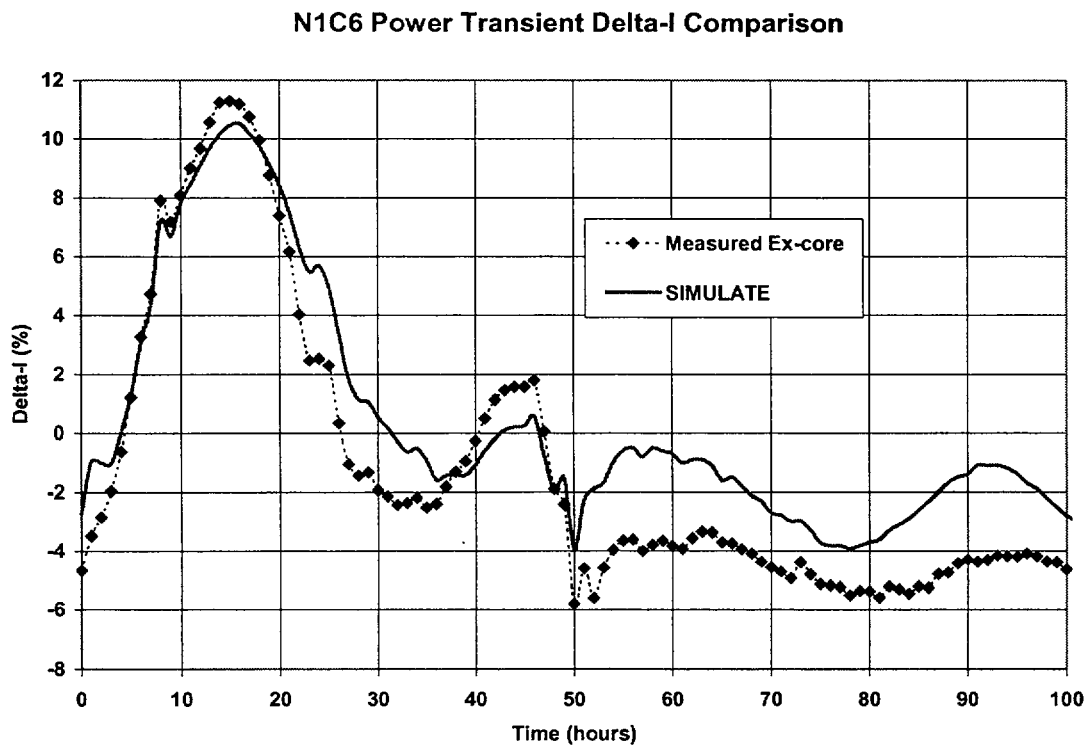
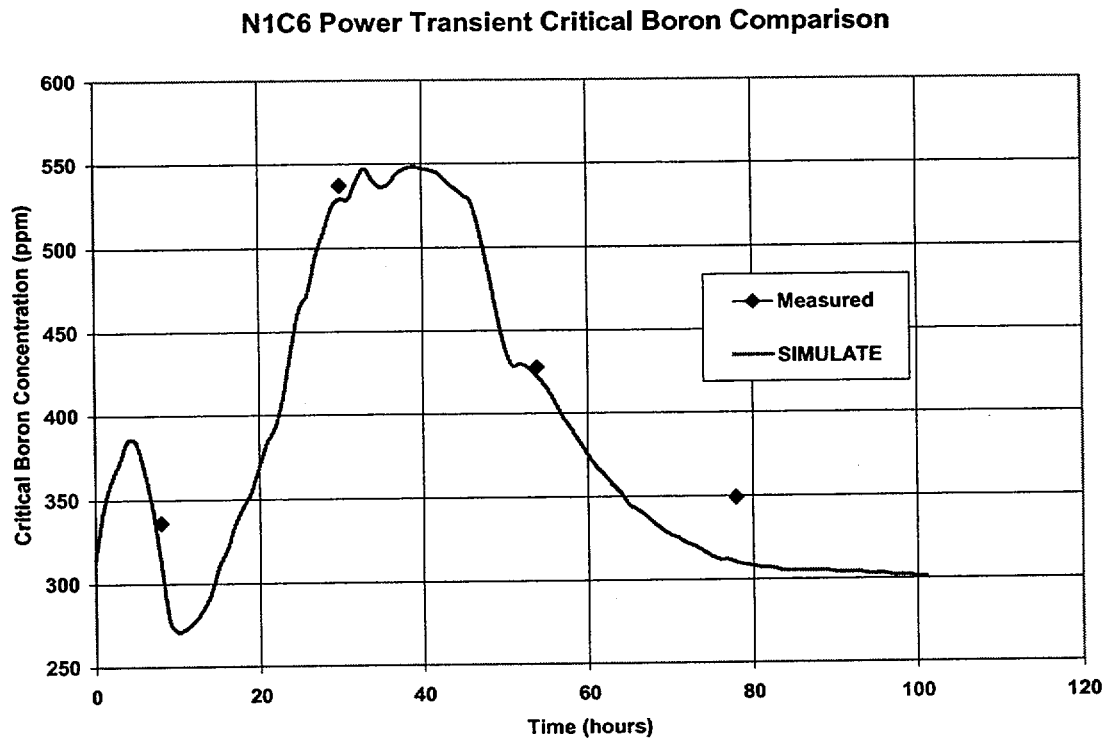


# Figure 38



### **N1C9 HFP MTC Measurement**

Modeling of the N1C9 HFP MTC measurement provides verification of the ability of SIMULATE to correctly calculate a moderator temperature driven axial transient in which no rod movement or significant power change occurs. Boron, temperature, and axial xenon effects are important contributors to this transient. The measurement was performed on 6/15/92 at 95% power.

Figure 39 provides the measured moderator inlet temperature and critical boron concentration versus time. Figure 40 shows the comparison of measured and predicted delta-I change versus time (set to zero at the beginning of the MTC measurement to eliminate bias). SIMULATE closely matches the measured delta-I change, indicating good performance of the Doppler, xenon, and moderator temperature components of the model.

Figure 41 shows the SIMULATE K-effective drift over time for each of the three statepoints of the MTC measurement (nominal, heatup, cooldown). Each statepoint is composed of four individual measurements. The reference K-effective for Figure 41 is the average SIMULATE K-effective for the four points in the nominal statepoint. Each statepoint represents a critical core condition with different combinations of individual reactivity components (primarily soluble boron and moderator temperature). Perfect agreement between measurement and prediction is indicated by eigenvalue drift of zero. SIMULATE eigenvalue drift for the individual measurements comprising the three statepoints varies from +5 pcm to -8 pcm. The maximum difference between statepoint averages is less than 7 pcm. This indicates that the tradeoff between soluble boron reactivity and HFP near EOC moderator temperature reactivity in SIMULATE closely matches the N1C9 core. The total reactivity worth for each component of this tradeoff (boron change and temperature change) is approximately 200 pcm.

In Section 3.3.4, the HZP BOC boron worth bias for SIMULATE was found to be negligible. Therefore, we can reasonably assume that the 7 pcm eigenvalue drift for the

HFP MTC measurement may be due to bias in the MTC. The core average moderator temperature change for this measurement between the first two statepoints is approximately 5 °F. Therefore for this measurement, the MTC difference between SIMULATE and measurement is approximately 7 pcm / 5 °F or 1.4 pcm/°F. The magnitude of this difference is consistent with the HZP ITC differences discussed in Section 3.3.3.



Figure 39

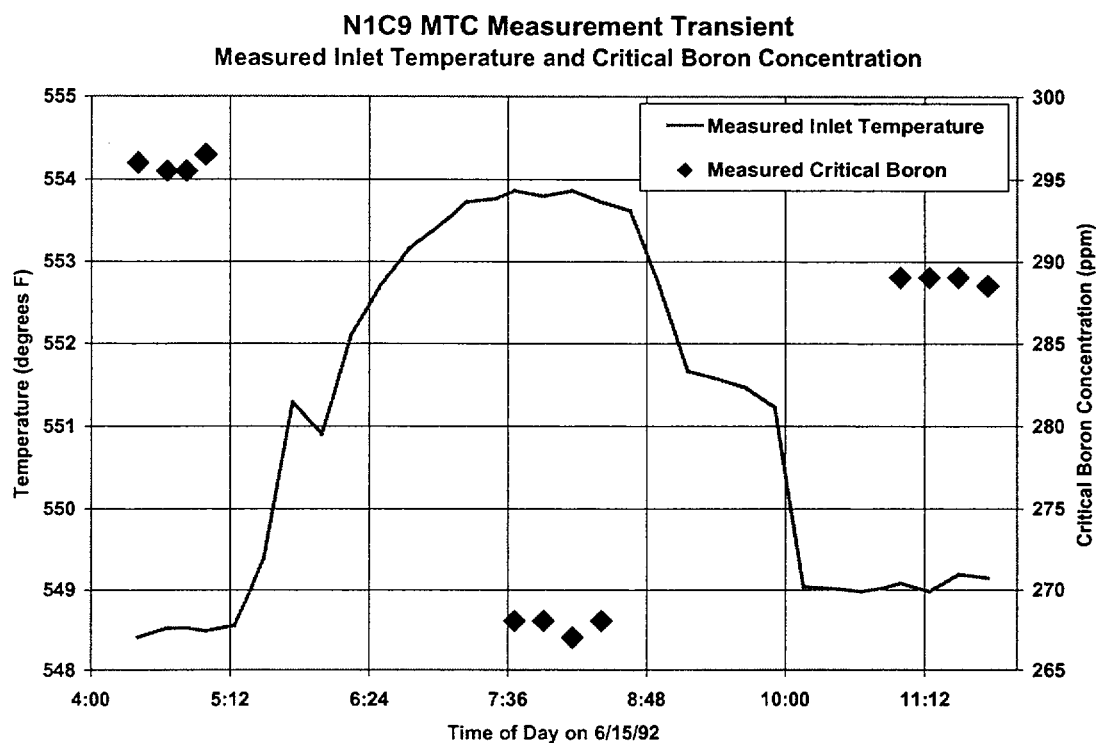
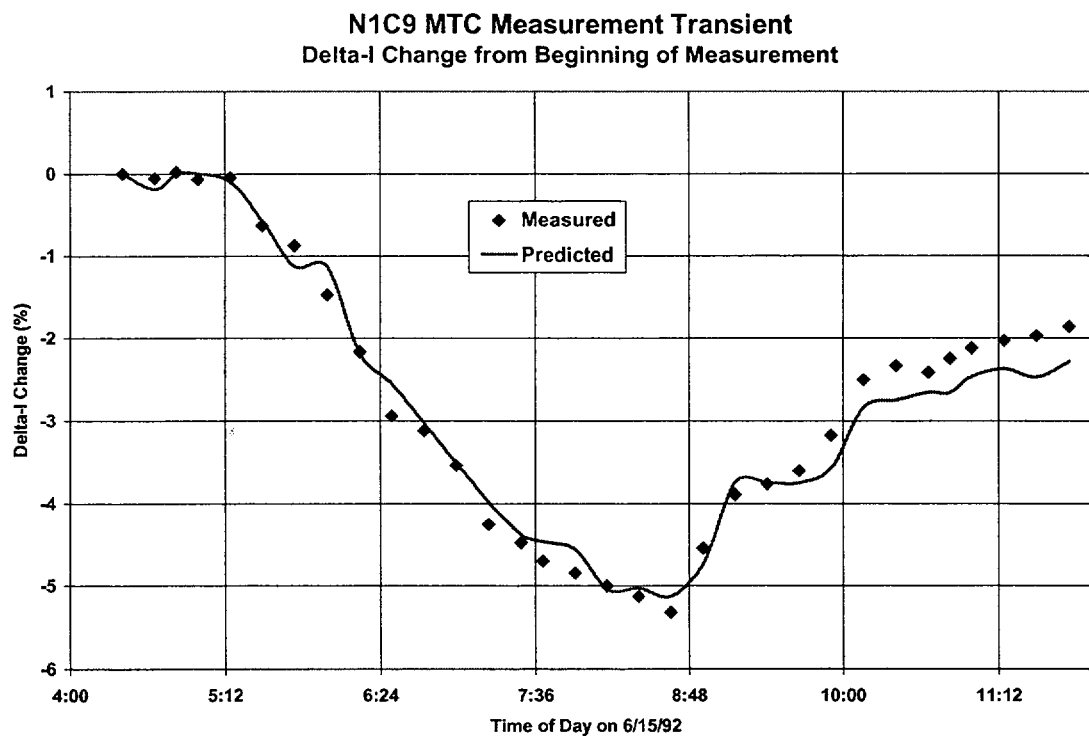
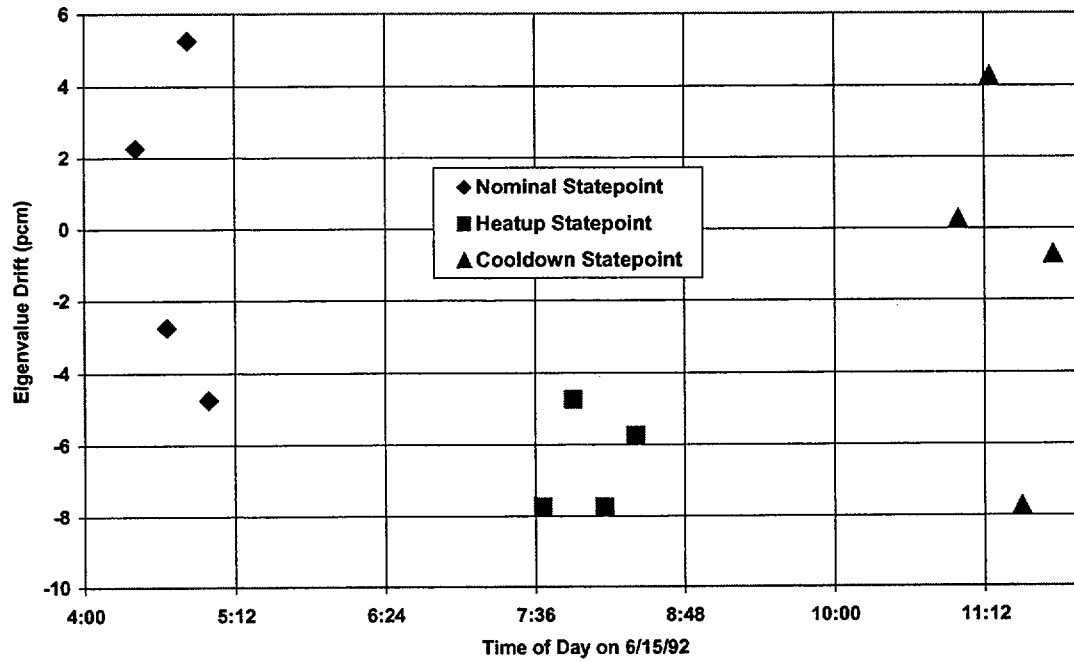


Figure 40



# Figure 41

N1C9 MTC Measurement Transient  
SIMULATE K-effective Drift



### **N1C11 Initial Power Ascension**

Modeling of the N1C11 initial power ascension is a test of many aspects of the SIMULATE model including thermal feedback (H2P-H2P), xenon (0 to equilibrium H2P), and control rods (D+C in overlap). Data collected on October 8-17, 1994 during startup physics testing was used for comparison of the measured and predicted delta-I and critical boron concentration during the transient. Figure 42 provides the core power and D-bank position as a function of time. Figures 43 and 44 show the comparison of SIMULATE and measured delta-I and critical boron concentration respectively. SIMULATE calculated delta-I versus time follows the measured values to within about  $\pm 2\%$ . SIMULATE critical boron values follow the measured values very closely (within +9 ppm / -13 ppm).

The N1C11 initial power ascension is of particular interest because full core flux maps were obtained during the power holds at 30% and 74% power (at approximately 21 and 75 hours, respectively). Figures 45-46 compare the measured and predicted core average axial power shapes ( $F(z)$ ) for the two initial power ascension maps. Agreement between measurement and prediction is excellent for both maps, which indicates that SIMULATE is capable of accurate power distribution calculations at low power, rodged configurations with changing xenon concentrations. Table 13 includes comparison statistics for measured and predicted flux thimble reaction rates for the two N1C11 maps. These data compare favorably with the data from all cycles discussed in Section 3.3.6.

# Figure 42

N1C11 Initial Power Ascension  
Power and D-Bank Position Versus Time

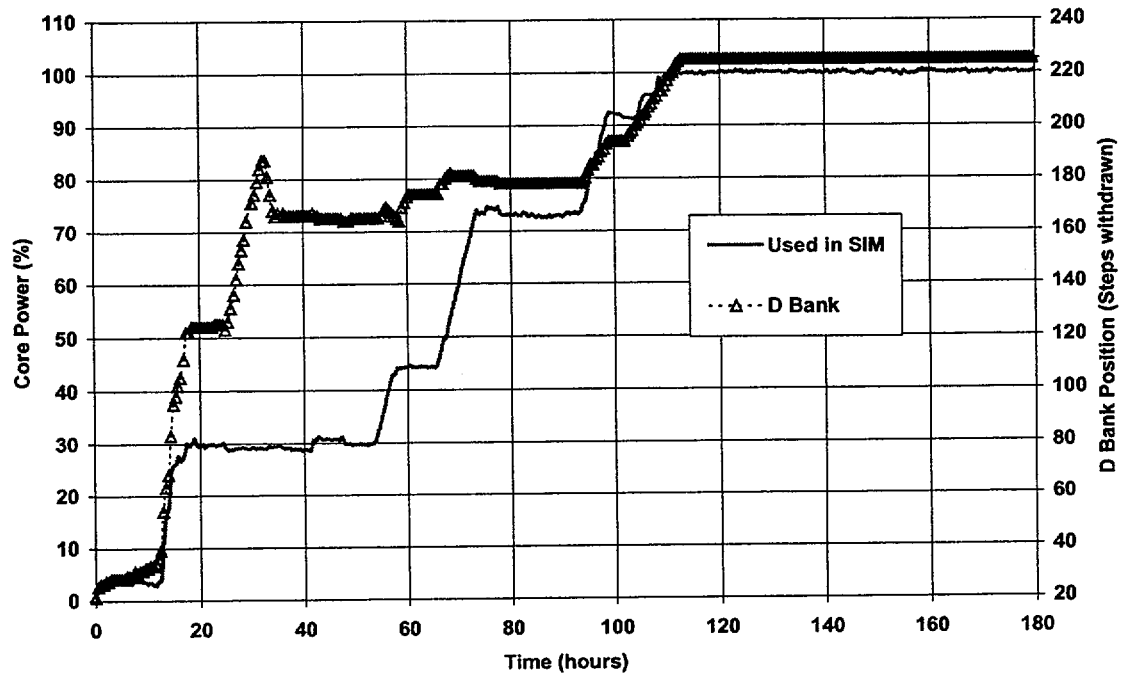


# Figure 43

N1C11 Initial Power Ascension Delta-I Comparison

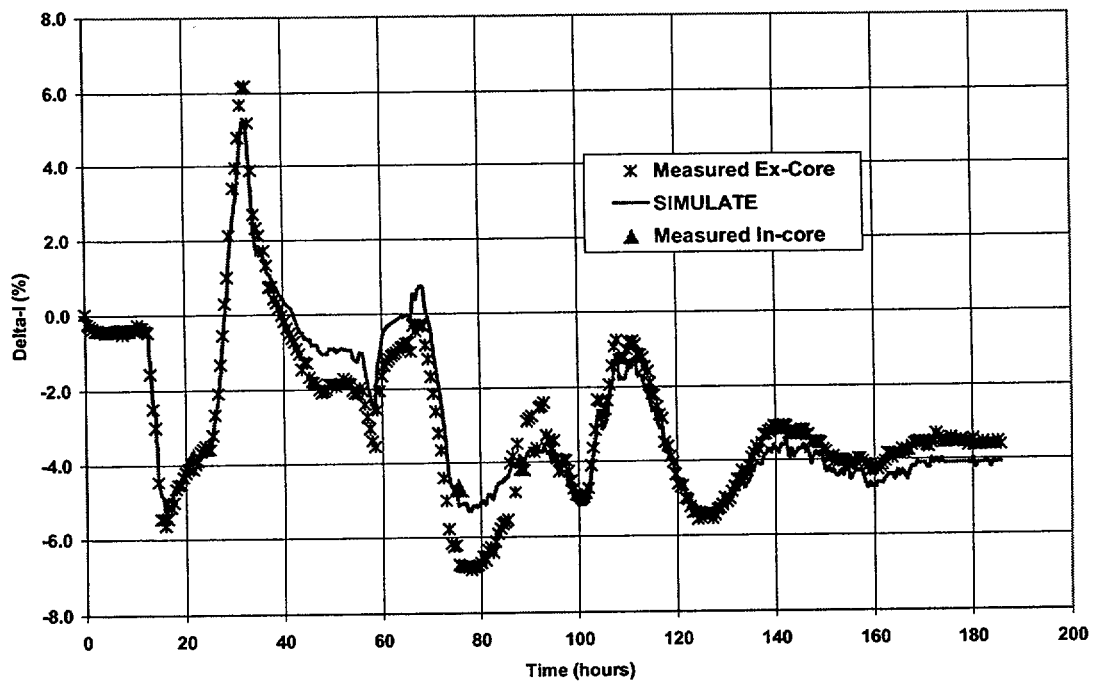


# Figure 44

## N1C11 Initial Power Ascension Critical Boron Comparison

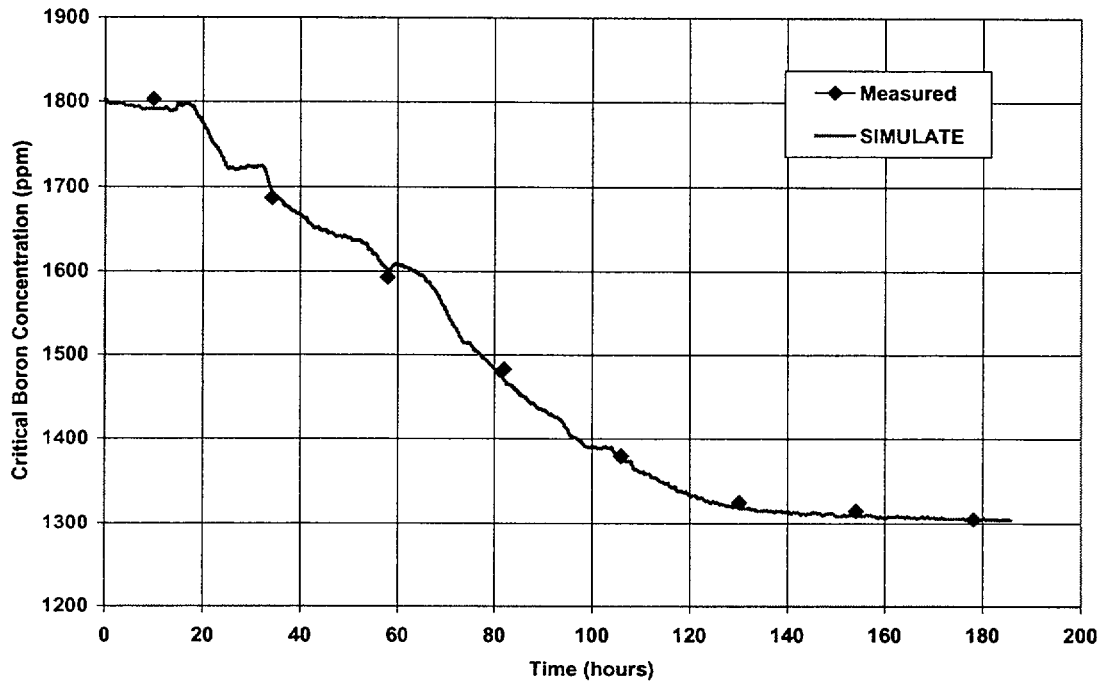


# Figure 45

## Core Average Axial Power Comparison N1C11 Flux Map 1, 29.9% Power, D@124

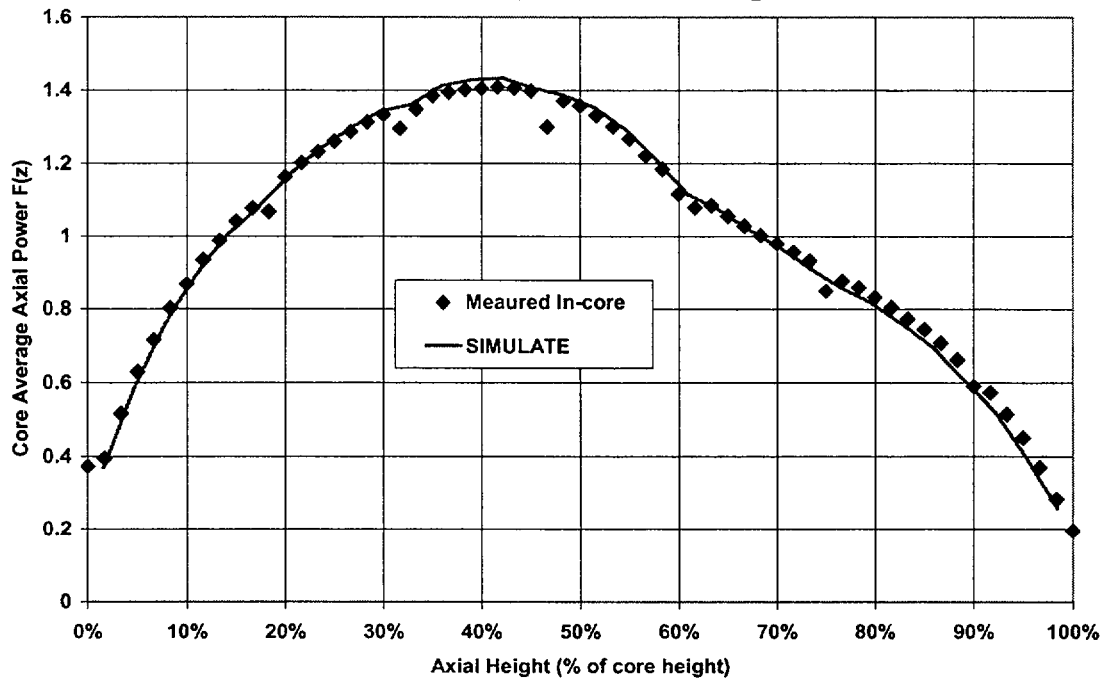


**Figure 46**

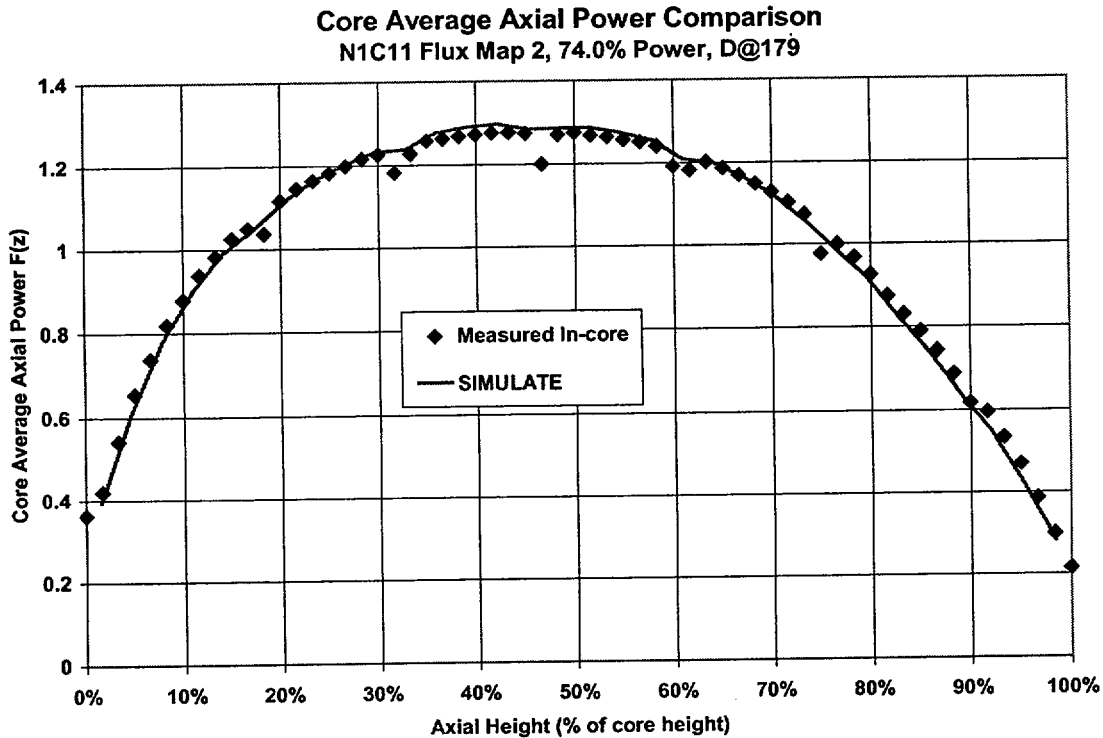


**Table 13**

**N1C11 Power Ascension Flux Map Reaction Rate Statistics**

Data Type	Mean (% Diff.)	Std. Dev. (% Diff.)	Number Of Obs.	Max. (%)	Min. (%)	Normal
Integral	0.4	1.8	61	4.1	-4.7	Yes
32 Node	0.2	2.2	1488	7.5	-6.1	No

**Note:** Reaction rate difference is  $((\text{Predicted} - \text{Measured}) / \text{Predicted}) \times 100\%$  for all normalized reaction rates  $> 1.0$ .

### **N2C14 Power Transient**

North Anna Unit 2 power was reduced from HFP equilibrium conditions to approximately 27% on 10/14/2000. After holding at low power for approximately 10 hours, a ramp to 100% over about 11 hours was initiated. Figure 47 provides the core power and D-bank position as a function of time. Figures 48 and 49 show the comparison of SIMULATE and measured delta-I and critical boron concentration respectively.

SIMULATE calculated delta-I versus time follows the measured values to within about  $\pm 5\%$ . This agreement is not as good as some other transients. One possible explanation is the extremely deep control rod insertions, which cause the ex-core detectors to be shadowed by C-bank between about 9 and 22 hours. Figure 48 shows SIMULATE delta-I results using both calorimetric (CAL) and ex-core nuclear instrumentation (NI) power. Below about 30% power, NI power is typically more accurate. Above 30% power, calorimetric power is considered more accurate. As shown in Figure 48, the difference is significant for the initial ramp down and for the period of low power operation (10-20 hours), but does not change the remainder of the transient.

SIMULATE critical boron values follow the trend in the measured values very closely, with a bias of about 60 ppm. The bias is attributable largely to a high degree of B-10 depletion due to low primary system leakage and very high load factor in N2C14.

A full-power undamped xenon oscillation begins at about 40 hours (see Figure 50). The measured delta-I indicates stable or slightly damped natural axial core power behavior. The good agreement of the measured and predicted magnitude of the axial oscillation over more than one full period is consistent with results from the N1C6 transient. The timing of the oscillation appears to be shifted by several hours. The reason for this shift is not known.

Results of a reduced moderator flow sensitivity case are presented in Figure 50. There is a strong correlation between the flow reduction (5%) and the change in the magnitude of the

positive and negative  $\delta I$  oscillation. These results are not intended to justify use of a value for core moderator flow rate other than measured, but are shown to demonstrate that uncertainty in the measured flow rate for the core is a significant source of uncertainty in transient modeling. The uncertainty in core moderator flow measurement is considered to be of the same order of magnitude as the calorimetric uncertainty (roughly 2%).



Figure 47

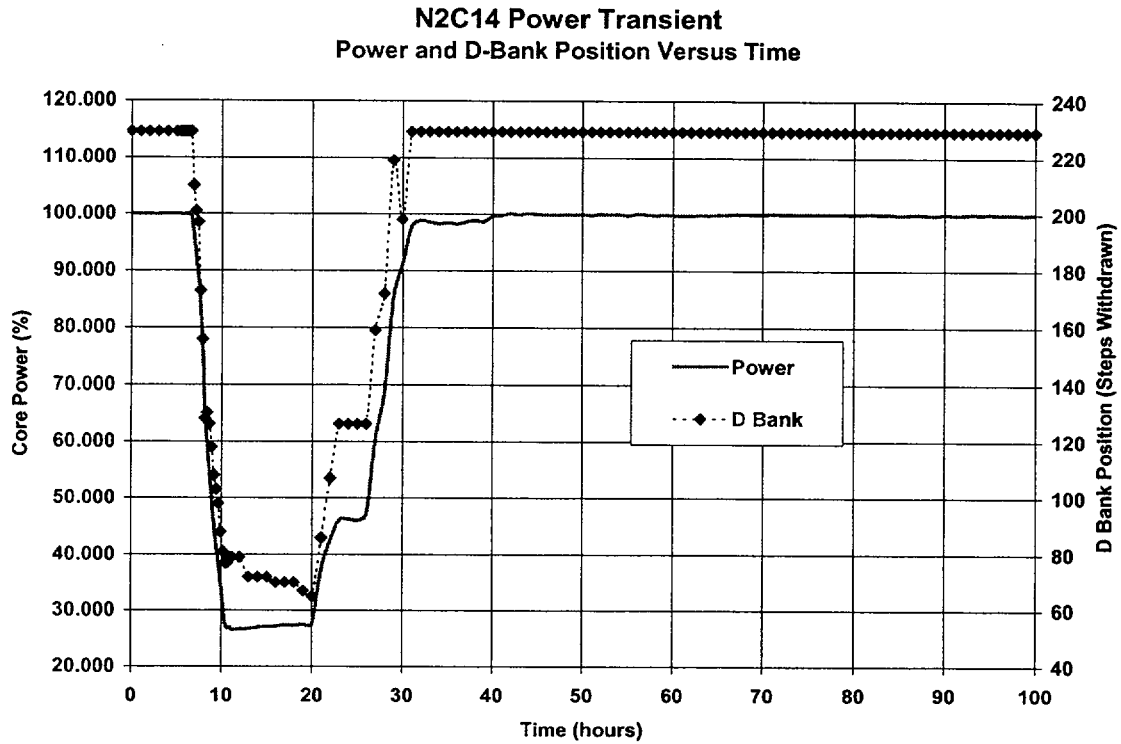
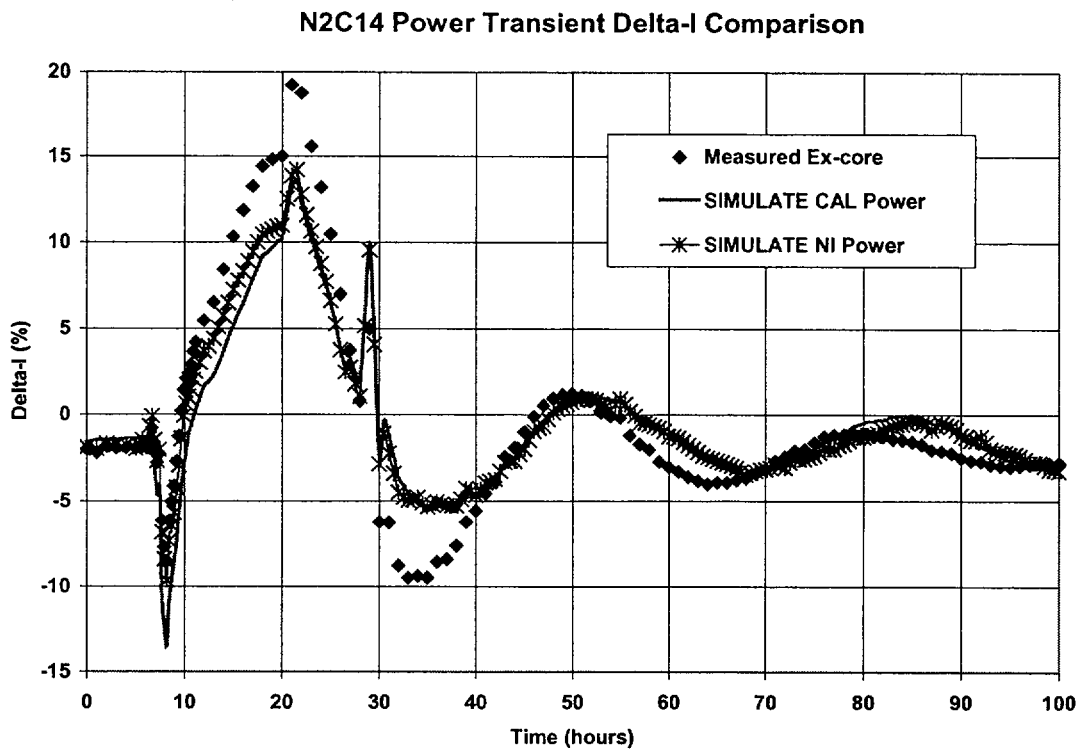
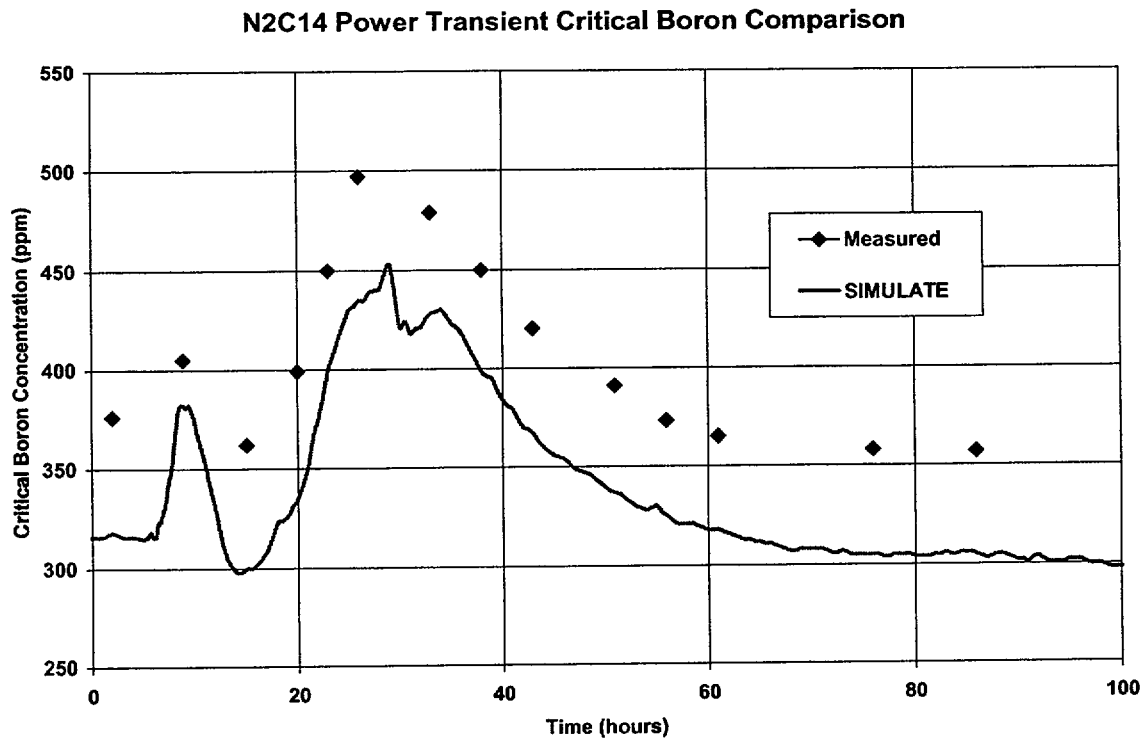


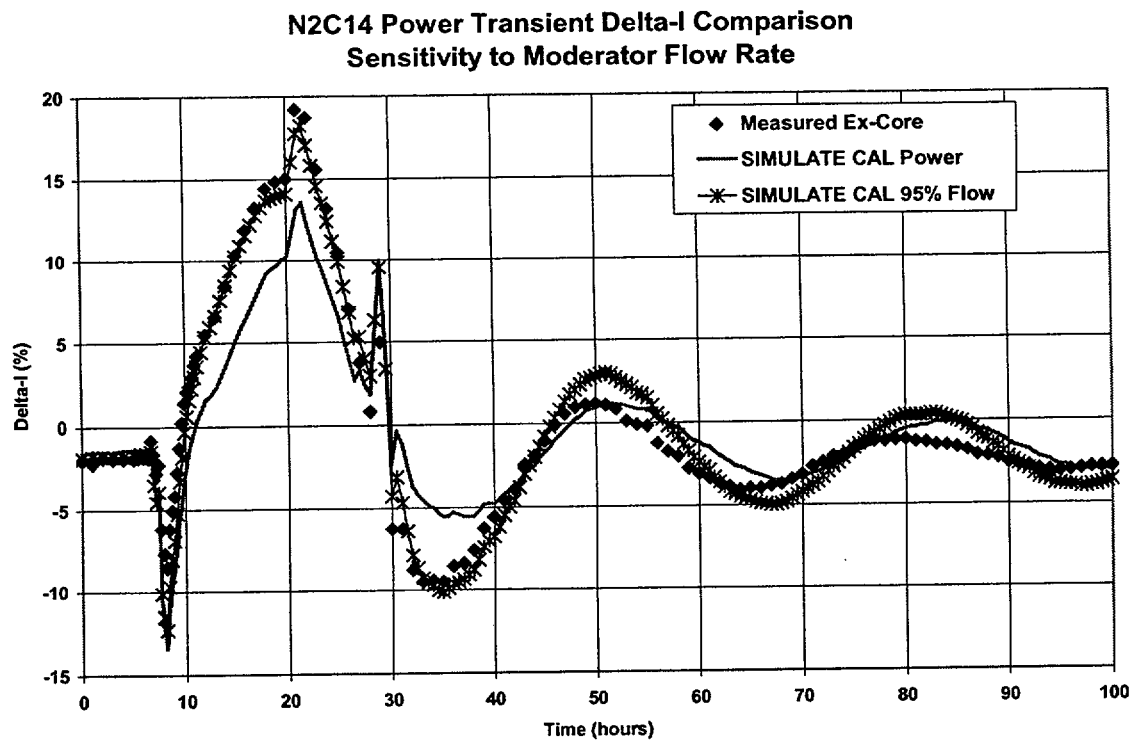
Figure 48



# Figure 49



# Figure 50



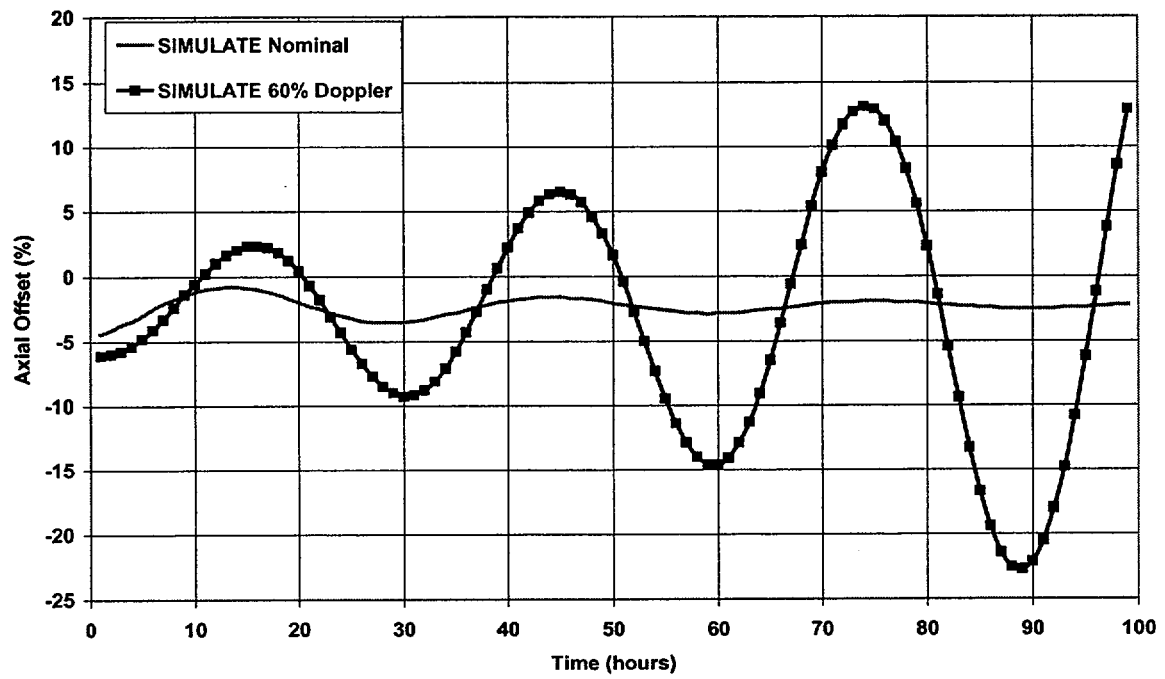
### **3.3.8 Xenon Oscillation Demonstration**

Verifying the ability of SIMULATE to accurately model plant transients provides evidence that SIMULATE can be used to verify acceptable design axial flux difference (AFD) operating bands via load follow simulations (FAC analysis) or via the free xenon oscillation technique (RPDC analysis, Ref. 11).

For RPDC analysis, axially skewed xenon distributions saved at different times during an unstable axial xenon oscillation are subsequently used to vary the axial power distributions for a matrix of core conditions at different power levels and control rod insertions. Instability is created by reducing Doppler feedback. This is normally accomplished by artificially changing the relationship between fuel rod power and fuel temperature. Figure 51 demonstrates an unstable xenon oscillation created using SIMULATE for the N1C15 core. Note that the nominal SIMULATE model is naturally damped, as is the actual core. The instability in Figure 51 was created by reducing Doppler feedback to 60% of nominal. Note that the change in Doppler feedback causes a large change in the amplitude of the xenon oscillation, but only a small change in the timing. This demonstration, coupled with the results presented in Section 3.3.7 shows that SIMULATE is fully qualified to perform FAC and RPDC analyses.

# Figure 51

N1C15 Xenon Oscillation Demonstration  
HFP, ARO 9000 MWD/MTU



## SECTION 4 – UNCERTAINTY AND RELIABILITY FACTORS

### 4.1 DEFINITIONS

Two terms will be discussed throughout this section. The Nuclear Uncertainty Factor (NUF) is defined as the calculational uncertainty for a core physics model parameter derived from a statistical analysis (where practical) of measurements and predictions of the parameter. If measurements are not available in sufficient quality or quantity to determine the NUF directly, comparisons can be made to higher order calculations, or the uncertainty can be inferred indirectly using observations of dependent quantities.

The Nuclear Reliability Factor (NRF) is defined as the allowance to be applied to a safety related core physics model design calculation to assure conservatism. For those parameters for which a NUF has been derived, the corresponding NRF is chosen to be equally conservative or more conservative than the NUF. A more complete description of the NRF including values approved for use in previous design models is provided in Reference 23.

Ideally, the NUF is determined such that when the NUF is applied to a model prediction, the result will be conservative compared to the corresponding measurement for 95% of the sample population with a 95% confidence level (when a sufficiently large sample population is available). The NUF is determined as a one-sided tolerance limit even for parameters for which both under and over-prediction may be important for safety analysis. A one-sided tolerance is acceptable for those parameters (such as differential boron worth) because the corresponding NRF is applied in the conservative direction for each analysis scenario. For example, if a boron dilution key analysis parameter is minimum boron worth and the differential boron worth NRF is 1.05 (max) / 0.95 (min), then the predicted differential boron worth is multiplied by 0.95. Another accident scenario may be sensitive to maximum boron worth. For that key parameter the predicted differential boron worth is multiplied by 1.05. Application of the NRF selectively as described meets the intent of 95% probability and 95% confidence. Some NRF's may be applied statistically

for safety evaluation calculations, but typically the application is for a one-sided parameter such as FQ, for which under-prediction is the only direction of concern.

It is important to note that when determining the NUF using comparisons of measurement and prediction, measurement uncertainty is inherently included in the statistically determined NUF. Measurement uncertainty can be of similar magnitude to the model uncertainty itself (see Section 3.3.4). Failure to address measurement uncertainty can lead to unreasonably large estimates of model predictive uncertainty. Approved NRF values for previous core design models are provided in Table 14.

### **Determination of the NUF from Tolerance Intervals**

In the statistics presented in Section 3.3, the sign convention used is such that a positive value indicates over-prediction of the magnitude of a parameter by SIMULATE, and a negative value indicates under-prediction by SIMULATE. The appropriate interpretation of the statistical data is therefore to determine an uncertainty factor in the opposite direction to be applied to SIMULATE predictions. For example, if a statistically determined tolerance interval for critical boron concentration is determined to be –35 ppm to +45 ppm, then the uncertainty factor to apply to predicted boron worth is +35 ppm when maximum boron concentration is conservative, and –45 when minimum boron concentration is conservative.

Similarly, statistics given in percent difference are defined as  $(\text{SIMULATE} - \text{Measured}) / \text{SIMULATE}$  in units of percent. The uncertainty factor in this case should be a multiplier on the SIMULATE value consistent with this definition. If a tolerance interval for a parameter is indicated to be –5% to +8%, then the appropriate multiplier range for SIMULATE predictions is 1.05 (when the maximum parameter estimate is desired) and 0.92 (when the minimum parameter estimate is desired).

**Table 14****Approved NRF Values for Previous Design Models**

<b>Parameter</b>	<b>NRF</b>	<b>Notes</b>
<b>Integral Control Rod Bank Worth (Individual banks)</b>	$\pm 10\%$	Multiply by 0.9 or 1.1, whichever is conservative.
<b>Integral Control Rod Bank Worth (Total of all banks)</b>	$\pm 10\%$	Bounded by individual bank NRF
<b>Differential Control Rod Bank Worth</b>	$\pm 2$ pcm/step	No current use.
<b>Critical Boron Concentration</b>	$\pm 50$ ppm	Add or subtract 50 ppm, whichever is conservative.
<b>Differential Boron Worth</b>	$\pm 5\%$	Inferred from dilution bank worth measurements
<b>Moderator Temperature Coefficient</b>	$\pm 3$ pcm/ $^{\circ}$ F	NRF is based on ITC measurements.
<b>Doppler Temperature Coefficient</b>	$\pm 10\%$	Not directly measured.
<b>Doppler Power Coefficient</b>	$\pm 10\%$	Not directly measured.
<b>Effective Delayed Neutron Fraction</b>	$\pm 5\%$	Not directly measured.
<b>Prompt Neutron Lifetime</b>	$\pm 5\%$	Not directly measured.
<b><math>F\Delta H</math></b>	1.05	One-sided multiplier.
<b>FQ</b>	1.075	One-sided multiplier. Includes bias for models with no explicit spacer grid modeling.

## 4.2 STATISTICAL METHODS

The difference between a predicted value,  $p_i$ , and a measured value,  $m_i$ , for the purpose of deriving the NUFs is defined as either

$$x_i = p_i - m_i$$

or

$$x_i = (p_i - m_i) \times 100\% / p_i$$

$x_i$  is assumed to be an observation of a distribution of size  $n$  whose mean  $x_m$  and variance  $\sigma^2$  are defined as:

$$x_m = \sum_{i=1}^n (x_i) / n$$

$$\sigma^2 = \sum_{i=1}^n (x_i - x_m)^2 / (n - 1)$$

In general,  $\sigma^2$  includes the statistical uncertainties due to both measurement and calculation. That is, the variance of  $x_i$  is given as

$$\sigma^2 = \sigma_m^2 + \sigma_c^2$$

Therefore, any standard deviation for calculational uncertainty is conservative since an additional margin for measurement uncertainty is included.

In deriving the NUFs, the assumption is made that individual cycle data may be pooled for a given nuclear unit because the data represents the same physical quantity for cores using essentially the same fuel design and undergoing similar operation. In addition, the measured data from various cycles has been derived using the same procedures and compared with predictions from the same computer code. Since the sister units of each station are of similar design, and fuel is often shuffled between sister units, analogous



arguments support the pooling of all cycle data for each station. These assertions are further supported by inspection of the descriptive statistics for cycles, which indicate that all cycle data for a given station are members of the same population.

Similarly, there is no reason to believe, based on Monte Carlo benchmarking (Section 3.1), that minor differences in geometry between 15x15 and 17x17 fuel designs cause Surry and North Anna statistical data to represent different populations. As with sister units for a station, the operational procedures and data measurement techniques for both stations are similar. For large samples, uncertainty factors derived from separate Surry and North Anna data support this assertion. For small samples, particularly those that do not pass normality tests, pooling was performed out of necessity because non-parametric methods cannot be used for very small samples.

Further reason to treat individual cycle data as a subset of a larger population is the process by which it will be treated for future use of the models. Uncertainty factors must be based on prior cycle benchmarking and applied to future cycle designs. It is not practical to determine unique uncertainty factors for each cycle design, because the choice of uncertainty factors for future cycles thereby becomes subjective.

The uncertainty factor is based on a one-sided upper tolerance limit  $TL$  defined as

$$TL = x_m + (K \times \sigma)$$

where  $K$  is chosen such that 95% of the population is less than the value of  $TL$ , applied in a conservative direction, with a 95% confidence level.

The value of  $K$  is most readily determined should the distribution, from which  $x_m$  and  $\sigma$  are derived, prove to be normal (Ref. 29). For those parameters whose uncertainty factor is derived from a population which is not assumed to be normal,  $TL$  is assumed to depend on the sample size  $n$ . In this case,  $TL$  is based on the  $m^{\text{th}}$  largest value in a ranking of the observations making up the distribution (References 26, 29).

Since no test for normality is foolproof, each having different strengths and weaknesses, the Kolmogorov-Smirnov (K-S) test previously used by Dominion (References 23, 30) has been supplemented by additional tests:

1. the Kuiper variant of the K-S test (Ref. 31),
2. the W test of Shapiro and Wilk (Ref. 32), and
3. the D' test of D'Agostino (Ref. 32).

Whereas the K-S and Kuiper tests were applied to samples of all sizes, the W test was applied only to samples of size 50 or less, and the D' test to sample sizes between 51 and 2000 inclusive.

The different normality tests were evaluated using samples whose normality or non-normality was known to a high degree of confidence. Included were normal samples of varying sizes, means and standard deviations generated by Monte Carlo methods. Consistent with the derivation of the nuclear uncertainty factors, all tests were performed for a 95% confidence level with a 0.05 level of significance being considered as adequate for the rejection of the assumption of normality.

As suspected, the various tests were not always in agreement in their rejection or non-rejection of some of the test samples. Of particular note, for the larger Monte Carlo generated normal distributions, the computed level of significance decreased with increasing sample size. The K-S and Kuiper tests occasionally demonstrated a type I error (rejecting the null hypothesis of normality when it is really true) for sample sizes greater than 100,000. Based on the nature of these tests, it is understandable that they might occasionally "fail" for such large sample sizes, as the probability of producing significant outliers by a random process increases with sample size.

The size of the Dominion data base for nodal reaction rates falls within such a large sample realm, leading to the suspicion that the conclusion that the reaction rate sample was not normal might be a type I error. Fortunately, in this realm the value of  $K$  for a non-

normal distribution converges with that derived for a normal distribution of similar mean and standard distribution.

### **4.3 DETERMINATION OF NUCLEAR UNCERTAINTY FACTORS**

The following sections will detail the derivation of NUFs for key core physics design parameters using the statistical methods described above. For parameters that cannot be directly evaluated using statistical techniques, the basis for arriving at conservative estimates for the NUF and NRF will be presented.

#### **4.3.1 Critical Boron Concentration**

Based on data presented in Table 5, the uncertainty factor for SIMULATE critical boron concentration predictions can be statistically determined. Table 15 presents upper and lower one-sided tolerance interval information (95% confidence) for North Anna data, Surry data, and combined data assuming normality. The NUF assuming normality was determined to be -19 /+39 ppm for the combined data. Therefore, use of the existing Table 14 NRF for critical boron concentration ( $\pm 50$  ppm) is conservative.

**Table 15**

**SIMULATE Critical Boron NUF**  
(Normality Assumed)

<b>Plant</b>	<b>Mean (ppm)</b>	<b>Std. Dev. (ppm)</b>	<b>Number Of Obs.</b>	<b>Std. Dev. Multiplier</b>	<b>Upper Tolerance Limit (ppm)</b>	<b>Lower Tolerance Limit (ppm)</b>
<b>North Anna</b>	-6.7	15.9	462	1.77	21	-35
<b>Surry</b>	-12.7	16.3	556	1.76	16	-41
<b>Combined</b>	-10.0	16.4	1018	1.76	19	-39

### 4.3.2 Integral Control Rod Worth

Based on data presented in Table 6, uncertainty factors can be statistically determined for the SIMULATE control rod worth predictions. Table 16 presents the upper and lower tolerance interval information (95% confidence) for North Anna data, Surry data, and combined data. Normality is assumed based on the results of tests as indicated in Table 6. Figure 52 is a plot of measured versus SIMULATE control rod worths along with upper and lower lines  $\pm 10\%$  about the SIMULATE worth. The measured and predicted values correlate well from very small rod worths to very large rod worths. The integral rod worth NUF range (a multiplier) for Surry and North Anna data combined was determined to be 0.911 to 1.062.

It is also useful to note that two sources of conservatism exist in the calculation of the rod worth NUF under either normality assumption. [

] In addition, an undetermined amount of other measurement uncertainty is inherently included in the measured versus predicted rod worth comparisons. Table 17 compares calculated and measured control rod worth for two pair of essentially identical cycles (N1C1/N2C1 and S1C1/S2C1). Minor differences in predicted rod worth are due to slight variations in as-built fuel enrichments. Measured rod worth differences are much larger than the slight predicted differences, which indicates the influence of measurement uncertainty (including reactivity computer bias). The calculated NUF is therefore estimated to be conservative for SIMULATE predicted rod worth uncertainty.

The NRF for integral rod worth in Table 14 of  $\pm 10\%$  (multiplier range 0.90 to 1.10) bounds the NUF and is therefore also conservative for SIMULATE integral rod worth calculations. No calculations have been performed to determine the NUF for total rod worth (the sum of all bank worths in the core). However, the uncertainty for the total rod worth cannot be larger than the uncertainty for individual banks, therefore a NRF of  $\pm 10\%$  (multiplier range 0.90 to 1.10) is also conservative for SIMULATE total rod worth calculations.

**Table 16**

**SIMULATE Integral Rod Worth NUF**  
(Normality Assumed)

<b>Plant</b>	<b>Mean (%)</b>	<b>Std. Dev. (%)</b>	<b>Number Of Obs.</b>	<b>Std. Dev. Multiplier</b>	<b>Upper Tolerance Limit (%)</b>	<b>Lower Tolerance Limit (%)</b>
<b>North Anna</b>	0.9	4.2	178	1.86	8.7	-6.8
<b>Surry</b>	1.8	4.2	184	1.85	9.6	-6.0
<b>Combined</b>	1.4	4.2	362	1.79	8.9	-6.2

Figure 52

Integral Control Rod Worth Comparison  
SIMULATE Versus Measured

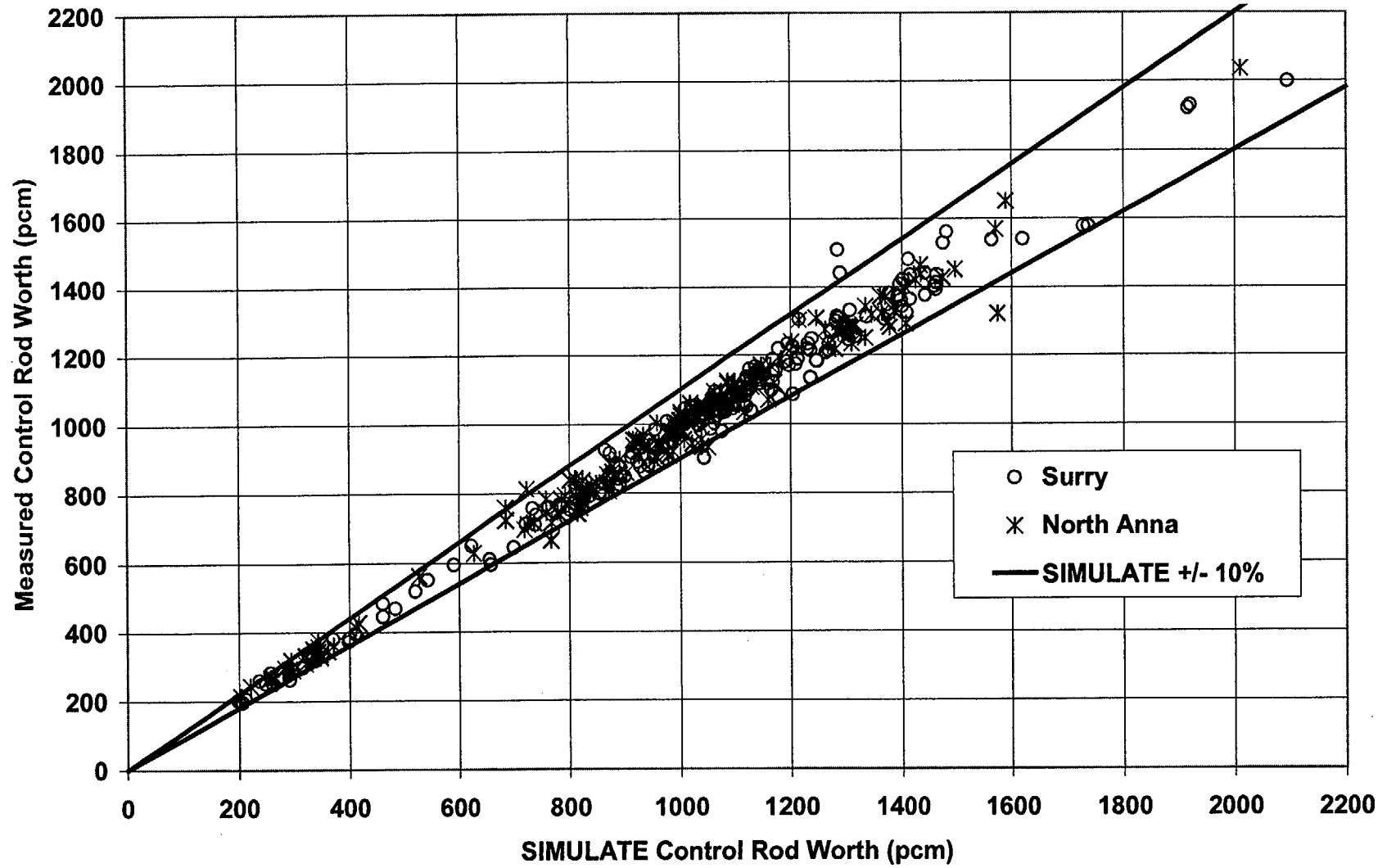




**Table 17**

**Rod Worth Measurement Uncertainty Estimate**

Cycle	Bank	Measured Worth (pcm)			Predicted Worth (pcm)		
		Unit 1	Unit 2	% Diff	Unit 1	Unit 2	% Diff
<b>North Anna Cycles 1</b>	D	1463	1437	1.8	1433	1434	-0.1
	C w/ D In	1303	1236	5.1	1215	1218	-0.3
	B w/ C+D In	2036	2002	1.7	2011	2017	-0.3
	A w/ B+C+D In	1309	1303	0.5	1246	1236	0.8
	SB w/ A+B+C+D In	1034	1046	-1.2	1037	1061	-2.3
		<b>Mean</b>		<b>1.6</b>	<b>Mean</b>		<b>-0.4</b>
		<b>Std. Dev.</b>		<b>2.3</b>	<b>Std. Dev.</b>		<b>1.1</b>
<b>Surry Cycles 1</b>	D	1480	1435	3.0	1411	1414	-0.2
	C	1300	1309	-0.7	1281	1285	-0.3
	B	1920	1929	-0.5	1916	1920	-0.2
	A	1440	1508	-4.7	1289	1284	0.4
		<b>Mean</b>		<b>-0.7</b>	<b>Mean</b>		<b>-0.1</b>
		<b>Std. Dev.</b>		<b>3.2</b>	<b>Std. Dev.</b>		<b>0.3</b>
<b>Combined</b>		<b>Mean</b>		<b>0.6</b>	<b>Mean</b>		<b>-0.3</b>
		<b>Std. Dev.</b>		<b>2.8</b>	<b>Std. Dev.</b>		<b>0.8</b>

### 4.3.3 Peak Differential Control Rod Worth

Based on data presented in Table 7, the uncertainty factor for peak differential rod worth can be determined statistically. Upper and lower one-sided tolerance limits based on Table 7 data are provided in Table 18. The existing Table 14 NRF for differential control rod worth of  $\pm 2$  pcm/step is not relevant (see discussion in Section 3.3.2). Based on this data, the NUF multiplier range is 1.10 to 0.79. Considering the significant amount of uncertainty involved in the measurement of the DRW, and the distribution of data shown in Figure 11, it appears to be prudent to set the NRF multiplier range at 1.15 to 0.8. This range bounds 90 of the 93 observations, with only one observation on each side exceeding this range significantly.

**Table 18**

**SIMULATE Peak Differential Rod Worth NUF**  
(Normality Assumed)

Plant	Mean (%)	Std. Dev. (%)	Number Of Obs.	Std. Dev. Multiplier	Upper Tolerance Limit (%)	Lower Tolerance Limit (%)
Combined	5.6	8.1	93	1.94	21.3	-10.2

#### 4.3.4 Isothermal Temperature Coefficient

Based on data presented in Table 8, the uncertainty factor for ITC can be determined statistically. Upper and lower one-sided tolerance limits based on Table 8 combined data are provided in Table 19. A NRF for ITC of  $\pm 2$  pcm/°F conservatively bounds the NUF of -1.9 / +0.7 pcm/°F and is therefore considered appropriate.

**Table 19**

**SIMULATE Isothermal Temperature Coefficient NUF**  
(Normality Assumed)

Plant	Mean (pcm/°F)	Std. Dev. (pcm/°F)	Number Of Obs.	Std. Dev. Multiplier	Upper Tolerance Limit (pcm/°F)	Lower Tolerance Limit (pcm/°F)
Combined	0.62	0.66	87	1.95	1.9	-0.7

#### 4.3.5 Differential Boron Worth

Based on data presented in Table 9, the uncertainty factor can be statistically determined for the SIMULATE DBW predictions. [

]

It is likely that boron measurement uncertainty, which has not been removed from the boron worth statistics, remains a significant source of uncertainty in these measurements. Boron measurement uncertainty in the determination of DBW was estimated to be as large as 8% in Section 3.3.4. Therefore, based primarily on the evidence of critical boron concentration difference data, a NUF and NRF of  $\pm 5\%$  (multiplier range of 1.05 to 0.95) is considered to be sufficiently conservative for SIMULATE differential boron worth predictions.

**Table 20**

**SIMULATE Differential Boron Worth NUF**  
(Normality Assumed)

<b>Plant</b>	<b>Data Adjustment</b>	<b>Mean (%)</b>	<b>Std. Dev. (%)</b>	<b>Number Of Obs.</b>	<b>Std. Dev. Multiplier</b>	<b>Upper Tolerance Limit (%)</b>	<b>Lower Tolerance Limit (%)</b>
<b>North Anna</b>	None	0.0	3.2	30	2.22	7.0	-7.0
<b>Surry</b>	None	0.3	4.2	35	2.17	9.3	-8.7
<b>Combined</b>	None	0.2	3.7	65	2.01	7.6	-7.3
<b>Combined</b>	[ ]	[ ]	[ ]	[ ]	[ ]	[ ]	[ ]

#### 4.3.6 Estimated Critical Position

Although there is no NRF for the ECP calculation, it is useful to develop uncertainty estimates based on the ECP data. ECP calculations involve all reactivity components of the SIMULATE model including control rod worth, xenon worth, power defect, and boron worth. The ECP uncertainty factor can be used as an estimator to make inferences about the maximum uncertainty associated with those components. Since uncertainty factors have been developed separately for at least three of the reactivity components (boron worth, control rod worth and moderator temperature coefficient via the ITC statistics), the remaining components can be approximated.

Table 21 presents the upper and lower tolerance interval information (95% confidence) for North Anna data, Surry data, and all ECP data combined. Normality is assumed based on the results of normality tests shown in Table 10.

A very crude approximation of the combined uncertainty of SIMULATE xenon and Doppler worth can be performed as follows. Using the assumption of normality, the major contributions to ECP uncertainty (variance) can be expressed as shown in Equation 3.

$$\sigma^2_{ECP} = \sigma^2_{Xe} + \sigma^2_{DPD} + \sigma^2_{MTD} + \sigma^2_{RW} + \sigma^2_{BW} + \sigma^2_{BC1} + \sigma^2_{BC1} \quad (\text{Eqn. 3})$$

The components, converted into units of pcm by weighting with typical reactivity contributions to the ECP calculation, are defined as follows:

$\sigma_{ECP}$  - combined standard deviation for ECP calculations from all sources  
(Table 21)

$\sigma_{Xe}$  - standard deviation associated with SIMULATE xenon change

$\sigma_{DPD}$  - standard deviation associated with SIMULATE Doppler defect

$\sigma_{MTD}$  - standard deviation associated with SIMULATE moderator defect

- $\sigma_{RW}$  - standard deviation associated with SIMULATE rod worth change
- $\sigma_{BW}$  - standard deviation associated with SIMULATE boron change
- $\sigma_{BC1}$  - standard deviation associated with at-power boron measurement
- $\sigma_{BC2}$  - standard deviation associated with zero power boron measurement

Using uncertainty estimates from previous sections, approximate values can be substituted into Equation 3 for ECP as indicated in Table 22. Note that most of the “typical” ECP reactivity components can vary widely depending on time in cycle life, outage duration, and outage recovery strategy. Substituting the estimated quantities into Equation 3 and rearranging terms results in Equation 4:

$$\sigma_{Xe}^2 + \sigma_{DPD}^2 = (124^2 - 40^2 - 40^2 - 87^2 - 21^2 - 23^2) = 60^2 \quad (\text{Eqn. 4})$$

The total Doppler change from HFP to HZP is on the order of 1000 pcm for all ECPs, and the xenon worth change can range from about +3500 pcm to –1500 pcm depending on the elapsed outage time. If the remaining 60 pcm standard deviation is assumed to be equally distributed between the Doppler defect and the xenon worth change, then the uncertainty of the Doppler component can be estimated. Using a standard deviation multiplier of 1.65, the Doppler uncertainty is estimated to be 1.65 x 30 pcm / 1000 pcm or 5%.

**Table 21**

**SIMULATE Estimated Critical Position NUF**  
(Normality Assumed)

Plant	Mean (pcm)	Std. Dev. (pcm)	Number Of Obs.	Std. Dev. Multiplier	Upper Tolerance Limit (pcm)	Lower Tolerance Limit (pcm)
North Anna	22	107	38	2.15	252	-208
Surry	42	142	33	2.19	353	-269
COMBINED	31	124	71	1.99	278	-216

**Table 22**

**Approximate Uncertainty Components for ECP Calculations**  
(Normality Assumed)

Component	Typical ECP variable change	Std. Dev.	Std. Dev. (pcm)
Control rod worth (From Table 6)	500 pcm	4.2 %	21
Boron worth (From Table 9; 8 pcm/ppm assumed)	350 ppm	3.1 %	87
Boron measurement (2 per ECP; 8 pcm/ppm assumed)	N/A	5 ppm	40
MTD (From Table 8)	35 °F	0.66 pcm/°F	23
Total (From Table 21)	N/A	N/A	124



#### 4.3.7 Reaction Rate Comparisons

Based on data presented in Table 12, the uncertainty factor can be statistically determined for the SIMULATE flux thimble reaction rate predictions. Although histograms of the reaction rate differences (%) appeared well distributed, the hypothesis of normality was rejected. Table 23 presents the one-sided upper tolerance interval information (95% confidence) for North Anna data, Surry data, and combined data for both integral and 32 node reaction rates assuming non-normality.

In order to use the data from Table 23 to determine NUFs for predicted  $F\Delta H$  and FQ, the tolerance limits must be combined with the CASMO/SIMULATE pin-to-box uncertainty factor from Section 3.1. Assuming that the reaction rate predictive uncertainty is independent of the Table 4 factors, the combination is performed by calculating the square root of the sum of the squares of the individual components (RSS). Table 24 presents the resulting  $F\Delta H$  and FQ NUFs.

The  $F\Delta H$  data supports a NUF of 1.03. This value is less than the 1.05 NRF approved for previous models (see Table 14) and reflects both improved modeling techniques (CASMO transport theory versus PDQ diffusion theory, 3D modeling in full core geometry, modeling of detector cross section variations in 3D, etc.) and a much larger database of reaction rate comparisons. A NRF for  $F\Delta H$  of 1.04 is therefore conservative. The FQ NRF approved for previous models is 1.075 (7.5%). However, this value included a bias of about 2.5% to account for grid effects. Previous models did not include a grid model that could account for the effect of grids on the axial power shape. The SIMULATE FQ NUF of 1.05 corresponds to a new NRF of 1.05. Use of SIMULATE with an FQ NRF of 1.05 (with no additional grid bias) is analogous to use of the previous NRF of 1.075 with prior models with no axial grid model.

**Table 23**

**SIMULATE Reaction Rate NUF**  
(Non-normality Assumed)

Plant	Data Type	Mean (%)	Std. Dev. (%)	Number Of Obs.	Limiting Tolerance Value	One Sided Tolerance Limit (%)
North Anna	Integral	-0.02	1.34	3453	150	-2.23
Surry	Integral	0.07	1.34	2322	98	-2.35
COMBINED	Integral	<b>0.01</b>	<b>1.34</b>	<b>5775</b>	<b>257</b>	<b>-2.25</b>
North Anna	32 Node	0.14	2.41	93070	4273	-3.96
Surry	32 Node	0.38	2.79	64354	2952	-4.53
COMBINED	32 Node	<b>0.24</b>	<b>2.58</b>	<b>157424</b>	<b>7233</b>	<b>-4.17</b>

**Table 24**

**SIMULATE FΔH and FQ NUF**

Plant	Data Type	Reaction Rate Tolerance Limit (Table 23)	[   ]	Combined Tolerance Limit (%)
North Anna	Integral / FΔH	-2.23	[   ]	-3.0
Surry	Integral / FΔH	-2.35	[   ]	-3.1
COMBINED	Integral / FΔH	<b>-2.25</b>	[   ]	-3.0
North Anna	32 Node / FQ	-3.96	[   ]	-4.4
Surry	32 Node / FQ	-4.53	[   ]	-5.0
COMBINED	32 Node / FQ	<b>-4.17</b>	[   ]	-4.6

#### 4.3.8 Doppler Coefficients and Defects

As discussed in a prior submittal (Ref. 23) direct determination of the NRF for Doppler feedback is very difficult. A value of 1.10 for the Doppler Temperature Coefficient and Doppler Power Coefficient was proposed in that submittal and accepted following NRC review. Although it is still very difficult to directly determine Doppler feedback uncertainty, there are three indirect indications (in addition to the development in Section 4.3.6) that support continued use of a  $\pm 10\%$  NRF (multiplier range 1.10 to 0.90):

- 1) Benchmarking of CASMO Doppler Temperature Defects to monte carlo methods enables a best-estimate correction to be performed that effectively eliminates the theoretical CASMO Doppler bias (as determined using higher order calculations) from the SIMULATE model.
- 2) Critical boron data from Sections 3.3.1 (BOC HZP and HFP critical boron data), 3.3.5, and 4.3.6 (ECP data) suggests that total Doppler feedback (HFP to HZP) is well predicted. Comparison of the mean biases for HZP and HFP BOC critical boron concentration shows only a 3 ppm (roughly 20 pcm) difference. ECP data spanning all times in core life also shows little HFP-HZP bias (31 pcm in the same direction as the critical boron bias). There are three significant reactivity components involved in the HZP-HFP statepoint transition: Doppler temperature defect, moderator temperature defect, and xenon build-in (all offset by reduced boron concentration). The data cited above indicates, at a minimum, that the sum of these factors is well predicted, and therefore that the Doppler defect is probably well predicted.
- 3) Several of the operational transients modeled in Section 3.3.7 included undamped xenon oscillations (N1C6, N1C9, and particularly N1C11). The degree of axial stability is determined by the relative balance between the axially shifting xenon distribution and opposing power-driven fuel temperature change. This phenomena is demonstrated graphically in Figure 50. The good agreement of the measured and predicted axial offset oscillation magnitude in the modeled operational transients demonstrates that the xenon-Doppler balance is well predicted. Since both the combination of xenon and Doppler feedback (item 2 above) and the balance between xenon and Doppler feedback are well predicted, it follows that the individual components are also well predicted.

#### 4.3.9 Delayed Neutron and Prompt Neutron Lifetime Data

The techniques used for calculating effective delayed neutron fractions for the core are described in reference 2 (CASMO, Section 9.7) and reference 6 (SIMULATE, Section 4.2). The treatment in CASMO uses a conventional six delayed neutron group approach based on basic nuclear data ( $\beta_{m,i}$  and  $\lambda_{m,i}$ ) for each fissioning nuclide  $m$  and delayed neutron group  $i$ . The data are weighted by nuclide fission rate and by energy group importance using the cell average adjoint flux in each energy group. CASMO data is passed to SIMULATE via the CMS-LINK cross section library. In the SIMULATE core model, CASMO data is integrated using the relative fission neutron production rate of each assembly weighted by the spatial adjoint flux.

There are three sets of basic delayed neutron data available in CASMO. ENDF/B-V data is available in a form which assumes a delayed group independent  $\nu$  (neutrons per fission) and in a form which uses a delayed group dependent  $\nu$  (the default data). The Tuttle 1979 evaluation for delayed neutron yield is also available. In practice, there is only a small difference between the Tuttle and ENDF/B-V data as indicated in reference 34.

Based on this review of the data and techniques used to calculate the effective delayed neutron fraction and decay constants for each delayed neutron group, it is reasonable to maintain the existing NRF of  $\pm 5\%$  for effective delayed neutron fraction. This value is consistent with the  $\pm 4\%$  value approved for the same use in a similar reactor in reference 35.

The techniques used for calculating prompt neutron lifetime ( $L_p$ ) for the core are described in reference 2 (CASMO, Section 9.7) and reference 6 (SIMULATE, Section 4.2). Although a variety of ways exist to define and calculate the prompt neutron lifetime, the technique described in reference 2 is similar to the description in reference 36. Reference 2 expands the calculation to a multiple

energy groups, and incorporates adjoint importance weighting. One difference is that instead of using the macroscopic absorption cross section in the denominator, the CASMO technique employs  $\nu\Sigma_f$ . The effect of this is that CASMO will tend to produce the value for  $L_p$  which would occur in a critical assembly (where  $\nu\Sigma_f = \Sigma_a$ ). CASMO data is passed to SIMULATE via the CMS-LINK cross section library. In the SIMULATE core model, CASMO  $L_p$  data is weighted using the spatial adjoint flux to obtain the core  $L_p$ .

[

]

Based on this review and validation of the techniques used to calculate  $L_p$ , it is reasonable to maintain the existing NRF of  $\pm 5\%$ . This value is consistent with the  $\pm 4\%$  value approved for the same use in a similar reactor in reference 35.

## Validation of CASMO-4 Prompt Neutron Lifetime Calculations

\_\_\_\_\_

Downloaded from <http://ajphaphysiol.physiology.org/> by guest on September 11, 2012

## SECTION 5 - SUMMARY AND CONCLUSIONS

Dominion (Virginia Power) has demonstrated in this report the accuracy of CASMO-4/SIMULATE-3 core models as well as Dominion's ability to develop and use these models for a variety of applications. The models have been validated by an extensive set of benchmarks to both higher order calculations and to over 60 cycles of measured data from the Surry and North Anna nuclear power stations. Based on those benchmarks, the following set of nuclear reliability factors (NRF) were determined to account for model predictive bias and uncertainty:

Parameter	NRF	
	Upper	Lower
Integral Control Rod Bank Worth (Individual banks)	1.1	0.9
Integral Control Rod Bank Worth (Total of all banks)	1.1	0.9
Differential Control Rod Bank Worth	1.15	0.8
Critical Boron Concentration	+50 ppm	-50 ppm
Differential Boron Worth	1.05	0.95
Isothermal and Moderator Temperature Coefficient	+2 pcm/°F	-2 pcm/°F
Doppler Temperature Coefficient	1.10	0.90
Doppler Power Coefficient	1.10	0.90
Effective Delayed Neutron Fraction	1.05	0.95
Prompt Neutron Lifetime	1.05	0.95
$F\Delta H$	1.04	N/A
FQ	1.05	N/A

Dominion concludes that the CASMO-4/SIMULATE-3 models, in conjunction with the indicated reliability factors, are fully qualified for use as equivalent replacements for prior models. Key aspects of core design and analysis methodology described in other Topical Reports (references 11-13, 18, 39) are not changed by the use of CASMO-4/SIMULATE-3 models as replacements. Furthermore, a robust model development process has been described that



benefits in part from the use of higher order models to identify and eliminate significant bias prior to use of the models for core calculations. This process, coupled with code and model quality assurance practices, provides assurance that future changes to core, fuel and burnable poison designs will be modeled with accuracy and appropriate conservatism. It is anticipated that additional model validation and improvement will continue as the CASMO-4/SIMULATE-3 models are applied to future core designs.

## SECTION 6 - REFERENCES

1. M. Edenius, K. Ekberg, B.H. Forssen, D. Knott, "CASMO-4 A Fuel Assembly Burnup Program User's Manual," Studsvik of America, Inc. and Studsvik Core Analysis AB, SOA-95/1, Rev. 0, September 1995.
2. D. Knott, B.H. Forssen, M. Edenius, "CASMO-4 A Fuel Assembly Burnup Program Methodology," Studsvik of America, Inc. and Studsvik Core Analysis AB, SOA-95/2, Rev. 0, September 1995.
3. J. D. Rhodes, K. Smith, "CASMO-4 v2.05 Modeling Changes and Additional Input Cards," Studsvik Scandpower, SSP-00/417, Rev. 0, June 2000.
4. T. Bahadir, A. S. DiGiovine, J. Rhodes, K. Smith, "CMS Microscopic Burnable Poison Option," Studsvik of America, SOA-97/36, Rev. 0, November 1997.
5. A. S. DiGiovine, J. D. Rhodes, "SIMULATE-3 User's Manual," Studsvik of America, SOA-95/15, Rev. 0, October 1995.
6. J. T. Cronin, K. S. Smith, D. M. Ver Planck, J. A. Umbarger, M. Edenius, "SIMULATE-3 Methodology," Studsvik of America, SOA-95/18, Rev. 0, October 1995.
7. R. A. Hall, "The PDQ Two Zone Model," Virginia Electric and Power Company, Topical Report VEP-NAF-1, July 1990.
8. Letter from W. L. Stewart (Virginia Electric and Power Company) to U.S. Nuclear Regulatory Commission, "Virginia Electric and Power Company, Surry Power Station Units 1 & 2, North Anna Power Station Units 1& 2 Topical Report – PDQ Two Zone Model," October 1, 1990.
9. S. M. Bowman, "The Vepco NOMAD Code and Model," Dominion Topical Report VEP-NFE-1-A, May 1985.
10. Letter from W. L. Stewart (Virginia Electric and Power Company) to U.S. Nuclear Regulatory Commission, "Virginia Electric and Power Company, Surry Power Station Units 1 & 2, North Anna Power Station Units 1& 2 Topical Report Use Pursuant to 10CFR50.59," November 25, 1992.
11. K. L. Basehore, et al., "Vepco Relaxed Power Distribution Control Methodology and Associated Fq Surveillance Technical Specifications," VEP-NE-1-A, March 1986.
12. D. Dziadosz, et al., "Reload Nuclear Design Methodology," Dominion Topical Report VEP-FRD-42 Rev. 1-A, September 1996.

## SECTION 6 – REFERENCES (Continued)

13. T. K. Ross, W.C. Beck, "Control Rod Reactivity Worth Determination by the Rod Swap Technique," Dominion Topical Report VEP-FRD-36A, December 1980.
14. R. W. Twitchell, "Fuel Management Scheme 2002," Dominion Technical Report NE-1313, Rev. 0, February 2002.
15. "SCALE: A Modular Code System for Performing Standardized Computer Analyses for Licensing Evaluation," NUREG/CR-0200, Rev. 6, Oak Ridge National Laboratory, December 1999.
16. J. F. Breismeister, "MCNP – A General Monte Carlo N-Particle Transport Code, Version 4C," LA-13709-M, December 2000.
17. J. G. Miller, "The ESCORE Steady State Fuel Performance Code," Dominion Technical Report NE-554, Rev. 0, November 1986.
18. T. W. Schleicher, "Reactor Power Distribution Analysis Using a Moveable In-core Detector System and the TIP/CECOR Computer Code Package," Dominion Topical Report VEP-NAF-2, November 1991.
19. [ ]
20. [ ]
21. K. Ekberg, "CASMO-4 Benchmark Against Yankee Rowe Isotopic Measurements," Tagungsbericht Proceedings, ISSN 0720-9207, Jahrestagung Kerntechnik '97, May 1997.
22. K. Terazu, et al., "Verification of the CASMO-4 Transport Method Based on BWR High-Burnup 9x9 Fuel Critical Experiments," Transactions of the American Nuclear Society, Volume 73, TANSO 73 1-522 (1995), ISSN 0003-18X, October 1995.
23. J. G. Miller, "Vepco Nuclear Design Reliability Factors," Dominion Topical Report VEP-FRD-45A, October 1982.
24. "American National Standard Reload Startup Physics Tests for Pressurized Water Reactors," ANSI/ANS-19.6.1-1997, August 1997.
25. M. G. Natrella, "Experimental Statistics," National Bureau of Standards Handbook 91, August 1963.

## SECTION 6 – REFERENCES (Continued)

26. P. N. Somerville, "Tables for Obtaining Non-Parametric Tolerance Limits," Ann. Math. Stat., Vol 29, 1958.
27. J. J. Duderstadt and L. J. Hamilton, "Nuclear Reactor Analysis," Table 2-4, ISBN 0-471-22363-8, John Wiley and Sons, 1976.
28. J. R. Lamarsh, "Introduction to Nuclear Reactor Theory," Table 3-10, Addison-Wesley Publishing Company, 1966.
29. "An Acceptance Model and Related Statistical Methods for the Analysis of Fuel Densification," U.S.N.R.C. Regulatory Guide 1.126, Rev. 1, March 1978.
30. M. A. Stephens, "Use of the Kolmogorov-Smirnov, Cramer-Von Mises and related statistics without extensive tables," J. American Statistical Association, 69:730, 1974.
31. M. A. Stephens, Biometrika, Vol. 52, pp. 309-321, 1965.
32. "American National Standard Assessment of the Assumption of Normality (Employing Individual Observed Values)," ANSI N15.15-1974.
33. T. Bahadir, J. Umbarger, M. Edenius, "CMS-LINK User's Manual," Studsvik of America, SOA-97/04 Rev. 2, April 1999.
34. M. C. Brady and T. R. England, "Delayed Neutron Data and Group Parameters for 43 Fissioning Systems," Nuclear Science and Engineering: 103, 129-149 (1989).
35. Letter from T. Kim, U. S. Nuclear Regulatory Commission to Mr. Joel Sorenson, Prairie Island Nuclear Generating Plant, "Prairie Island Nuclear Generating Plant, Units 1 and 2 – Safety Evaluation on Topical Report, NSPNAD-8101, Revision 2, Qualification of Reactor Physics Methods for Application to Prairie Island Units and 2," September 13, 2000.
36. J. R. Lamarsh, "Introduction to Nuclear Reactor Theory, 2<sup>nd</sup> Edition," Chapter 7.1, Addison-Wesley Publishing Company, 1983.
37. M. M. Bretscher, "Evaluation of Reactor Kinetic Parameters Without The Need For Perturbation Codes," Argonne National Laboratory under DOE contract # W-31-109-ENG-38, Presented at the 1997 International Meeting on Reduced Enrichment for Research and Test Reactors, October 5-10, 1997.

## **SECTION 6 – REFERENCES (Continued)**

38. L. M. Petrie, et al, "KENO-V.a: An Improved Monte Carlo Criticality Program With Supergrouping," NUREG/CR-0200, Rev. 6, Volume 2 Section F11.5.14, Oak Ridge National Laboratory, March 2000.
39. C. A. Ford and T. W. Schleicher, "Reactor Vessel Fluence Analysis Methodology," Dominion Topical Report VEP-NAF-3A, April 1999.

**Attachment 3**

**Application for Withholding From Public Disclosure**  
**and**  
**Affidavit of Leslie N. Hartz**

**Virginia Electric and Power Company  
(Dominion)**

**APPLICATION FOR WITHHOLDING**  
**AND**  
**AFFIDAVIT OF LESLIE N. HARTZ**

I, Leslie N. Hartz, Vice President – Nuclear Engineering, state that:

1. I am authorized to execute this affidavit on behalf of Virginia Electric and Power Company (Dominion).
2. Dominion is submitting Topical Report DOM-NAF-1, "Qualification of the Studsvik Core Management System Reactor Physics Methods for Application to North Anna and Surry Power Stations," for NRC review and approval. The Proprietary Version of the Topical Report DOM-NAF-1 contains proprietary commercial information that should be held in confidence by the NRC pursuant to the policy reflected in 10 CFR §§ 2.790(a)(4) because:
  - a. This information is being held in confidence by Dominion.
  - b. This information is of a type that is held in confidence by Dominion, and there is a rational basis for doing so because the information contains sensitive commercial information concerning Dominion's reactor physics analysis methodology.
  - c. This information is being transmitted to the NRC in confidence.
  - d. This information is not available in public sources and could not be gathered readily from other publicly available information.
  - e. Public disclosure of this information would create substantial harm to the competitive position of Dominion by disclosing confidential Dominion internal reactor physics analysis methodology information to other parties whose commercial interests may be adverse to those of Dominion. Furthermore, Dominion has expended significant engineering resources in the development of the information. Therefore, the use of this confidential information by competitors would permit them to use the information developed by Dominion without the expenditure of similar resources, thus giving them a competitive advantage.
3. Accordingly, Dominion requests that the designated document be withheld from public disclosure pursuant to the policy reflected in 10 CFR §§ 2.790(a)(4).

Virginia Electric and Power Company

  
Leslie N. Hartz

Vice President –Nuclear Engineering

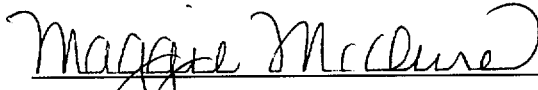
STATE OF

Virginia

COUNTY OF

Henrico

Subscribed and sworn to me, a Notary Public, in and for the County and State  
above named, this 13<sup>th</sup> day of June, 2002.

  
Maggie McClure

My Commission Expires: 3-31-04

